



**Politecnico
di Torino**

POLITECNICO DI TORINO

Master's degree course in Electrical Engineering
A.y. 2020/2021
Graduation session October 2021

String inverter control design for photovoltaic applications

Supervisors:

Academic:
Prof. Radu Bojoi
Company:
Dr. Francisco Freijedo

Co-supervisor:

Alvaro Moralez

Candidate:

Vincenzo Barba
s268910

Acknowledgements

The work presented in this thesis was carried out as an intern at the Huawei Nuremberg Research Center thanks to the collaboration between it and the Politecnico di Torino (PoliTo).

First of all, I would like to express my deep gratitude to my supervisors, Professor Radu Bojoi, for having given me several times the opportunity to gain didactic-scientific experience during my entire university studies, and Dr. Francisco Freijedo, for having allowed me to carry out this thesis as a member of his team and for having been an excellent guide. With their trust, scientific expertise, and also patience, they pushed me in the right direction, while giving me ample space to develop my ideas.

I would like to thank my co-supervisor, the PhD student Alvaro Morales, and the entire Huawei team for supporting me in this project, which has been very interesting and educational.

This experience allowed me to grow my work skills and gain more my resourcefulness and self-confidence. It has consolidated my university background and has enriched my knowledge about grid-stability, converter's control design, the use of PLECS simulation software even more. I have improved my own problem-solving skills, self-study, and learnt from the advice and knowledge of those with more experience than me. In addition, I have learnt the importance of company and teamwork choices. Working in a multicultural environment enriched my experience too.

I am also grateful to all the professors I had during my years of study for enhancing my knowledge with such professionalism and competence.

Finally, my greatest gratitude goes to my parents and family members, who believed in my abilities and supported me in every situation, to my course mates at PoliTo with whom we interacted and collaborated to grow together, and to my roommates in Nuremberg for helping me and welcoming me.

Now, my intention is to pursue improving my skills with a PhD at PoliTo.

Forza e onore...
...sempre!

List of contents

Introduction	1
1 State of the art	3
1.1 Synchronous machine classical power system.....	3
1.2 Problem of the Power Electronic dominated renewable grid.....	18
1.2.1 Transition to low rotational inertia system	18
1.2.2 Three phase short circuit with a power converter.....	21
1.2.3 Short and long term solutions	26
1.3 Grid following and grid forming.....	28
1.3.1 Grid following.....	32
1.3.2 Grid forming - Droop control	35
1.4 The Virtual Synchronous Machine control.....	39
2 Average model of string inverters	45
2.1 Motivation.....	45
2.2 Averaging versus switching models	45
2.3 Lumped model of a string	46
2.4 Current control	55
2.5 DC-link control	64
3 Frequency control with power electronic converter.....	67
3.1 Motivation.....	67
3.2 Power reference generation.....	71
3.3 Modification to the grid control	76
3.4 Enabling/Disabling state of the storage.....	83
3.5 Case PV's power generation bigger than load's request.....	91
3.5.1 Without energy supplier.....	92
3.5.2 With energy supplier.....	95
Conclusions	98

List of Figures

Figure 1.1-1	Steam turbine's schematic	4
Figure 1.1-2	Synchronous machine frequency regulation.....	5
Figure 1.1-3	Trends of frequency variation and power variation at the step load's power variation- Reference's machine	7
Figure 1.1-1	SNPS trend in the years 2018 light purple, 2019 dark purple and 2020 green in different places: (a) NEM; (b) New South Wales; (c) Queensland; (d) South Australia; (e) Tasmania; (f) Victoria [7].....	20
Figure 1.2-2	Stator current of the synchronous machine during a short circuit event.....	21
Figure 1.2-3	Voltage and current of the converter during a short circuit event... ..	22
Figure 1.2-4	PLL dynamic during a short circuit time interval of 0,05 s and 0,1 s.	23
Figure 1.3-1	Grid following converter topology on the left and its phasors diagram on the right [21].....	28
Figure 1.3-2	Grid following converter control block diagram.....	29
Figure 1.3-3	Grid following converter control principle: droop control.....	29
Figure 1.3-4	Grid forming converter control block diagram.....	30
Figure 1.3-5	Grid forming converter control principle: droop control.....	30
Figure 1.3-6	Grid forming converter topology on the left and its phasors diagram on the right [21].....	30
Figure 1.3-7	Topology of the power electric circuit: converter connected to the RLE grid trough RLC filter.....	31
Figure 1.1.1-1	Grid following converter control schematic block.....	32
Figure 1.1.1-2	Grid following converter control: active and reactive power dynamics at a step reference variation.....	34
Figure 1.1.1-3	Grid following converter control: dq-axis current dynamic at a step reference variation.....	35
Figure 1.3.2-1	Grid forming converter droop control schematic block... ..	36
Figure 1.1.2-2	Topology of the power electric circuit used in simulation: converter connected to the RL grid trough RLC filter.....	37
Figure 1.1.2-3	Grid forming converter control: active power and frequency dynamic at step load request, reference power, frequency reference and voltage drop variations.....	38
Figure 1.1.2-4	Grid forming converter control: phase voltage and current dynamic at step load request, reference power, frequency reference and voltage drop variations.....	39

Figure 1.4-1 Grid forming converter Virtual Synchronous Machine control schematic block: in orange the part coming from a typical GFM control; in green the part that simulates the synchronous machine frequency regulation's behavior.....	41
Figure 1.4-2 Grid Forming Virtual Synchronous Machine converter control: phase current dynamic at step load request.....	41
Figure 1.4-3 Grid Forming Virtual Synchronous Machine converter control: power and frequency dynamics at step load request.....	42
Figure 1.4-4 Grid Forming Virtual Synchronous Machine converter control: dynamic of the power and frequency responses of the simulated machines' system -dynamic response at step load request.....	43
Figure 2.3-1 String PV obtained connecting several PV panel in series.	47
Figure 2.3-2 Parallel of more string PV. Output current and voltage are managed by a converter.....	47
Figure 2.3-3 Electrical circuit of the power system formed by a converter connected to the grid trough a LCL filter.....	48
Figure 2.3-4 ZOH frequency response. The yellow zone corresponds to alias region [49].....	50
Figure 2.3-5 String inverter obtained connecting N inverter in parallel.	52
Figure 1.1-6 A generic n LCL filter between the N_{inv} inverter ant the point of connection PCC.....	53
Figure 1.1-7 Point of connection of the N_{inv} inverters composing the string inverter.....	54
Figure 2.4-1 Power arrangement: PV generation for N inverters composing a string; LCL filers between inverters and point of connection: transformer to connect with the grid.....	56
Figure 2.4-2 Equivalent AC system arrangement.....	57
Figure 2.4-3 Current's control loop block diagram.....	60
Figure 2.4-4 Current's control loop block diagram with saturators and anti-windup.....	62
Figure 2.4-5 Plot of currents for a 50% step variation of the d-axis reference current.....	63
Figure 2.4-6 Plot of currents for a 50% step variation of the q-axis reference current on the right.....	63
Figure 2.5-1 Equivalent DC system arrangement.....	64
Figure 2.5-2 Equivalent DC system arrangement for power control action	64
Figure 2.5-3 DC-link voltage's control loop block diagram	66
Figure 2.5-4 Plot of DC voltage for a step PV's power of 1MW and 10% step variation of the DC voltage's reference	66
Figure 3.1-1 Entire AC power system: string converter, filter, loads and synchronous alternators in frequency regulation	67
Figure 3.1-2 Synchronous machine's schematic block in dq-axis.....	69

Figure 3.2-1 DC-link voltage and energy calculation schematic block and energetic inputs for the DC voltage control.....	72
Figure 3.2-2 DC-link voltage control with energetic inputs.....	73
Figure 3.2-3 Storage introduction in the power DC arrangement.....	74
Figure 3.2-4 Power system arrangement with storage in action according with the control strategy.....	74
Figure 3.2-5 Emulated inertia energy in the power reference generation.....	75
Figure 3.2-6 Schematic block of the entire control structure of the converter control.....	75
Figure 3.3-1 Inertial energy calculation for the power reference calculation.....	76
Figure 3.3-2 Complete AC electric circuit: string converter, equivalent filter, short circuit transformer's inductance, load request, synchronous alternator.....	77
Figure 3.3-3 Dynamic behavior of the DC-link voltage- initial transient.....	78
Figure 3.3-4 Dynamic behavior of the load's power and of the sources. - initial transient.....	78
Figure 3.3-5 Mechanical speed measured on both the synchronous machines- initial transient.....	79
Figure 3.3-6 Dynamic behavior of the converter's reference power- initial transient.....	79
Figure 3.3-7 Dynamic behavior of the phase AC voltage and current	81
Figure 3.3-8 Dynamic behavior of the DC-link voltage- long time simulation..	81
Figure 3.3-9 Dynamic behavior of the load's power and of the sources. - long time simulation.....	82
Figure 3.3-10 Mechanical speed measured on both the synchronous machines- long time simulation.....	82
Figure 3.4-1 Working area of storage technologies [60].....	83
Figure 3.4-2 Schematic block of the storage activation control	84
Figure 3.4-3 Dynamic behavior with storage of the DC-link voltage and of the storage's current- initial transient.....	85
Figure 3.4-4 Dynamic behavior with storage of the load's power and of the sources. - initial transient	86
Figure 3.4-5 Dynamic behavior with storage of the phase AC voltage and current.....	86
Figure 3.4-6 Mechanical speed measured on both the synchronous machines- initial transient with storage	87
Figure 3.4-7 Dynamic behavior of the DC-link voltage and storage's current- step change of PV's power of 200 kW at time $t=60$ s.....	91
Figure 3.4-8 Dynamic behavior of the load's power and of the sources - inertial energy is activated at time $t = 0,4$ s.- initial transient.....	90
Figure 3.5.1-1 Dynamic behavior of the DC-link voltage- power generation bigger than load's request.....	92
Figure 3.5.1-2 Dynamic behavior of the load's power and of the sources - power generation bigger than load's request.....	93

Figure 3.5.1-3	Mechanical speed measured on both the synchronous machines- power generation bigger than load's request.....	93
Figure 3.5.1-4	Dynamic behavior of the converter's reference power- power generation bigger than load's request.....	94
Figure 3.5.1-5	Dynamic behavior of the load's power and of the sources - power generation bigger than load's request- initial transient	94

List of Tables

Table 1.1-1	Data of the reference's synchronous machine.....	6
Table 1.1-2	Dynamic results at the step load's power variation - One synchronous machine in first frequency regulation.....	8
Table 1.1-3	Open loop poles, closed loop poles and damping for various synchronous machine in first frequency regulation.....	10
Table 1.1-4	Data of the two different machines in first frequency regulation end of the one non participant	11
Table 1.1-5	Dynamic results at the step load's power variation- Two different synchronous machines in first frequency regulation and one non participant.....	13
Table 1.1-6	Data of the machines in first frequency regulation, in secondary frequency regulation and one non participant.....	15
Table 1.2-1	Short-term solutions and long-term solutions for low inertia systems	26
Table 3.1 1	Data of the droops and time constants of the synchronous machines used in the simulation.....	69
Table 3.1-2	Data of synchronous machines for the simulation.....	71
Table 3.1-3	Data of the synchronous machine in secondary regulation used in the simulation	71

List of Acronyms and Symbols

Symbol	Meaning
E_{dec}	Deceleration energy during fault
E_P	Regulated permanent energy
E_T	Regulated transient energy
E_{acc}	Accumulated energy during fault
E_c	Energy of rotating loads
E_{ecc}	Eccitation's voltage
E_w	Inertial energy
G_f	Transfer function of the regulator
H_{OL}	Open loop transfer function
P_L	Load's power request
P_P	Power delivered by SM in first frequency regulation

P_{as}	Asynchronous power of the machine's damping windings
P_c	Power of rotating loads
P_e	Electrical power
P_m	Mechanical power
P_s	Power delivered by SM in secondary frequency regulation
P_w	Inertial power
$R(\theta)_{\alpha\beta\rightarrow dq}$	Rotational transformation
R_{th}	Boiler's thermal resistance
T_0	Secondary frequency regulation time constant
$T_{123\rightarrow\alpha\beta}$	Parke transformations
$T_{a c}$	Start-up time of the converter
T_a	Start up time
T_p	Pole time constant
T_s	Sampling period
T_z	Zero time constant
V_{amp}	Amplitude value of the converter reference voltage
Y_c	Equivalent admittance of converter and filter
Y_g	Equivalent admittance of converter, filter and transformer
Z_{0g}	Equivalent impedance of grid and transformer
b_p	Permanent droop
b_T	Transitory droop
$\frac{d}{dt}$	Time derivate
f_s	Sampling frequency
k_p	Proportional gain of the regulator
k_0	Secondary frequency regulation gain
k_{ad}	Active damping gain
k_d	Direct feedthrough gain of anti-windup
$k_{d.c.}$	Droop control gain
k_{fdb}	Feedback gain of anti-windup
k_i	Integral gain of the regulator
m	Modulation index
p_{\pm}	Poles
p_{conv}	Converter's pole
ω_c	Crossover pulsation
ω_{nat}	Natural pulsation
$\wedge T$	Transposed
$_0$	Initial value

<i>_l</i>	Fundamental value
<i>_abc , _123</i>	Three-phase
<i>_b</i>	Base value
<i>_band</i>	Bandwidth
<i>_C</i>	Value on filter capacitance
<i>_cr</i>	Critical value
<i>_dq</i>	Two-phase rotating frame of reference. d-axis's direction equal to voltage phase.
<i>_f</i>	Value of filter component
<i>_ff</i>	Feedforward
<i>_g</i>	Grid's value
<i>_i</i>	Relative to the current control loop
<i>_inv</i>	Value on converter output
<i>_load</i>	Load's value
<i>_LPF</i>	Low pass filter
<i>_max</i>	Maximum value
<i>_min</i>	Minimum value
<i>_n</i>	Nominal value
<i>_r</i>	Rotor
<i>_ref</i>	Reference value
<i>_res</i>	Value of resonance
<i>_s</i>	Stator
<i>_sat</i>	Saturation limit
<i>_sc</i>	Short circuit value
<i>_tot</i>	Equivalent total value
<i>_v</i>	Relative to the voltage control loop
<i>_σ</i>	Leakage value due to the transformer
<i>cosφ</i>	Power factor
DAC	Digital-to-analog converter
<i>F , _F</i>	Control function of the converter
GFL	Grid following converter
GFM	Grid forming converter
<i>h</i>	Enthalpy variation
HP	High pressure step of the steam turbine
J	System inertia constant
LP	Low pressure step of the steam turbine
PCC	Point of connection
PI	Proportional integral controller
PLL	Phase locked loop
PV	Photovoltaic

<i>PWM</i>	Pulse width modulation
<i>qf</i>	Quality factor
ROCOF	Rate of change of frequency
<i>s</i>	Laplace variable
SM	Synchronous machine
SMES	Superconducting magnetic energy storage
VSC	Voltage source converter
VSM	Virtual Synchronous Machine control
VSM	Virtual Synchronous machine methodology
<i>z</i>	Z-domain variable
ZOH	Zero Order Hold
Δ	Small variation
Δq	Fuel flow rate of the steam turbine
ω	Pulsation
<i>D</i>	Damping coefficient
<i>S</i>	Complex power
<i>SNSP</i>	System non-synchronous penetration
<i>Z</i>	Impedance
<i>f</i>	Frequency
<i>pm</i>	Phase margin
δ	Load angle
ζ	Damping
θ	Angle of rotation from three-phase to dq frame

Introduction

The objective of this thesis is to realize the converter control model for the PV TRUST Task 5 project. In this project, the companies Huawei and ENEL collaborate to allow higher PV penetration levels by improving the operational stability at the point of connection and ensure grid friendliness. Huawei's Nuremberg Research Center has the task of designing the model of the converter control strategy while Enel will produce detailed models of the components integrated in the simulation.

The converter used is a string inverter formed by connecting several inverters in parallel. The aim is to study the dynamics of the grid when such a converter is introduced to power it.

The work therefore is articulated in the following points:

- To study the environment where the converter will be introduced.
- Qualitatively evaluation of what changes, advantages and disadvantages there are in the grid as a result of its introduction
- To know which converter control strategies are present nowadays and what principles they are based on
- Construction of the electrical power circuit model of the grid
- Design the control model of the converter in the various loops
- Evaluate the limits of control and take additional measures, such as introducing storage into the power system.

In the contemporary power system, the electric power generation is mainly provided by synchronous generators, which are regulated to preserve the correct operation of the electric grid. In particular, the active power balance is guaranteed by keeping the grid frequency at the reference value, i.e., 50 Hz or 60 Hz. During a load power variation, the whole system reacts by decelerating or accelerating and transferring the inertial energy of the synchronous generators into electrical power. In a second phase, the primary and secondary regulations of the frequency operate to recover this energy and restore the reference frequency in the power grid.

This control paradigm is severely challenged in case of a large penetration of converters connected to non-synchronous sources (e.g. solar PV). Given the exponential growth of such technologies, new control strategies are necessary. This thesis develops an advanced control strategy to be used in a future grid perspective controlled by a system with little inertia.

At first, the state-of-the-art regulation system for synchronous generators and the impact on the system of the various system parameters (e.g. inertia constant) are observed. To obtain the aim of the thesis, different control strategies are investigated and developed using simulation software solutions such as MATLAB and PLECS. Especially, control strategies for grid following converters (GFL), such as the ones interfacing PV arrays to the grid, which can adapt to the behaviour

of the grid, and grid forming (GFM), which can generate an electric grid in islanded operation, are analysed and developed. The block schematics of the control is built. In smart grid applications Virtual Synchronous machine (VSM) methodology simulates the typical regulation system for synchronous generators to estimate the reference power of the converter control. Given the GFM overcurrent and GFL overvoltage issues, the proposed idea is to interconnect the two controls.

The study focuses on the dynamics of the entire grid and not on the strategy for regulating the electrical variables of the converter. For this reason, the high-frequency dynamics and the discontinuities that it presents are neglected. The string inverter in question uses LCL filters. The active damping coefficient is introduced into the control, specially calculated to guarantee passivity and to ensure the system stability. Furthermore, a study that considers electrical variables and the behaviour of all connected inverters is too detailed and requires too much computing power. Their lumped equivalent model is created at average values, reducing the order of the system.

Once the basics are in place, the cascade control that returns the voltage reference is built. The internal current control loop with PI controller in the dq-axis reference system rotates at the mains frequency. It is achieved using a phase locked loop (PLL). The external DC-link voltage control is realised with energetic inputs controlling its square value in order not to introduce non-linearity between DC and AC part of the convert.

Finally, it is ready to introduce the control design of the frequency control. An energy quantity representing the virtual inertia of the converter is added. PLECS simulations tests are carried out to evaluate the operation of the converter when it works supplied by the photovoltaic source and together with synchronous machines at different power levels. Having highlighted functional limitations, an energy storage is added in the power circuit to support the DC-link voltage.

In conclusion, the designated control demonstrates the ability to work frequency regulation as desired under conditions of high and low load demand or photovoltaic output power, cooperating in state-of-the-art regulation.

1 State of the art

It is desired to study what is the principle of frequency regulation used today with synchronous alternators. This is aimed at understanding the salient points of the regulation system and this will be useful in implementing the control for the converter. In fact, the converter must be able to work to meet the load demand of the grid. This means that the control to be implemented must take into account the working environment in which it will operate, whether it can influence the existing system and vice versa. In this section it is explained the state of the art of the grid's structure and, in particular, how frequency regulation is realized today and what changes the introduction of converters in the system will bring in the future.

Subsequently, different types of control for converters are explored. In particular, the fundamental differences between grid following and grid forming control are analyzed. Simulations are carried out to study their principles and collect all their details.

1.1 Synchronous machine classical power system

Today the grid is organized to satisfy the request of load electrical power through two system regulations.

The frequency of the power grid is related to the speed of rotation of the machines according to the equation [1]:

$$\begin{cases} \Delta P_m - \Delta P_e = -\Delta P_W = (T_a \cdot S_n / f_n) \cdot \frac{d\Delta f}{dt} = J \cdot \frac{d\Delta f}{dt} \\ \Delta P_e = \Delta P_L + E_c \cdot \Delta f \end{cases} \quad (1.1-1)$$

where:

- Δ indicates the small signal deviation;
- P_m is the mechanical power;
- T_a is the time that the alternator needs to arrive at the rotation speed of the nominal frequencies f_n starting from zero with a constant acceleration;
- S_n is the nominal complex power;
- J is the full system's inertia constant of alternators connected to the grid;
- P_e is the electrical power. It is obtained as the sum of a power given by static load P_L and another given by rotating loads E_c , proportional to the variation of frequency Δf ;
- E_c is the energy deviation of rotating loads; from a control point of view, it can be considered as a friction.

The frequency should be kept as constant as possible at the nominal value, trying to ensure a balance between the power pairs of the production units and the consumption ones due to the presence of the users. Controllers with zero pole

transfer function are used but the impossibility to set a pole to zero, for reasons of stability, creates a non-null steady state frequency deviation from the nominal value if rotating loads are present in the grid.

Considering a simple model of a steam turbine with high pressure (HP) and low pressure (LP) steps, the mechanic power delivered in function of the frequency is delivered as a sum of the two steps. The low pressure step must wait the regulation of the fuel flow rate Δq made with valves and for this reason its delivered power has a delay respect to the high pressure step. h indicates the specific henthalpy variation [J/kg]. Steam turbine's schematic is represented in the Figure 1.1-1.

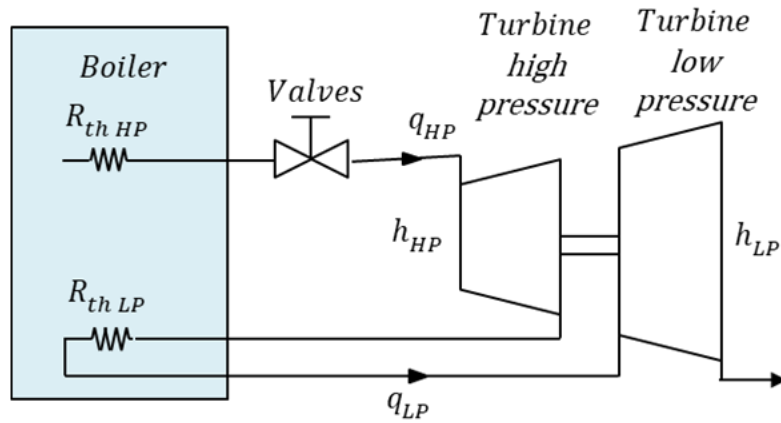


Figure 1.1-1 Schematic of a steam turbine.

The equation that describes the mechanical power variation is [2]

$$\Delta P_m = \Delta P_{HP} + \Delta P_{LP} = h_{HP} \cdot \Delta q_{HP} + h_{LP} \cdot \Delta q_{LP} = h_{HP} \cdot \Delta q_{HP} + h_{LP} \cdot \frac{\Delta q_{HP}}{1 + s \cdot T_p} \quad (1.1-2)$$

The variable s indicates the Laplace variable and T_p is the pole time constant representing the delay of the low-pressure part after a change in flow rate driven by the valves.

The transfer function of the regulator is below reported.

$$G_f(s) = \frac{\Delta P_m}{\Delta f_{ref} - \Delta f} = E_p \cdot \frac{1 + s \cdot T_z}{1 + s \cdot T_p} = E_T + \frac{E_p - E_T}{1 + s \cdot T_p} \quad (1.1-3)$$

where:

- $T_z = \alpha \cdot T_p$ is the zero time constant and $\alpha \leq 1$.
- E_p, E_T are called regulated permanent and transient energies. Their values are calculated in every kind of turbine from the declaration values of permanent and transitory droops $b_p b_T$.

$$\begin{cases} E_P = \frac{P_n}{b_P \cdot f_n} \\ E_T = \frac{P_n}{b_T \cdot f_n} \\ b_T = \frac{b_P}{\alpha} \end{cases} \quad (1.1-4)$$

The whole system is described with the following open loop transfer function.

$$H_{OL} = E_P \cdot \frac{1+s \cdot T_Z}{1+s \cdot T_P} \cdot \frac{1}{E_c+s \cdot J} \quad (1.1-5)$$

As a goal, it's wanted to study what it the system's response at a load power step variation for different values of the parameters. What it's intention to do is to use simulation and mathematical softwares, such as PLECS and MATLAB, to analyse the impact that individual parameter values have on the complex system and the control dynamics. Therefore, it's chosen to carry out simulations and calculations for a reference case, using specific values for the variables. After that, further simulations are carried out changing one parameter at a time and making comparisons with the reference case.

Through the PLECS simulation software, a model has been realized that allows to show the behavior of the system. The schematic block of a first frequency regulation performed by a synchronous machine (SM1°f) is reported in Figure 1.1-2.

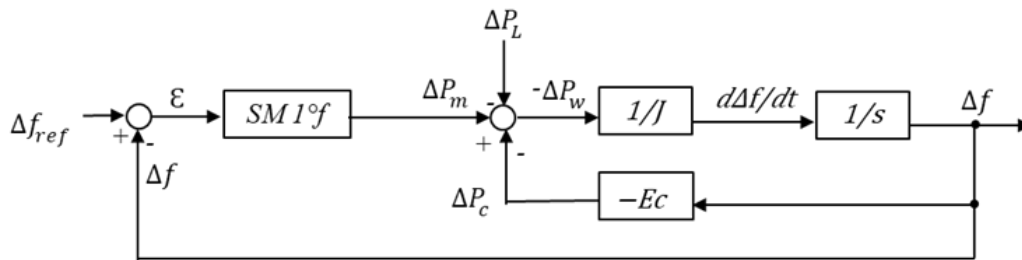


Figure 1.1-2 Synchronous machine frequency regulation.

The alternator receives as input the frequency variation error ϵ and load's variation references ΔP_L . The frequency variation reference Δf_{ref} is null because it is intended that the frequency is totally recovered by the action of the regulator.

The information on the frequency variation error is passed to the blocks represented by the synchronous alternator. Depending on the values of permanent and the regulated energies, it returns the produced mechanical power. Subtracting the load demand variation from this value and adding the inertial power variation of the rotating loads ΔP_c , the inertial power variation of the full system ΔP_w is calculated. Knowing the inertia of every individual generator and the total inertia given by their interconnection, the frequency variation present at that moment is obtained.

The following data reported in the Table 1.1-1 are used as a reference. It is used only a synchronous machine participating at the first regulation of frequency ($SM\ 1^\circ f$).

T_a [s]	T_p [s]	T_z [s]	E_c [p.u.· s]	J [p.u.· s ²]
12	10	2,5	0,01	0,24

Table 1.1-1 Data of the reference's synchronous machine.

For the simulation, a step of $\Delta P_L = 0,1\ p.u.$ is applied at the time $t = 1\ s$. The trends of frequency variation, mechanical power variation provided by the controller, the variation in inertial power caused by the machines and the power variation that the rotating loads have, are graphed respectively in Figure 1.1-3.

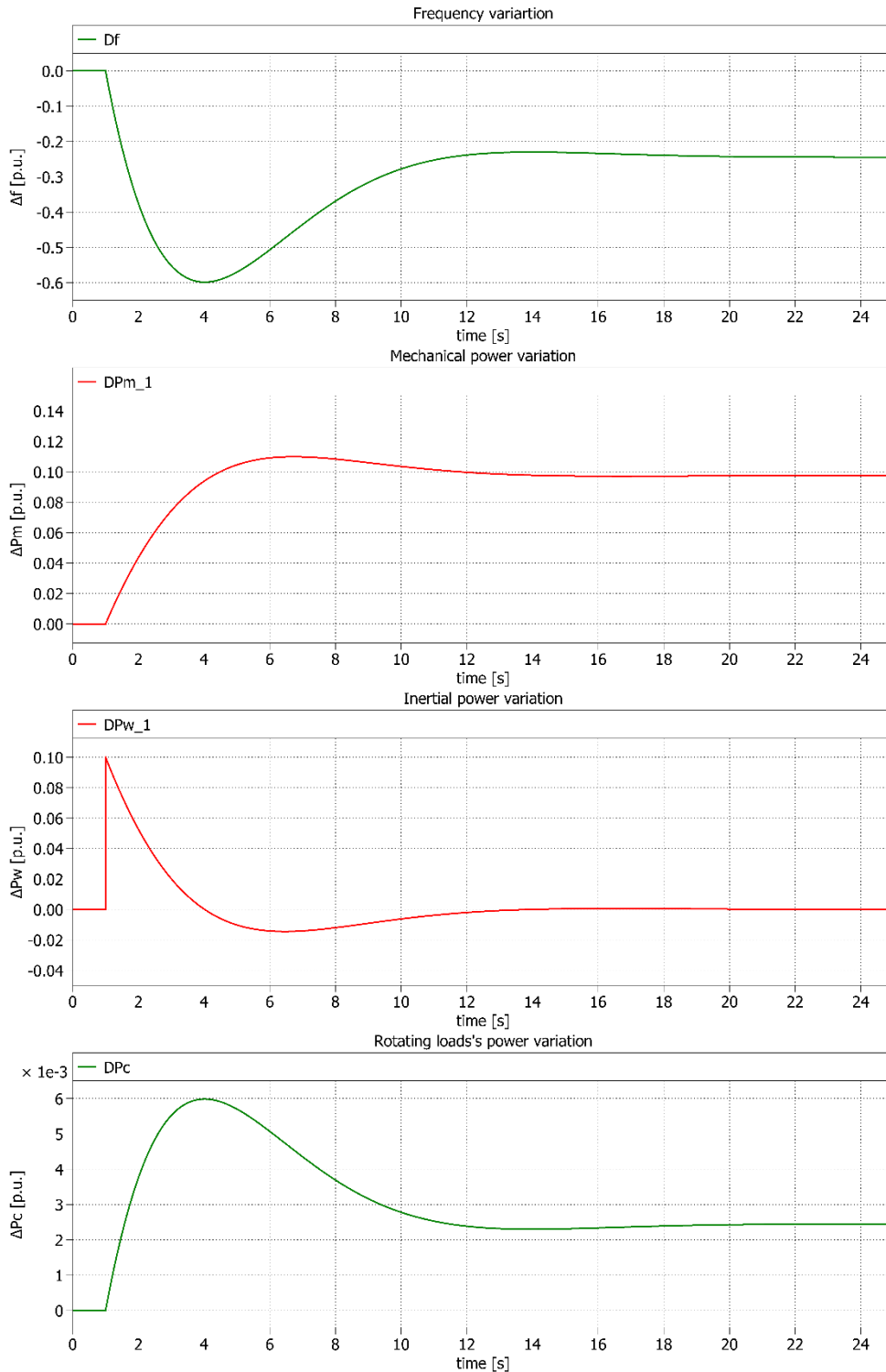


Figure 1.1-3 Trends of frequency variation and power variation at the step load's power variation- Reference's machine.

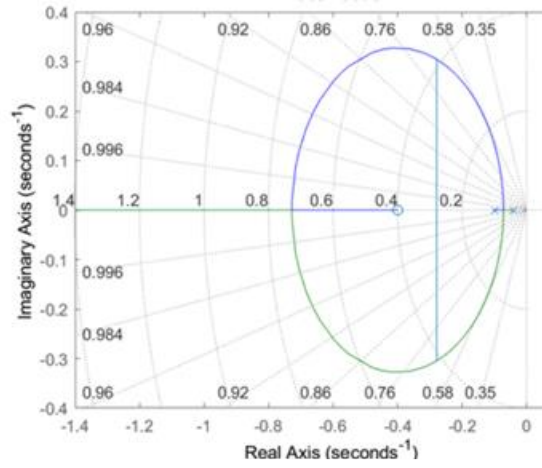
In the Table 1.1-2 are shown the values of the maximum frequency variation, called nadir, and the medium frequency variation time derivate value, called slew rate and measured from the 5% till the 95% of the maximum amplitude. If these values are both too high, they imply the activation of the protections and the load release [3]. For this reason, they must be observed. For have a good frequency regulation, it must be return that the frequency variation is null at the steady state.

In this table, also follow the value of the mechanical power variation's overshoot and its value when the steady state condition is reached. The subscript ∞ indicates the steady state values.

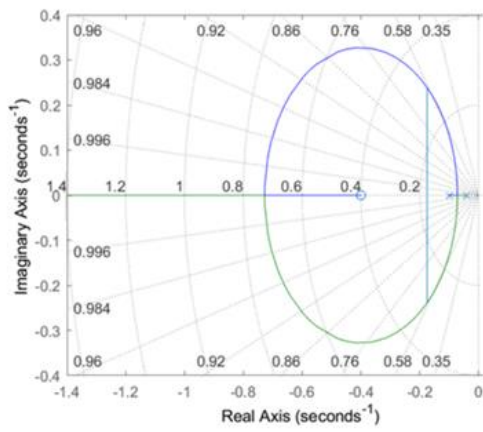
	<i>Reference data</i>	$b_p' = 0,1$	$E_t' = 0$ [p.u.· s] $T_z' = 0$ [s] $\alpha' = 0$	$E_c' = 0$ [p.u.· s]	$T_a = 8$ [s] $J = 0,16$ [p.u.· s ²]
Δf nadir [p.u.]	-0,576	-0,6	-0,992	-0,595	-0,624
Δf slew-rate (5%)	-154,5	-159,9	-387,7	-166,3	-307,1
Δf_∞ [p.u.]	-0,245	-0,46	-0,245	-0,25	-0,245
ΔP_m overshoot	14,37%	17%	32,7%	17%	11,8 %
$\Delta P_{m\infty}$ [p.u.]	0,0974	0,0935	0,0976	0,1	0,0975

Table 1.1-2 Dynamic results at the step load's power variation - One synchronous machine in first frequency regulation.

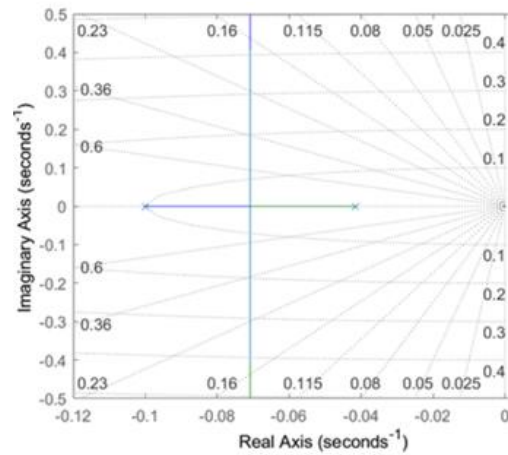
Through the study of the root locus is possible to understand how the poles of the closed-loop transfer function move compared to the open-loop ones when the gain varies. For this purpose, the MATLAB software data has been used. The poles and damping values are shown in Figure 1.1-4 for the reference machine and for each test that differs for only a parameter from the reference. Circles and crosses represent the position of zeros and poles of the open loop transfer function (1.1-5). The blu vertical lines represent the segment connecting the closed loop poles.



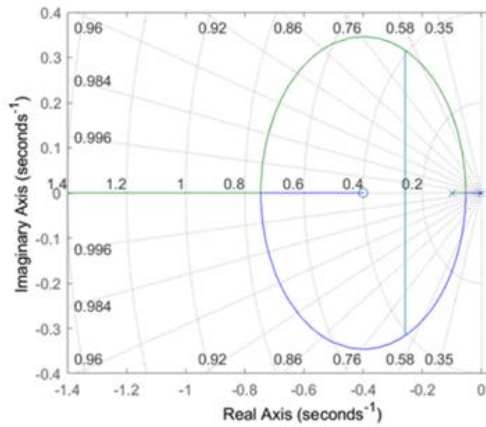
reference data



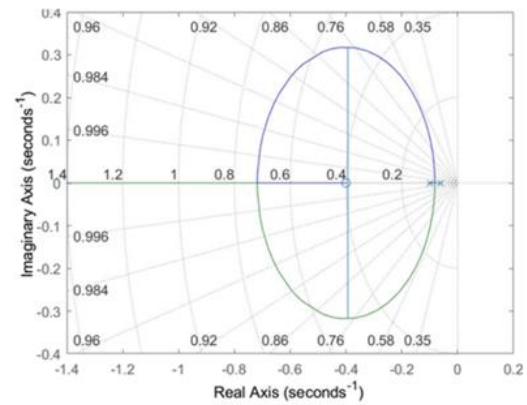
$b'_p = 0,1$



$T'_z = 0 [s]$



$E'_c = 0 [p.u. s]$



$T_a = 8 [s]$

Figure 1.1-4 Root locus of different synchronous machines:
reference data; $b'_p = 0,1$; $T'_z = 0 [s]$; $E'_c = 0 [p.u. s]$; $T_a = 8 [s]$

The values of poles and the damping for every test is reported in the Table 1.1-3.

	<i>Reference data</i>	$b_p'=0,1$	$E'_t = 0$ [p.u.· s] $T'_z = 0$ [s] $\alpha' = 0$	$E'_c = 0$ [p.u.· s]	$T_a = 8$ [s] $J = 0,16$ [p.u.· s ²]
Open loop poles	0,0417 0,1	0,0417 0,1	0,0417 0,1	0 0,1	0,065 0,1
Closed loop poles	-0,279 + 0,305i -0,279 - 0,305i	-0,175 + 0,2385i -0,175 - 0,2385i	-0,071 + 0,407i -0,071 - 0,402i	-0,258 + 0,316i -0,258 - 0,316i	-0,394+318i -0,394-318i
damping	0,6754	0,5916	0,1714	0,6328	0,778

Table 1.1-3 Open loop poles, closed loop poles and damping for various synchronous machine in first frequency regulation.

As it is possible to observe from the results, the desired values of frequency and mechanical power variation are not always achieved at the steady state. The steady state values of frequency and mechanical power's variation are equal to [4]:

$$\Delta f_\infty = -\Delta P_L / (E_P + E_C) \quad (1.1-6)$$

$$\Delta P_{m\infty} = \Delta P_L \cdot E_P / (E_P + E_C) \quad (1.1-7)$$

In the various cases analyzed, there are the following differences from the reference case:

- The case in the absence of rotating loads connected to the grid $E'_c = 0$ presents a pole in the origin in the open-loop transfer function (1.1-5). This implies that the alternators are producing all the required power alone, and not even the rotating machines of the load.
- Using a $b_p' = 2 \cdot b_p = 0,1$ permanent droop twice than the one of the reference case, entails that $E_P' = E_P/2$ the permanent energy is equal to half. It makes the system more under-damped by increasing the frequency variation's error and extending the settling time.
- Using a null transient energy $E'_T = 0$ causes that the zero of the open loop transfer function moves away from the poles and it tends to the negative infinite value $\omega_z \rightarrow -\infty$. The system becomes very under-damped and

oscillating. The overshoot of the ΔP_m mechanical power variation and the Δf frequency variation derivatives become very large.

- Using a lower J inertia value causes the root locus poles to move away from the origin and increasing the system's damping. There are curves with much larger derivatives and during the load take-off the frequency variation is more relevant. The power variation's overshoot is reduced because with a shorter start time it is faster to reach the nominal speed.

To use multiple interconnected machines even if not all participants in the primary frequency regulation gives the advantage of increasing the overall inertia of the system. To show this, a PLECS simulations is carried out using three regulators with their datas reported in the Table 1.1-4. The first two alternators participate at the frequency regulation but they differ for the values of inertia, nominal power's size and regulation's energies ($SM1\ 1^\circ f$ and $SM2\ 1^\circ f$). Last regulator is equal to the first one but doesn't participate at the frequency regulation $SM\ No\ Reg$. The frequency regulation schematic block with this configuration is reported in Figure 1.1-5.

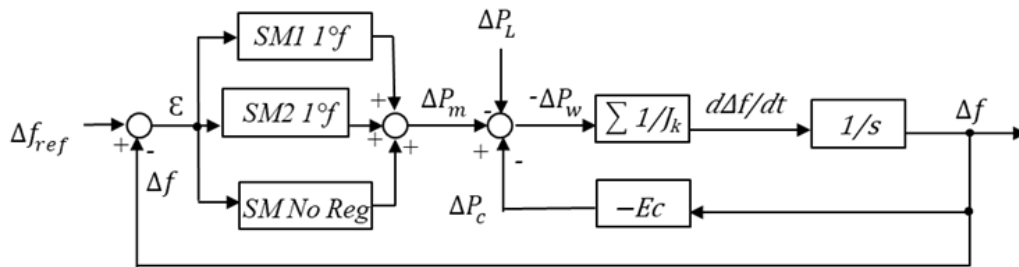


Figure 1.1-5 Frequency regulation with two different machines in first frequency regulation end one non participant.

	P_n [p.u.]	J [p.u.· s ²]	T_a [s]	E_P [p.u.· s]	E_T [p.u.· s]
$SM1\ 1^\circ f$	1	0,24	12	0,4	0,1
$SM2\ 1^\circ f$	0,5	0,16	8	0,1	0,025
$SM\ No\ Reg$	1	0,24	12	0	0

Table 1.1-4 Data of the two different machines in first frequency regulation end of the one non participant.

Results of the simulation are reported in the Figure 1.1-6 and in the Table 1.1-5, where:

- the curves in red refer to $SM1\ 1^\circ f$;
- the curves in blue refer to $SM2\ 1^\circ f$;
- the curves in yellow refer to $SM\ No\ Reg$;
- the curves in green refer to the full system.

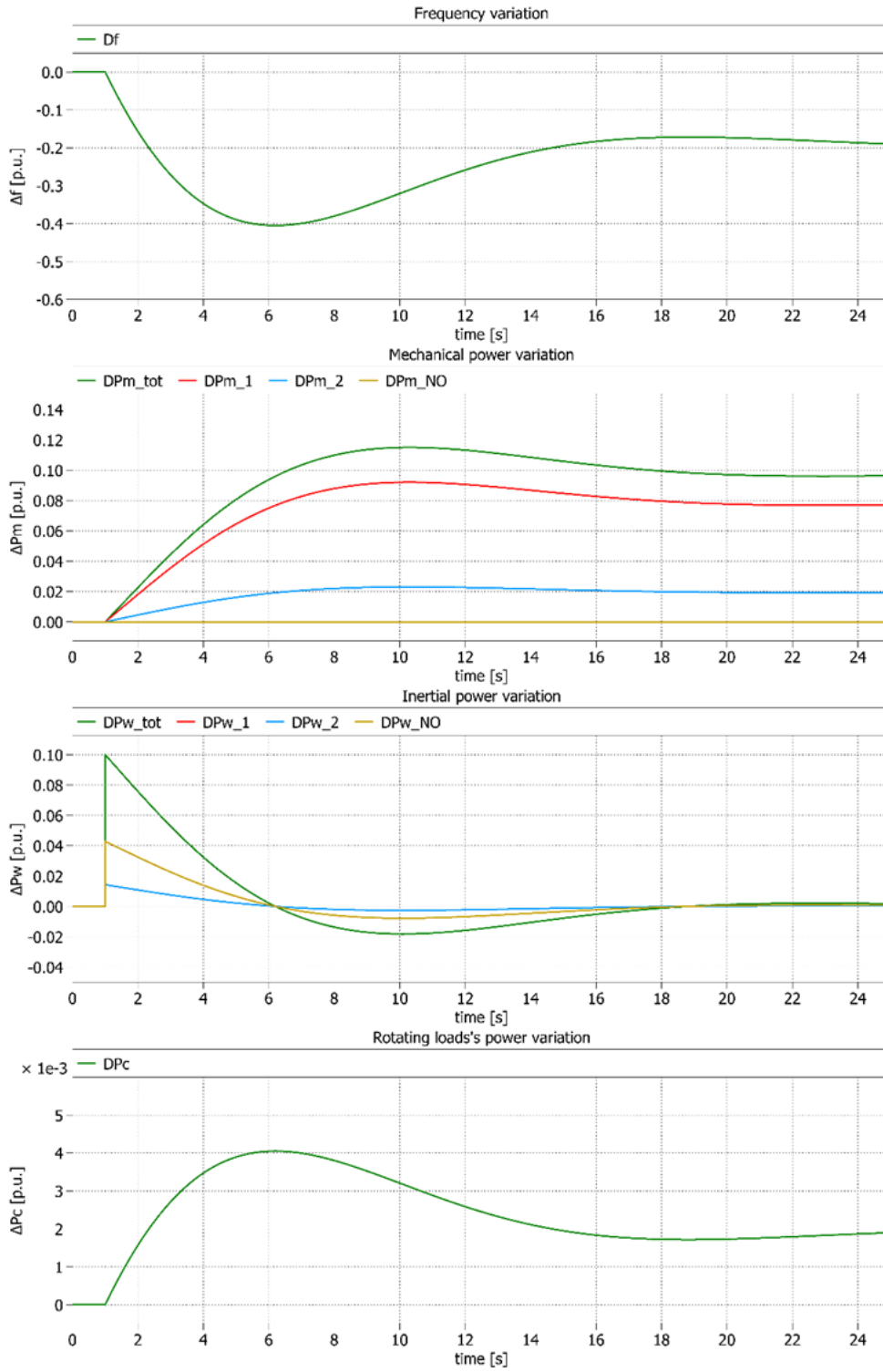


Figure 1.1-6 Trends of frequency variation and power variation at the step load's power variation- Two different synchronous machines in first frequency regulation and one non participant.

Δf Nadir [p. u.]	Δf slew-rate (5%)	Δf_∞ [p. u.]	ΔP_m overshoot	$\Delta P_{m\infty}$ [p. u.]
-0.4	-160%	-0,245	14,37%	0,098

Table 1.1-5 Dynamic results at the step load's power variation- Two different synchronous machines in first frequency regulation and one non participant.

Unlike the previously simulations, in the load takeover's transient also the inertial power of machines not participating in the regulation intervenes, helping those who participate. In fact, considering the whole system, there are all the opposite effects that have been seen in the previously simulation done with

$$T'_a = 8 \text{ s } (J' = 0,16 \text{ p. u. } \cdot \text{ s}^2)$$

Furthermore, it can be observed that the participating controllers do not respond proportionally to their nominal power. To achieve it, there are to make the following arrangements:

- The inertial power variation of the generic k^{th} machine is

$$\Delta P_{w_k} = -s \cdot \Delta f \cdot J_k \cong -s \cdot \Delta f \cdot T_{a_k} \cdot P_{n_k} / f_n \quad (1.1-8)$$

The condition

$$T_{a_k} = T_a = \text{cost}$$

is needed for all the interconnected machines to have inertial power variation proportional to the nominal one.

$$\Delta P_{w_k} \propto P_{n_k}$$

- In the steady state operation, the mechanical power variation of the generic k^{th} machine is

$$\Delta P_{m\infty k} = \Delta P_{e\infty k} = -\Delta f \cdot E_{P_k} = -\Delta f \cdot P_{n_k} / (b_{P_k} \cdot f_n) \quad (1.1-9)$$

The condition

$$b_{P_k} = b_P = \text{cost}$$

is needed for all the interconnected machines participating to the frequency regulation to have mechanical power variation proportional to the nominal one.

$$\Delta P_{m\infty k} \propto P_{n_k}$$

- During the transient operation, the mechanical power variation of the generic k^{th} machine is

$$\Delta P_{m_k} = \Delta P_{e_k} = -\Delta f \cdot E_{T_k} = -\Delta f \cdot P_{n_k} / (b_{T_k} \cdot f_n) \quad (1.1-10)$$

The condition

$$b_{T_k} = b_T = \text{const}$$

is needed for all the interconnected machines participating to the frequency regulation to have mechanical power variation proportional to the nominal one.

$$\Delta P_{m_k} \propto P_{n_k}$$

Overall, there is a non-zero error on the frequency's variation at the steady state.

Using a pole transfer function would originally give zero error at the steady state but achieving this is prevented by the fact that the distribution of the primary control on multiple units would be indeterminate.

The solution is to introduce a secondary controller with full action. The secondary controller's block diagram is set out in Figure 1.1-7 and subsequently commented on.

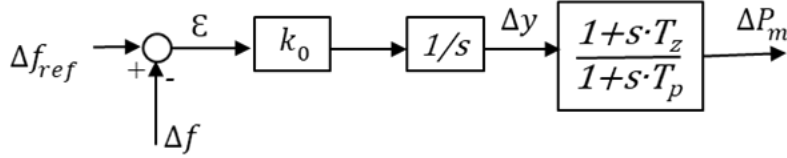


Figure 1.1-7 Secondary frequency regulation controller.

The secondary controller receives the frequency error in input and processes this signal. Compared to a control with only the primary one, for those that also participate in the secondary regulation an additional outer loop with integral action is added. It allows to generate the mechanical power necessary to increase the speed and restore the dynamic synchronism between all machines. The outer loop returns a new signal which is then sent to the first frequency controllers. Therefore, it can be deduced that the alternators participating in secondary regulation are also participating in primary regulation. However, while participating in the primary regulation is mandatory, the second one is optional.

The Laplace transfer function of these regulators is

$$G_s(s) = \frac{\Delta P_s}{\Delta f_{ref} - \Delta f} = \frac{k_0}{s} \cdot \frac{1+s \cdot T_z}{1+s \cdot T_p} \quad (1.1-11)$$

where T_z and T_p are the zero and pole time constant. k_0 is the gain of the regulator and its value is obtained as

$$k_0 = (E_p + E_c)/T_0 \quad (1.1-12)$$

where T_0 is the approximate time constant of the controller. This formulation is obtained imposing the value of the transfer function equal to unity at the steady state.

$$G_s(j\omega \rightarrow 0) = \frac{\Delta P_s}{\Delta f_{ref} - \Delta f} = (k_0 \cdot T_0) \cdot \frac{1}{E_p + E_c} = 1$$

A new PLECS model is realized. It takes into account that there are regulators participating in the primary frequency regulation only ($SM 1^{\circ}f$), another participants to both ($SM 2^{\circ}f$), another non-participant ($SM No Reg$). The frequency regulation schematic block with all kinds of participation at the frequency regulations performed by the machines is reported in Figure 1.1-8.

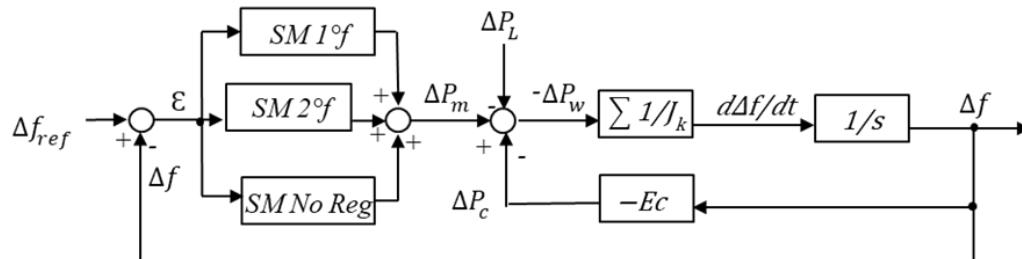


Figure 1.1-8 Frequency regulation with a machine in first frequency regulation, one in secondary frequency regulation and one non participant.

The carried-out simulation considers the presence of equal synchronous machines, one for each type of participation in the frequency regulation, with the following data in Table 1.1-6.

	P_n [p.u.]	J [p.u.· s ²]	T_a [s]	E_p [p.u.· s]	E_T [p.u.· s]
$SM 1^{\circ}f$	1	0,24	12	0,4	0,1
$SM 2^{\circ}f$	1	0,24	12	0,4	0,1
$SM No Reg$	1	0,24	12	0	0

Table 1.1-6 Data of the machines in first frequency regulation, in secondary frequency regulation and one non participant.

In addition, the secondary regulator of $SM 2^{\circ}f$ has been set with $T_0 = 40 s$, resulting in $k_0 = 0,0103$.

As example, in Figure 1.1-9 is shown the overall response given by synchronous machines interconnected to a 10% load power request variation.

- Red curves refer to $SM 1^{\circ}f$
- Blue curves refer to $SM No Reg$
- Yellow curves refer to $SM 2^{\circ}f$
- Green curves refer to the full sistem.

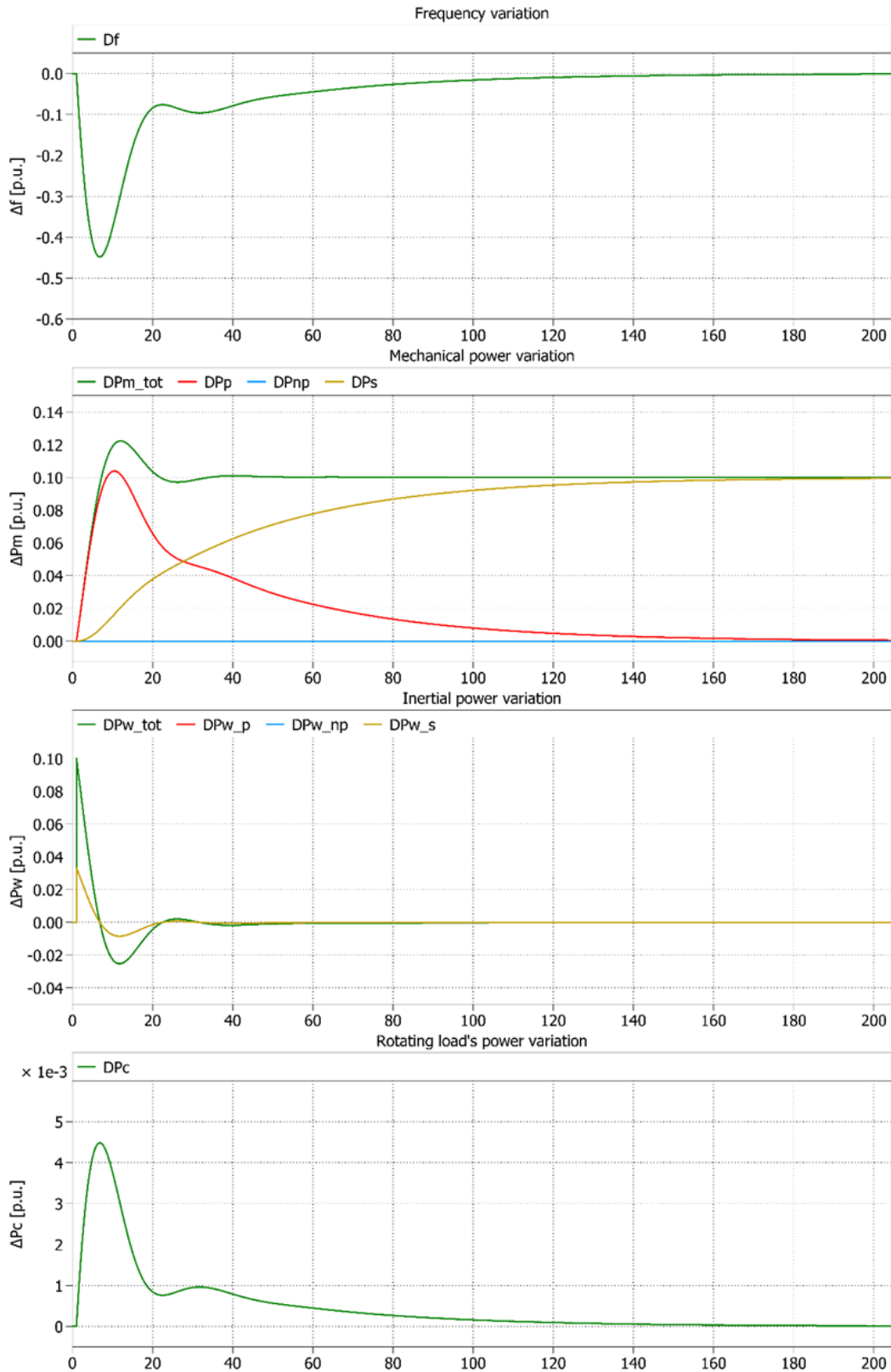


Figure 1.1-9 Trends of frequency and power variations at a step power variation - Machines in first frequency regulation, in secondary frequency regulation and non-participant.

Inertial power variation ΔP_w plots of every machine are overlapped curves because the inertia values are the same for all machines. Secondary regulation

mainly works at the steady state by replacing the primary regulation. The transitory trend remains almost unchanged. The frequency and mechanical power variation of the system at the steady state are

$$\begin{cases} \Delta f_{\infty} = 0 \\ \Delta P_{m\infty} = \Delta P_L + E_c \cdot \Delta f = \Delta P_L \end{cases} \quad (1.1-13)$$

and the mechanical power provided by the alternators is

$$\begin{cases} \Delta P_{p\infty} = -E_p \cdot \Delta f = 0 \\ \Delta P_{s\infty} = \Delta P_m - \Delta P_p = \Delta P_L \end{cases} \quad (1.1-14)$$

In the first moments, the load variation ΔP_L is fed by the inertial power of all interconnected machines. The frequency decreases and generates a speed error compared to the reference (synchronization frequency). The first response action is the primary regulation but this cannot compensate the whole load request because of the disturbance caused by the rotating loads. The integral action of the controller participating in the secondary regulation leads to the cancellation of the frequency variation's error by restoring the reference frequency and the synchronism between all the machines, by delivering the proper value of mechanical power. Through a slower dynamic it replaces the primary regulation.

As done in the primary regulators, it is possible to allocate the power supplied by the machines participating in the secondary regulation in proportion to their nominal power:

$$\begin{cases} \Delta P_{S_k} = \rho_k \cdot P_{S_k} \\ \sum \rho_k = 1 \end{cases} \quad (1.1-15)$$

Where k indicates a generic k^{th} regulator among all the regulators participating in the secondary regulation.

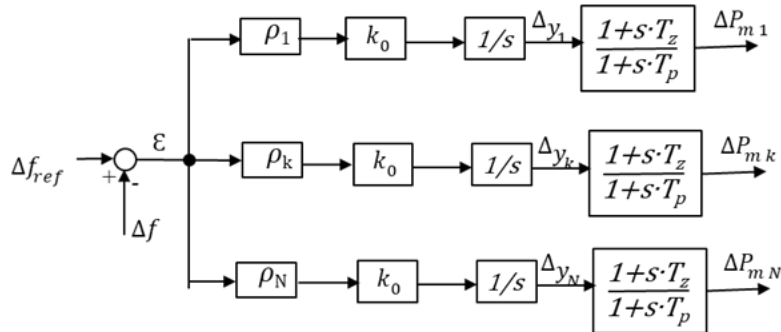


Figure 1.1-10 Controllers for power allocation in machines participating in the secondary adjustment.

This complete frequency regulation control ensures the stability of the electrical system.

1.2 Problem of the Power Electronic dominated renewable grid

Having enough inertia in the system, thanks to the generators connected to the grid, makes it possible to limit the speed at which the maximum frequency variation occurs as a result of a load power request. The frequency and the speed at which machines rotate must be kept within a limited range for reasons of quality of service and system's stability. For example, under- or over-excitation of synchronous machines may occur, or their operation may take place at operating points that are outside the limits of the capability curves.

The use of more and more static converters reduces the amount of inertia associated with the grid of consequences. For the reasons mentioned above, it is therefore necessary to study what the grid will be like in the future and what measures should be taken as a result of the changes.

1.2.1 Transition to low rotational inertia system

In our time we are living in a new energy and ecological revolution with a global impact. Nations have programs and projects to reduce 'carbon intensity' in different economic sectors, with particular emphasis on energy production and consumption, transport, and industrial activities. The aim is to reduce greenhouse effect, gas emissions and encourage renewable energy sources. According to this, an increase in the production of electrical energy produced by renewable sources is promoted by new energy plans.

This will lead to future grid changes in several levels [5]:

- Operation: the system will work with machine learning and no more with human workers, so it will be without the autonomous choice of the worker but made by computers.
- Production: from large and non-renewable production centers, they will switch to be smaller, renewable, non-rotating and intermittent. This will create a system with less rotational inertia.
- Market: there will be no more interconnections of the energy sources between areas / nations. The control will be regional.
- Distribution grid: previously the power direction was only from sources to loads. In the future, the opposite will also be possible and so the distribution will become bidirectional. There will be more small power lines with integrated storages.
- Transmission grid: it will have to carry less power but they will have more energy storage centers.
- Consumer: from being passive only, it will also be active. It will be able to produce energy and deliver it into the grid. Therefore, it must participate in the decisions on how to make the market.

In this new era there is a tendency to have a completely sustainable system dominated by power converters. Photovoltaic and wind power plants, storage

systems, residential and industrial utilities, all points on the grid, from loads to production, will need the presence of an electronic power converter. It is therefore necessary to take into account all the consequences that this transition has on the power system and how its dynamic response changes. The System Non-Synchronous Penetration index (*SNSP*) has been introduced to assess how far the power converter penetrated. It is defined in [6]

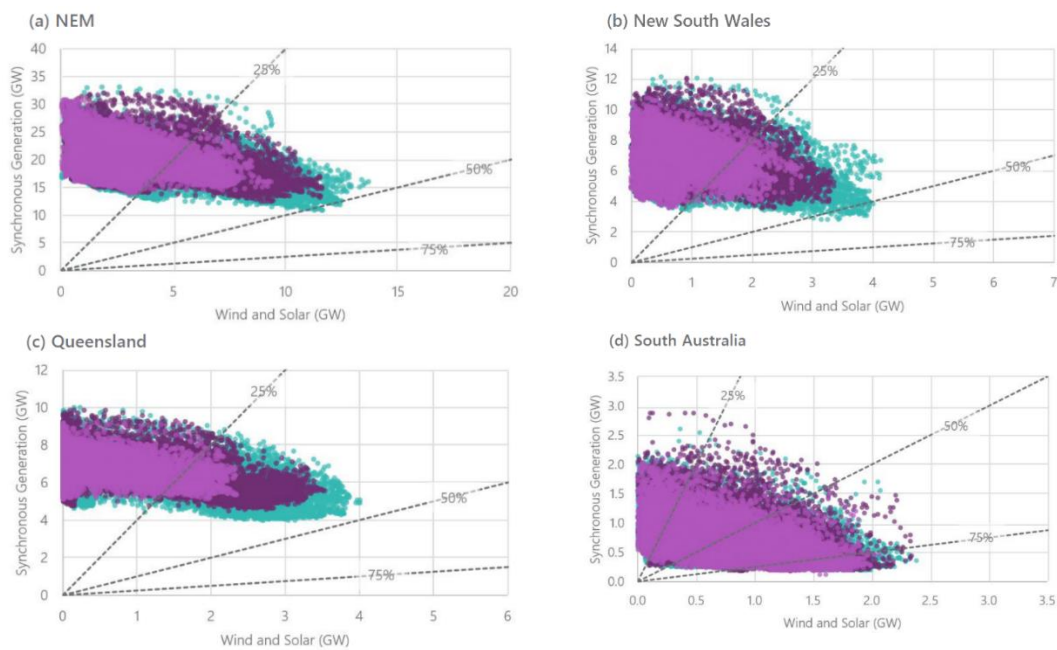
$$SNSP = \frac{P_{non-synchronous\ production} + P_{interconnection}}{P_{load} + P_{exported\ with\ interconnection}} \quad (1.2-1)$$

where P indicates the power in W.

This index is the ratio of the real time power contribution of the non-synchronous production and the net import of the loads plus the net exports.

In the past with few power converters installed, the index was very low and not many situations with little equivalent inertia were measured. Therefore, the safe operation of the system was assured. After 50% of renewable energy produced, the system starts to have high penetration of non'synchronous production and there is the risk of no-safety of the electrical system. Nowadays, if the level of the 75% is exceeded, the renewable sources are disconnected.

SNSP's graphs with the non-synchronous production as abscissae and the power demand in the ordinates are shown below. The Figure 1.2.1-1 shows actual wind and solar generation versus synchronous generation in several places for each half-hour period for the 2018, 2019 and 2020 calendar year.



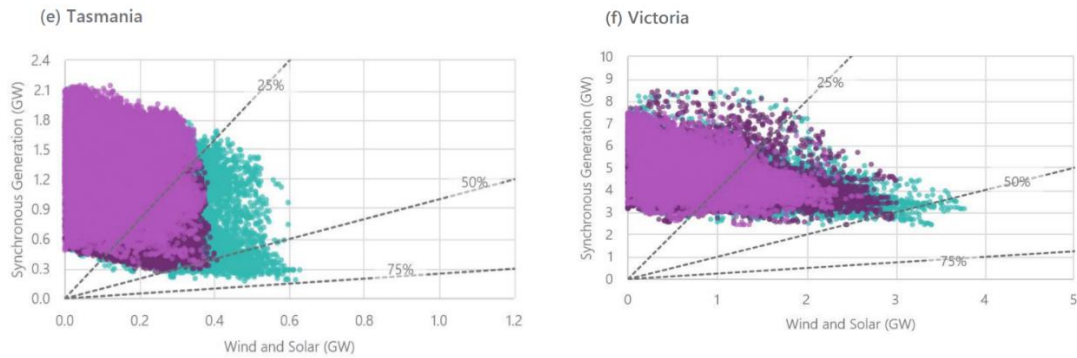


Figure 1.2.1-1 SNPS trend in the years 2018 light purple, 2019 dark purple and 2020 green in different places: (a) NEM; (b) New South Wales; (c) Queensland; (d) South Australia; (e) Tasmania; (f) Victoria [7]

With the growing application of power converters, the points tend to locate near straight with less inclination. In 2018 the measured points are very concentrated at low *SNSP* values. Year after year, the measured points tend to spread out by increasing the number of critical situations with low total production and high non-synchronous production. It is observed that not only the power generation from wind and photovoltaic sources is increasing, but also that the amount of energy fed into the grid from synchronous generators is decreasing. This is explained by the fact that the electrical energy produced by renewable sources is replacing the energy produced by fossil sources.

Differences to be taken into account for the transition from synchronous machine and power converter are [8]:

- the converter cannot withstand overloads while a synchronous machine is able to do it;
- the converter has no energy accumulation. By the contrary, a synchronous machine has inertia and mechanical energy storage;
- a synchronous machine uses a control system made by a frequency control and an AC voltage control. A converter needs at least also a DC voltage control and it can become more complex adding other additional controls.
- the converter must take into account the measures of both voltages, DC and AC, and of the currents that it supplies, the measures of active and reactive power, the reference values for power and voltage. If they are not at all available, it doesn't work.
- the converter performs inner loop (current) in microseconds and the outer loop (voltage) in seconds. It is very fast in regulation.

By focusing on the stability of the system, it must be guaranteed under all conditions. When using power electronic converters system instability can manifest itself as [9]

- undamped oscillations between the power electronic converter and the grid. They manifest themselves at the grid frequency or at the sub-synchronous resonance. It is a phenomenon in which one or more of the resonant frequencies of the turbine shaft, which is part of a thermal power unit, coincides with a natural resonant frequency of the electrical system.

- loss of synchronism is possible for power converter-based technologies. This could be due to an inertia not adequately defined. Virtual inertia is generated by storage systems associated with inverters, to keep the rate of frequency variation low in case of active power imbalances, especially under sub-frequency conditions.
- loss of fault ride through capability. Synchronous generators can 'slip' and become unstable if the stator voltage drops below a certain threshold. When a voltage drop occurs even a power converter can become unstable.

The cause may be due to the incorrect converter control interacting with the grid [10].

While with synchronous machine the stability is guaranteed ensuring the rotor angle stability, the frequency stability and the voltage stability, using power converter the power system's stability is obtained by the stability of resonance and the converter driven stability [11].

1.2.2 Three phase short circuit with a power converter

A situation where the attention should be paid is also on the short circuit event. During and after a short circuit event, the dynamics of the power converter's current and voltage are different from those of a synchronous generator [12].

A simulation has been carried out considering a three-phase short circuit that happens at time $t = 1.5\text{ s}$ of the duration of $\Delta t = 0,05\text{ s}$. After this time the situation returns to normal operating conditions. The simulation and the parameters used are the same as those used in Chapter 3.4.

The plots of the stator current of the synchronous machine and the voltage and current of the power converter are reported in Figure 1.2.2-1 and Figure 1.2.2-2.

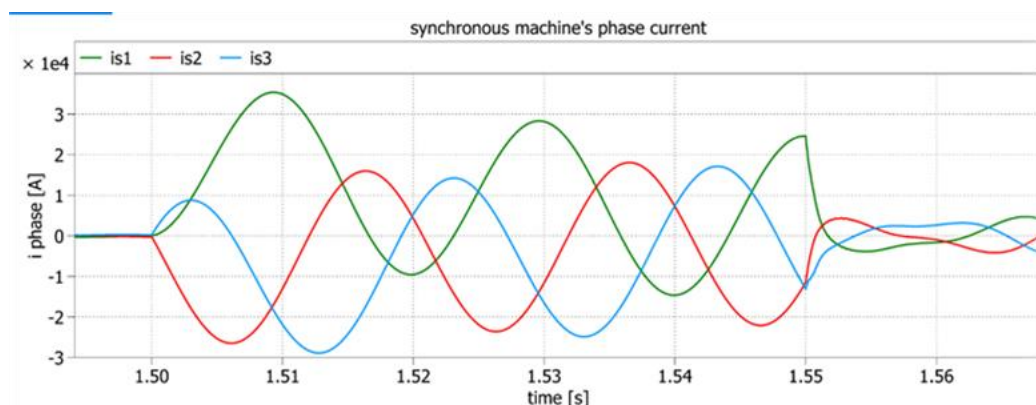


Figure 1.2.2-1 Stator current of the synchronous machine during a short circuit event.

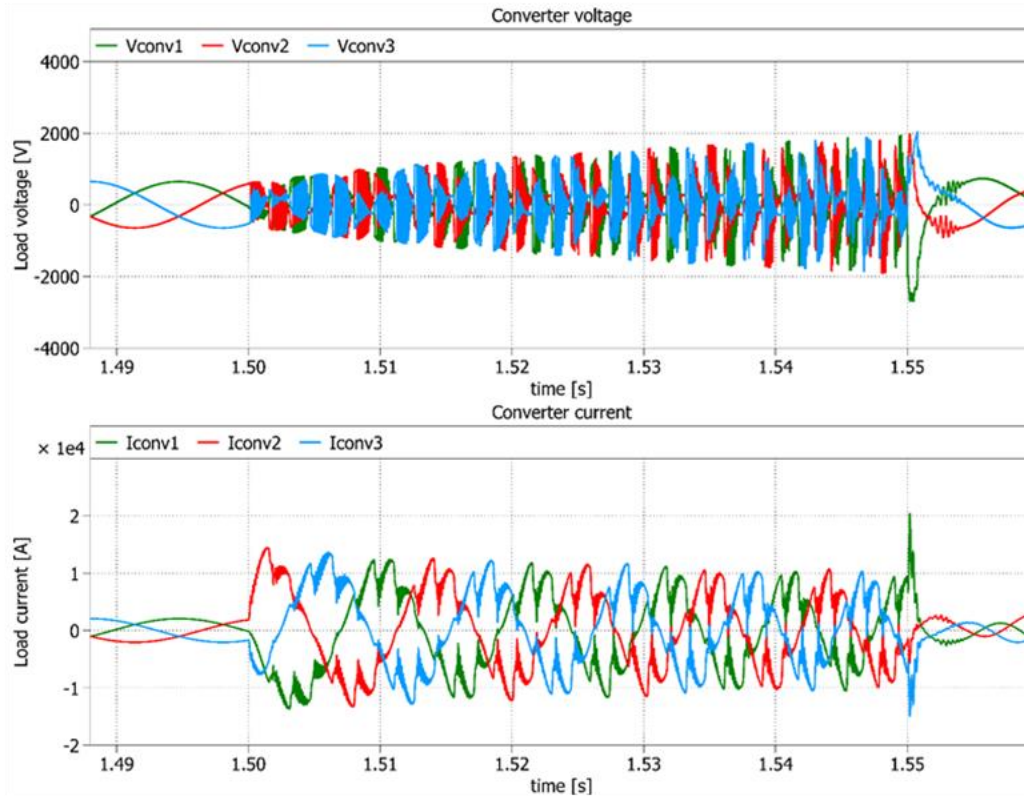


Figure 1.2.2-2 Voltage and current of the converter during a short circuit event.

Looking at the waveforms of the currents, the first thing that emerges is the different amplitude of the short-circuit currents. The synchronous generator can deliver a higher current because it allows overload, while this is forbidden in a converter. This must be taken under observation because when a short circuit occurs and the power becomes too low, the loss of synchronism and therefore unstable situation can happen. During faults, the typical behavior of the grid dominated by synchronous generators is modified to a greater or lesser extent depending on the amount of non-synchronous production. In situations of high *SNSP* there can be such a reduction in short-circuit current that the correct functioning of the typical protection devices can be compromised. For example, the opening of circuit breakers and the localization of the fault point may be more difficult.

More importantly, the voltage dynamics at the converter terminals is consequence of the very high frequency trend. This fact tests the converter's PLL and it must be able to follow these high-frequency variations in order to maintain stability.

During the failure, the voltage on the grid drops. In a dead three phase short circuit it is null for all the phases. When the fault ends, if the voltage drop is not too large or the duration of fault is not too long, then the PLL is able to re-synchronizes with the grid. Otherwise, the PLL fails to follow the grid and oscillations that enter in the system are generated. [13] [14]

A similar simulation has been carried out imposing a dead three phase short circuit of the duration of 0,1 s, twice bigger than the previous simulated situation.

The PLL dynamics of both the simulation, short circuit time duration $\Delta t = 0,05$ s and $\Delta t = 0,1$ s respectability, are shown in Figure 1.2.2-3.

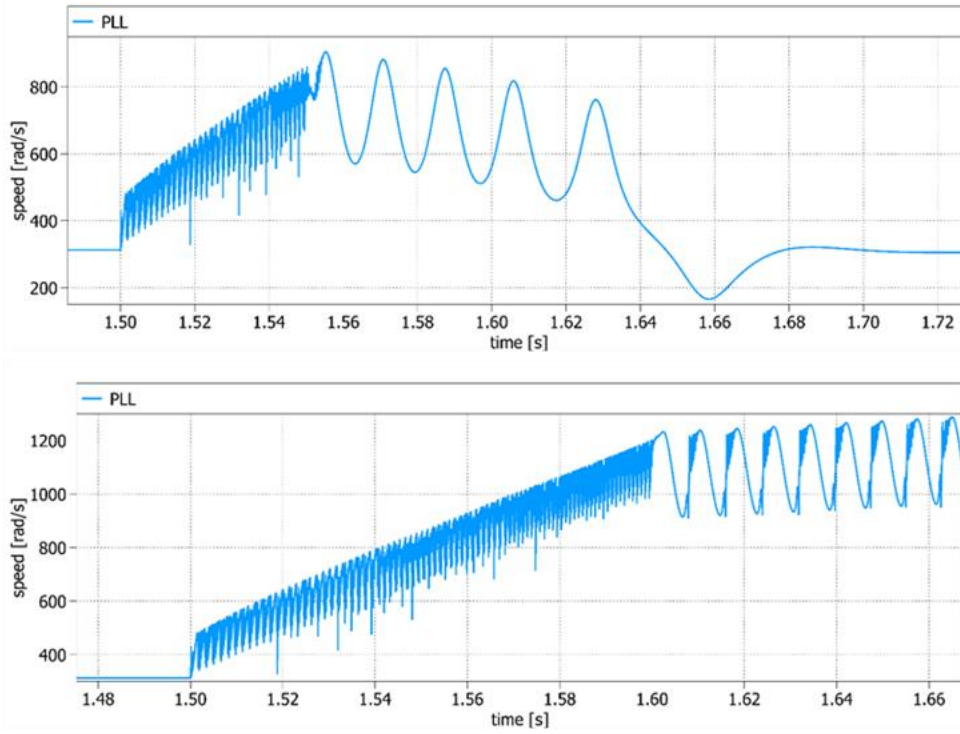


Figure 1.2.2-3 PLL dynamic during a short circuit time interval of 0,05 s and 0,1 s.

If the PLL allows it, the recovery dynamics are fast for the first seconds but for total recovery it takes more time.

The maximum time allowed to resolve the fault without interrupting the system operation is called critical clearing time t_{cr} . Considering an electrical machine, it can be calculated starting from the swing equation (1.1-1) without using small signal variations and considering the angle δ as the phase angle between the excitation's voltage V_{ecc} and the grid's voltage V_g [15].

$$P_m - P_e = \frac{T_a}{\omega_n} \cdot \frac{d^2\delta}{dt^2} \quad (1.2.2-1)$$

Considering only a reactance X between the two voltage sources, the electric power is

$$P_e = \frac{V_{ecc} \cdot V_g}{X} \cdot \sin\delta = P_{max} \cdot \sin\delta \quad (1.2.2-2)$$

Combining the two equations (1.2.2-1) and (1.2.2-2), it is given the differential equation

$$\frac{d^2\delta}{dt^2} = \frac{\omega_n}{T_a} \cdot P_m - \frac{\omega_n}{T_a} \cdot P_{max} \cdot \sin\delta \quad (1.2.2-3)$$

It is hypothesized that:

- δ_0 is the angle's value just before that the fault occurs;

- P_e is null during the fault;
- there is the critical clearing angle δ_{cr} after the fault.

The system remains stable if the fault is solved before this time or if the angle of the synchronous machine is smaller than the critical clearing angle δ_{cr} . Otherwise, if the fault is not fixed before the critical time and the angle exceeds the critical value, the machine accelerates and the rotor angle increases until diverging. The unstable equilibrium point is $\delta_{max} = \pi - \delta_0$. If the angle δ reaches a value larger than δ_{max} there is insufficient decelerating energy and so it leads to instability. The Figure 1.2.2-4 shows the plane δ -Power. The areas E_{acc} and E_{dec} indicates that the condition of recovering stability is possible only if the energy accumulated during the fault E_{acc} is smaller than the one that remain to decelerate the machine E_{dec} .

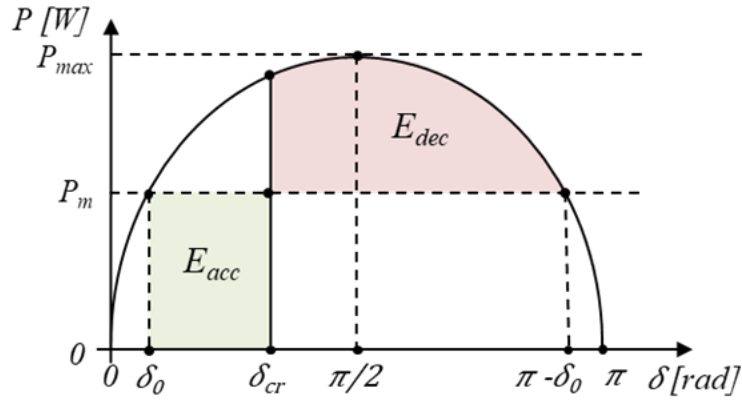


Figure 1.2.2-4 Plane load angle δ - power P . Acceleration and deceleration energies are the highlighted areas.

From these considerations, the equation that can be used to find the critical clearing angle's value is

$$E_{acc} = E_{dec} \rightarrow \int_{\delta_0}^{\delta_{cr}} P_m d\delta = \int_{\delta_{cr}}^{\pi - \delta_0} P_{max} \cdot \sin \delta d\delta \quad (1.2.2-4)$$

Solving it, the critical clearing angle δ_{cr} is equal to

$$\delta_{cr} = \cos^{-1}((\pi - 2 \cdot \delta_0) \cdot \sin \delta_0 - \cos \delta_0) \quad (1.2.2-5)$$

Knowing this value, the critical time t_{cr} can be calculated integrating the equation (1.2.4) two times in the time.

$$t_{cr} = \sqrt{2 \cdot \frac{\delta_{cr} - \delta_0}{P_m \cdot \omega_n} \cdot T_a} \quad (1.2.2-6)$$

Considering that the set up time T_a is proportional to the system inertia, this means that if inertia decreases, critical time also decreases and the risk of losing stability is greater.

In addition, reconsidering the equation (1.2.2-2) and using small signal variation it becomes

$$\Delta P_e = P_{max} \cdot \cos \delta_0 \cdot \Delta \delta \quad (1.2.2-7)$$

Let introduce an asynchronous power P_{as} term of the damping windings as consequence of the currents that flow in the rotor induced by the stator. It's proportional to the change in speed from ω_0 , when the fault occurs by the damping coefficient D [16].

$$P_{as} = D \cdot (\omega_0 - \omega) = -\frac{D}{\omega_n} \cdot \frac{d\delta}{dt} \quad (1.2.2-8)$$

The system's differential equation in small variation signals is

$$\Delta P_m = \Delta P_e - \Delta P_{as} + \frac{T_a}{\omega_n} \cdot \frac{d\Delta\omega}{dt} = P_{max} \cdot \cos \delta_0 \cdot \Delta \delta + \frac{D}{\omega_n} \cdot \frac{d\Delta\delta}{dt} + T_a \cdot \frac{d^2\Delta\delta}{dt^2} \quad (1.2.2-9)$$

In control matrix form the system is expressed as

$$\frac{d}{dt} \begin{bmatrix} \Delta\omega \\ \Delta\delta \end{bmatrix} = \begin{bmatrix} -\frac{D}{T_a} & -P_{max} \cdot \cos \delta_0 / T_a \\ \omega_n & 0 \end{bmatrix} \cdot \begin{bmatrix} \Delta\omega \\ \Delta\delta \end{bmatrix} + \begin{bmatrix} \Delta P_m \\ 0 \end{bmatrix} \quad (1.2.2-10)$$

Eigenvalues are derived from the state matrix. $\text{Det}(_)$ indicates the determinant operator applied to the matrix between the brackets.

$$\text{Det} \left(\begin{bmatrix} -\frac{D}{T_a} - p & -P_{max} \cdot \cos \delta_0 / T_a \\ \omega_n & -p \end{bmatrix} \right) = p^2 - \frac{D}{T_a} \cdot p + \omega_n \cdot \frac{P_{max} \cdot \cos \delta_0}{T_a} = 0$$

$$p_{\pm} = -\frac{D}{T_a} \pm j \sqrt{\frac{P_{max} \cdot \cos \delta_0 \cdot \omega_n}{T_a} - \left(\frac{D}{2 \cdot T_a}\right)^2} \quad (1.2.2-11)$$

Reducing inertia, the damping ζ and the natural frequency of the mechanical motion ω_{nat} increase.

$$\omega_{nat} = \sqrt{\frac{P_{max} \cdot \cos \delta_0 \cdot \omega}{T_a}} \quad (1.2.2-12)$$

$$\zeta = \frac{-\frac{D}{T_a}}{2 \cdot \sqrt{\frac{P_{max} \cdot \cos \delta_0 \cdot \omega}{T_a}}} \quad (1.2.2-13)$$

The result is that by decreasing inertia, the synchronous machines decelerate faster reaching a lower minimum frequency (nadir).

1.2.3 Short and long term solutions

To solve problems that come from the power converter's high penetration in the grid it's possible to take some measures.

There are short-term solutions and long-term solutions. Some of them are listed in Table 1.2.3-1 [17].

Short-term solutions:	Long-term solutions:
<ul style="list-style-type: none"> • Grid connection codes • Mitigation measures • Ancillary services • Synchronous condenser 	<ul style="list-style-type: none"> • Synthetic inertia • Grid forming control: advanced use of storages or HVDC

Table 1.2.3-1 Short-term solutions and long-term solutions for low inertia systems.

An example of short-term method is to check the equivalent inertia of the complex system. Starting with measurements taken over time intervals, the minimum equivalent inertia is calculated. Depending on its value and the power required for primary frequency control, the emergency condition is determined if the critical inertia limit is exceeded.

The graph in Figure 1.2.3-1 [18] shows for different values of system's inertia:

- the trends of the frequency's nadir in red;
- of frequency's ROCOF in blue;
- the minimum level of nearly-steady-state frequency in green.

ROCOF means Rate of Change of Frequency and it's calculated as the maximum frequency variation divided by the time interval taken by the tangent to the frequency deviation in the initial time to reach the nadir value (see Figure 1.2.3-3). The secure working area is delimited where all these limits are not exceeded and it is highlighted in gray in Figure 1.2.3-1.

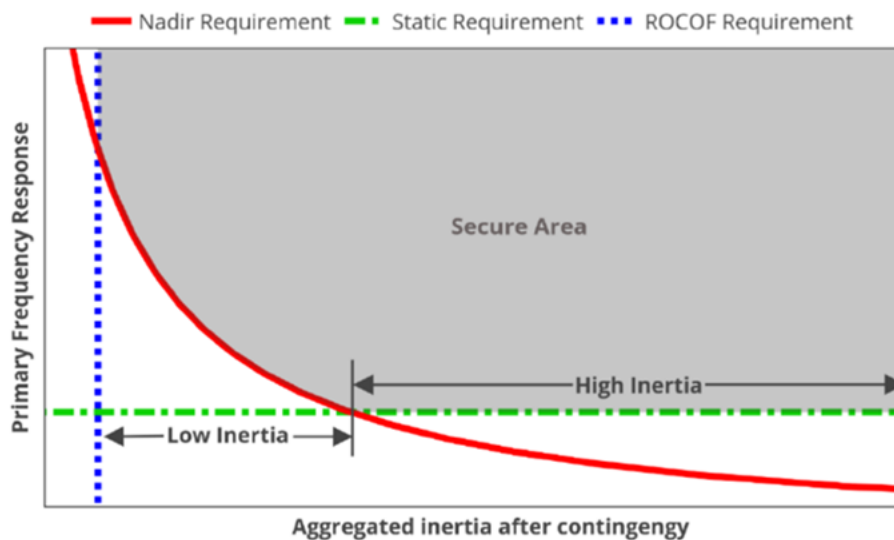


Figure 1.2.3-1 Safe area and limits for minimum equivalent inertia [18].

The conditions of minimum total inertia are determined by an acceptable limit of nadir frequency, ROCOF, and power demand. When leaving the safe area, protections are activated to return to acceptable inertia conditions.

An example of a long-term solution is the Fast Active Power Control (FAP) controller and its control schematic block is in Figure 1.2.3-2. It uses a derivative proportional controller that receives as input the grid's frequency value and returns the reference power value as output. After this, follows a power and current control. In Figure 1.2.3-3 shows a typical power and frequency response at a load step request using the FAP controller [19].

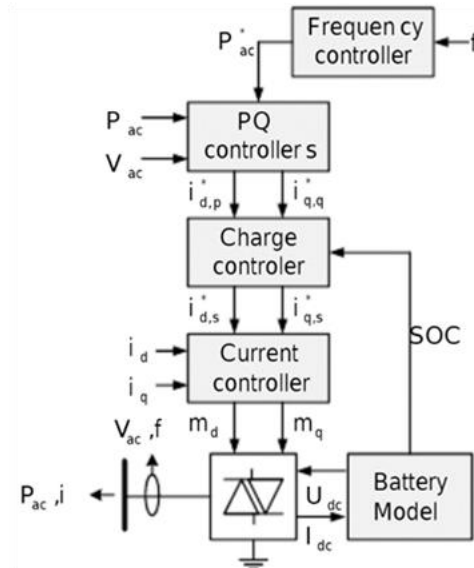


Figure 1.2.3-2 Fast Active Power Control (FAP) controller: control schematic block [19].

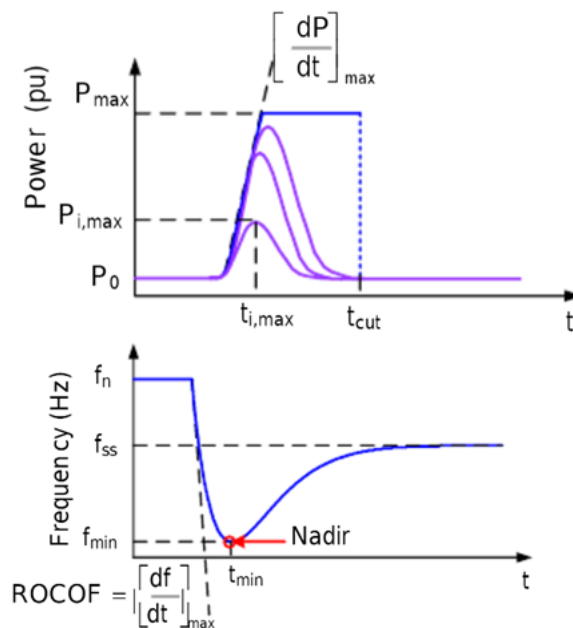


Figure 1.2.3-3 Fast Active Power Control (FAP) controller: power and frequency typical dynamics on the right [19].

The proportional coefficient k_p can have a dead band to keep the power constant in that frequency range and saturators for the maximum bidirectional power.

The derivative coefficient k_d determinates the ROCOF [20]:

$$\Delta P = k_d \cdot \frac{df(t)}{dt} \quad (1.2.3-1)$$

Its value is chosen so that applying a frequency pulse $f_{min} - f_n$ a power variation of $\Delta P = P_{max} - P_0$ is generated.

With these considerations in mind, a closer look at the possible control strategies for power converters in the grid is given in the next sub-chapters.

1.3 Grid following and grid forming

In a future low-inertia power system, the functionalities of the frequency regulation must be provided by an appropriate control of the converters operation.

In this sub-chapter two possible control strategies for converters connected to the grid are compared and evaluated. Then, the work continues looking for how to realize one for the project converter.

Grid-following converters (GFL) are controlled current source. They can be modelled as current source with a high parallel impedance Z_c . They achieve their purposes of power injection and voltage regulation by controlling the injected currents. The instantaneous reaction of the GFL converter is to maintain the grid current vector $i_{g \ 123}$ constant in terms of magnitude and phase, causing therefore an inevitable variation of the converter output voltage vector $v_{c \ 123}$. This is due to the necessity of the new phase angle's detection of the grid voltage vector $v_{g \ 123}$ to calculate the new current setpoint.

The Figure 1.3-1 shows a Grid following converter topology on the left and its phasors diagram on the right.

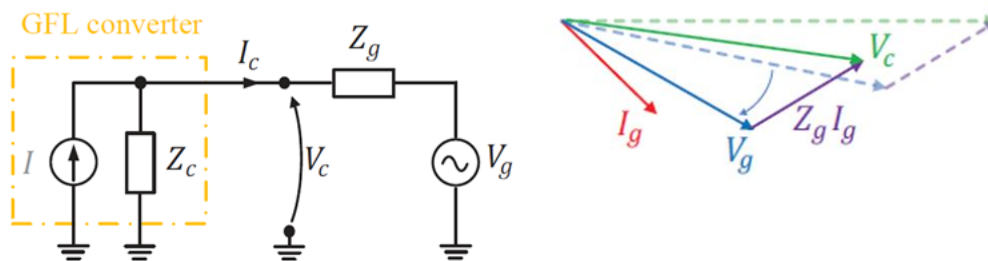


Figure 1.3-1 Grid following converter topology on the left and its phasors diagram on the right [21].

Grid following converter requires a dedicated unit such as a Phase Locked Loop (PLL) to identify the grid voltage angle of $v_{g \ 123}$ and calculate a proper phase shift θ of the converter currents to inject the defined amount of active and reactive power. This converter control follows the grid angle and its frequency and doesn't

actively control its output frequency. The aim is to generate a quantity of power according to the frequency variation present on the grid. This can be achieved in the simplest way using a droop control, which is a type of control that makes the two quantities directly proportional: when the frequency's value is known, the value of power to be delivered by the generator is obtained. When the main frequency is equal to the reference value, which is set as the nominal value, the power value that will be provided will be exactly equal to the nominal one. If, on the other hand, there is a non-null difference between the main frequency and the nominal frequency, the power generated will be higher or lower than the nominal value in proportion to it. In this way, the main frequency is "followed", producing a power reference that depends on it [22] [23] [24] [25].

Figure 1.3-2 shows a grid following converter control block diagram. A simplified representation of its power reference generation principle is shown in the Figure 1.3-3.

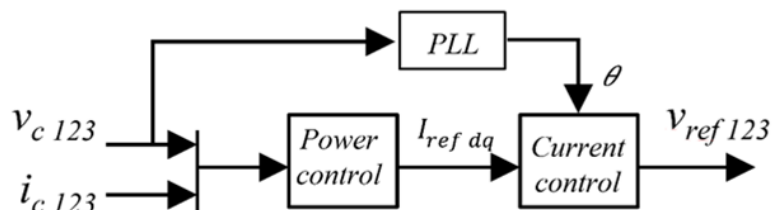


Figure 1.3-2 Grid following converter control block diagram.

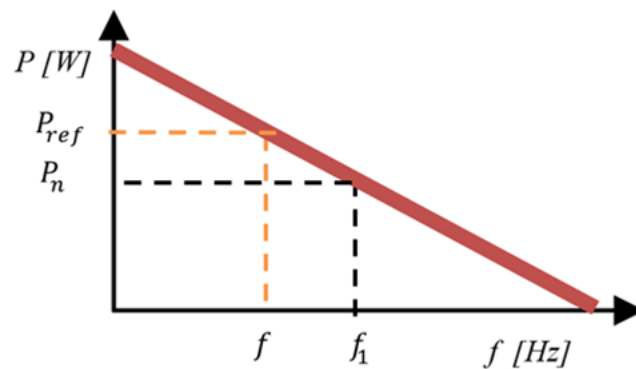


Figure 1.3-3 Grid following converter control principle: droop control.

The Grid forming (GFM) converter regulates the power by directly controlling the voltage v_{inv123} measuring the voltage and the current at its output terminal, v_{c123} and i_{c123} . Unlike the GFL control, the aim is to generate an AC voltage with frequency that is function of the power variation on the grid. The GFM control can be realised in a simple way using again a droop control and therefore by connecting frequency and power's values. It's necessary to know the value of the power required by the grid and then the control can calculate the frequency at which the voltages, coming out of the source feeding the grid, must be generated. In this way, the grid frequency is "formed", imposed by the source and the grid must follow the frequency imposed by the converter. When the mains power is equal to the nominal value, which is set as the reference value, voltage will be generated at

exactly the nominal frequency. If, on the other hand, the main power varies and therefore differs from the nominal value, the frequency at which the voltages are generated will be bigger or smaller than the nominal value depending on this difference. For example, in the case droop control they will be proportional as in Figure 1.3-5.

Another aspect of the GFM implementation is that it is able to self-synchronize to the grid without the need of a dedicated unit, even by emulating the power synchronization principle of a synchronous machine [26] [27] [28].

In Figure 1.3-4 is shown a Grid forming converter control block diagram. A simplified representation of its reference frequency generation principle is shown in the Figure 1.3-5.

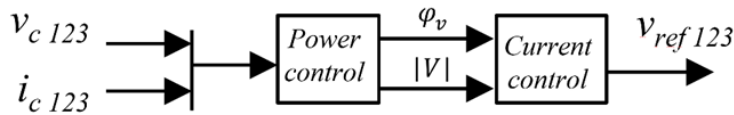


Figure 1.3-4 Grid forming converter control block diagram.

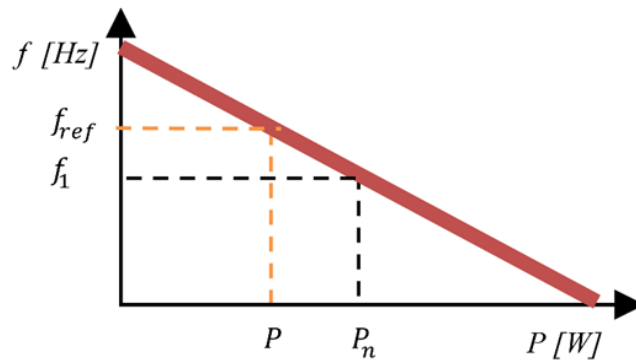


Figure 1.3-5 Grid forming converter control principle: droop control.

Grid forming converter are represented as a voltage source with low series impedance. The internal voltage phasor v_c of the converter is initially not affected by the perturbation, causing an almost instantaneous variation of the phasor i_g . This might cause a rapid growth of the converter current. The Figure 1.3-6 shows a grid forming converter topology on the left and its phasors diagram on the right.

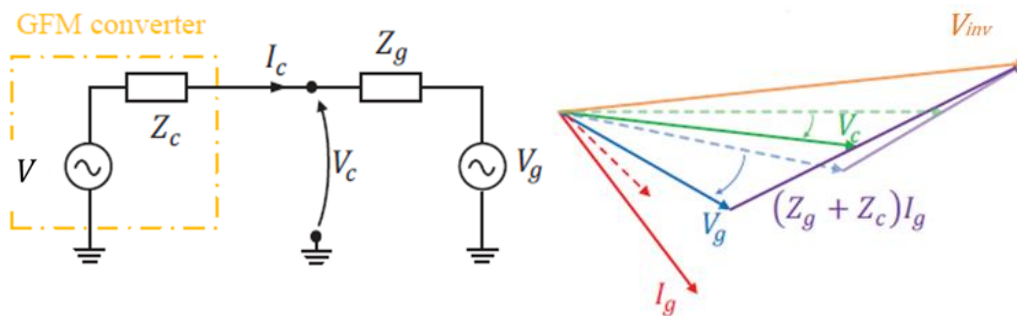


Figure 1.3-6 Grid forming converter topology on the left and its phasors diagram on the right [21]

When it is connected to the grid, GFM control actively controls the grid's frequency and the output voltage. The rotational speeds of synchronous generators are directly linked to the electrical output frequency, causing these generators to act as grid-forming sources.

To fully understand how these two types of control work, simulations carried out with PLECS software are made where these control strategies have been implemented in a simple and simplified manner. The focus is on the converter frequency control, which is the main mechanism that makes a converter operating as grid-forming or grid-following.

The range of frequencies of interest for grid power system study are much lower than when is analyzed the inverter with its PWM operation and the switching non-linearity. Focusing the study on the frequency level of the grid, it's assumed that the inverter is an ideal voltage or current source that works in combination with some output filter. It operates by feeding a three-phase grid with an RLE load (subscription *load*) and it uses an RLC filter (subscription *f*) at the output.

Figure 1.3-7 shows the topology of the power electric circuit.

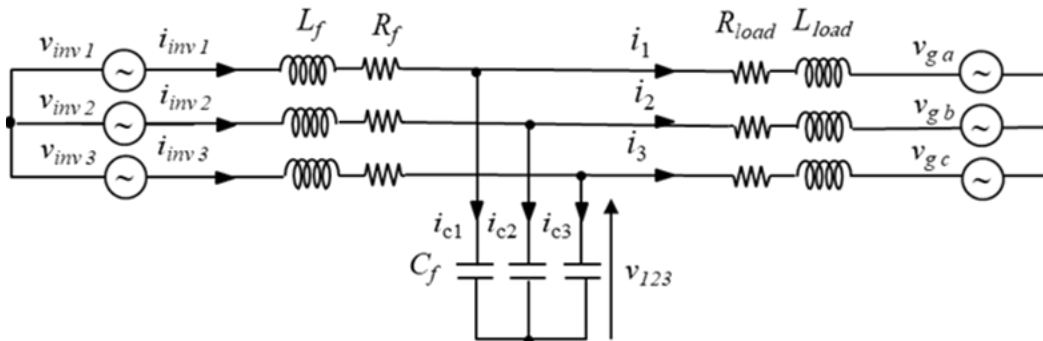


Figure 1.3-7 Topology of the power electric circuit: converter connected to the RLE grid trough RLC filter.

The electrical variables are measured at the connection point between the converter and grid and then plotted. The grid works with sinusoidal phase voltage $V_{g\ rms}$ at the nominal frequency of $f_1 = 50\ Hz$. In it is present a symmetrical load for the three phases with L_{load} inductance and R_{load} resistance.

The control receives as input the values of the electrical variables measured at each stage and generates as output the reference voltage for the converter, which in this case is modelled with three voltage-sources.

The filter of the converter has been set to obtain a resonant frequency of $f_{res} = 3000\ Hz$ so that it is far enough from the grid nominal frequency of $50\ Hz$ and can cut high frequencies.

$$2 \cdot \pi \cdot f_{res} = \frac{1}{\sqrt{L_f \cdot C_f}} \quad (1.3-1)$$

If the filter's circuit has also a series resistance, his value is chosen obtaining a quality factor [29] equal to $qf = 1$.

$$qf = \frac{1/R_f}{\sqrt{\frac{L_f}{C_f}}} \quad (1.3-2)$$

The values chosen for the simulations are in Table 1.3-1.

$V_{g\ rms}$ [V]	R_{load} [Ω]	L_{load} [mH]	R_f [m Ω]	L_f [mH]	C_f [μ F]
230	10	1	1,88	28	1

Table 1.3-1 Values of the grid and filter's parameters used in the simulation.

1.3.1 Grid following

An example of a simple control of the grid following type is first implemented. This is shown in the Figure 1.3.1-1 and then explained.

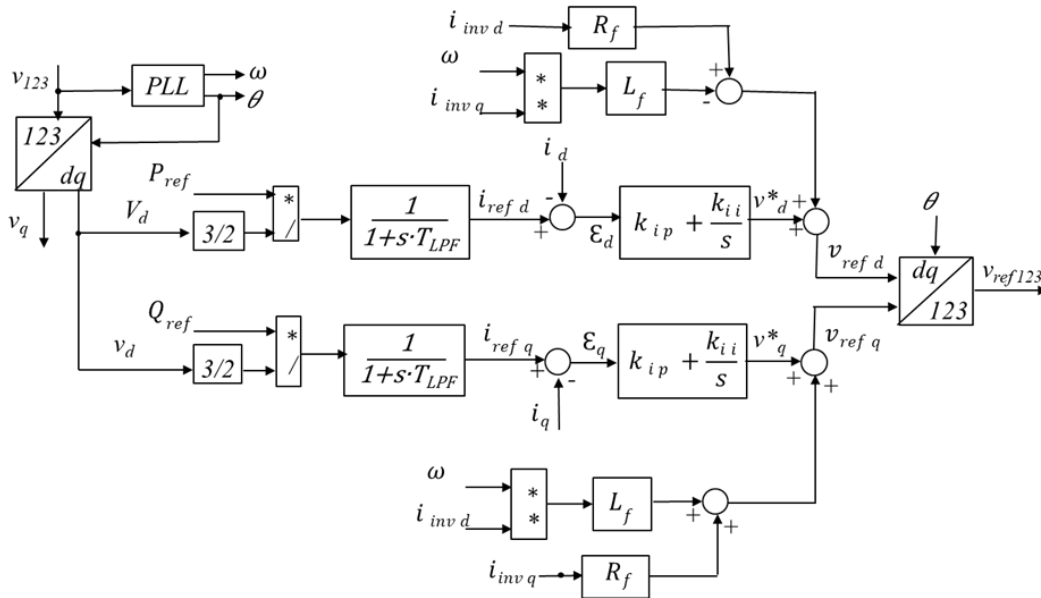


Figure 1.3.1-1 Grid following converter control schematic block.

To obtain the desired pulsation and the angle with respect to the fixed-axis reference system, a PLL is used which receives as input the three-phase voltages measured on the point of connection between the converter's filter and the grid. Using the Plank's transformation (2.4-3) and the rotational transformation (2.4-4) from the fixed 3-phases axis abc to the rotating 2-phases axis dq , the value of power is calculated as follow:

$$\begin{aligned} P + j \cdot Q &= \frac{3}{2} \cdot (\mathbf{v}_{dq} \cdot \mathbf{i}_{dq}^T) = \frac{3}{2} \cdot (v_d + j \cdot v_q) \cdot (i_d - j \cdot i_q) = \\ &= \frac{3}{2} \cdot (v_d \cdot i_d + v_q \cdot i_q) + \frac{3}{2} \cdot j \cdot (v_q \cdot i_d - v_d \cdot i_q) \end{aligned} \quad (1.3.1-1)$$

Thanks to the PLL, the grid voltage is assumed to always be aligned with the d-axis. In this way, the q-voltage is always $v_q = 0$ in the steady state and the power equations could be simplified [30]:

$$P + j \cdot Q = \frac{3}{2} \cdot (\mathbf{v}_{dq} \cdot \mathbf{i}_{dq}^T) = \frac{3}{2} \cdot (v_d \cdot i_d) - \frac{3}{2} \cdot j \cdot (v_d \cdot i_q) \quad (1.3.1-2)$$

Reversing the equation is possible to obtain the reference currents for the active and reactive power respectively, simply dividing the power for the peak grid voltage:

$$\begin{cases} i_{ref\ d} = \frac{P_{ref}}{1,5 \cdot v_d} \\ i_{ref\ q} = \frac{Q_{ref}}{1,5 \cdot v_d} \end{cases} \quad (1.3.1-3)$$

In the schematic block, a simple low pass filter LPF is added to eliminate the high frequency noisy and to decouple the power response from the current response. It helps the system calculating the error of current. In this model a value of $T_{LPF} = 0,1\ s$ is used [31]. The equation expressing the voltage of the connection point between converter and grid in the steady state is:

$$\mathbf{v}_{dq} = R_{load} \cdot \mathbf{i}_{dq} + j \cdot \omega_g \cdot L_{load} \cdot \mathbf{i}_{dq} + \mathbf{v}_{g\ dq} \quad (1.3.1-4)$$

Using a PI controller that receives as input the current value of \mathbf{i}_{dq} , the reference voltage value \mathbf{v}_{dq}^* in the point of connection between the filter and the grid is obtained. Considering that the voltage on the filter capacitor is equal to the one in input of the grid, by measuring the output current of the converter $\mathbf{i}_{inv\ dq}$, is possible to determine the voltage value to be supplied by the converter.

$$\mathbf{v}_{inv\ dq} = R_f \cdot \mathbf{i}_{inv\ dq} + j \cdot \omega_g \cdot L_f \cdot \mathbf{i}_{inv\ dq} + \mathbf{v}_{dq} \quad (1.3.1-5)$$

Using the pulsation ω in output of the PLL, the reference voltage $\mathbf{v}_{ref\ dq}$ can be calculated as [32]

$$\mathbf{v}_{ref\ dq} = R_f \cdot \mathbf{i}_{inv\ dq} + j \cdot \omega \cdot L_f \cdot \mathbf{i}_{inv\ dq} + \mathbf{v}_{dq}^* \quad (1.3.1-6)$$

In the current loop, the PI regulator is used to determinate the reference grid voltage for the d and q axis, using gains

$$\begin{cases} k_{ip} = L_f \cdot \omega_{band} \\ k_{ii} < k_{ip} \cdot \omega_{band} \end{cases} \quad (1.3.1-7)$$

Values $k_{ip} = 6$ and $k_{ii} = 500$ has been used.

As example, a simulation has been carried out:

- the start active and reactive power values are

$$P_{ref}(t = 0\ s) = 2\ kW$$

$$Q_{ref}(t = 0 \text{ s}) = 666 \text{ VAr}$$

- at time $t = 1 \text{ s}$ an active power step of 50% is applied

$$\Delta P_{ref} = 50\%$$

- at time $t = 2 \text{ s}$ a reactive power step is applied to reach the value of

$$Q_{ref} = 1 \text{ kVAr}$$

This reference reactive power is calculated according to obtain power factor $\cos\phi = 0,95$ and so $Q_{ref} \approx P_{ref}/3$.

- at time $t = 3 \text{ s}$, a step grid voltage's (v_g) frequency drop is set.

$$\Delta f_g = -10\%$$

The plots of the power reference P_{ref} in green and calculated in the measurement point P in red are shown in Figure 1.3.1-2.

The plots of the current reference i_{ref} in red and measured i_{dq} in green are shown in Figure 1.3.1-3.

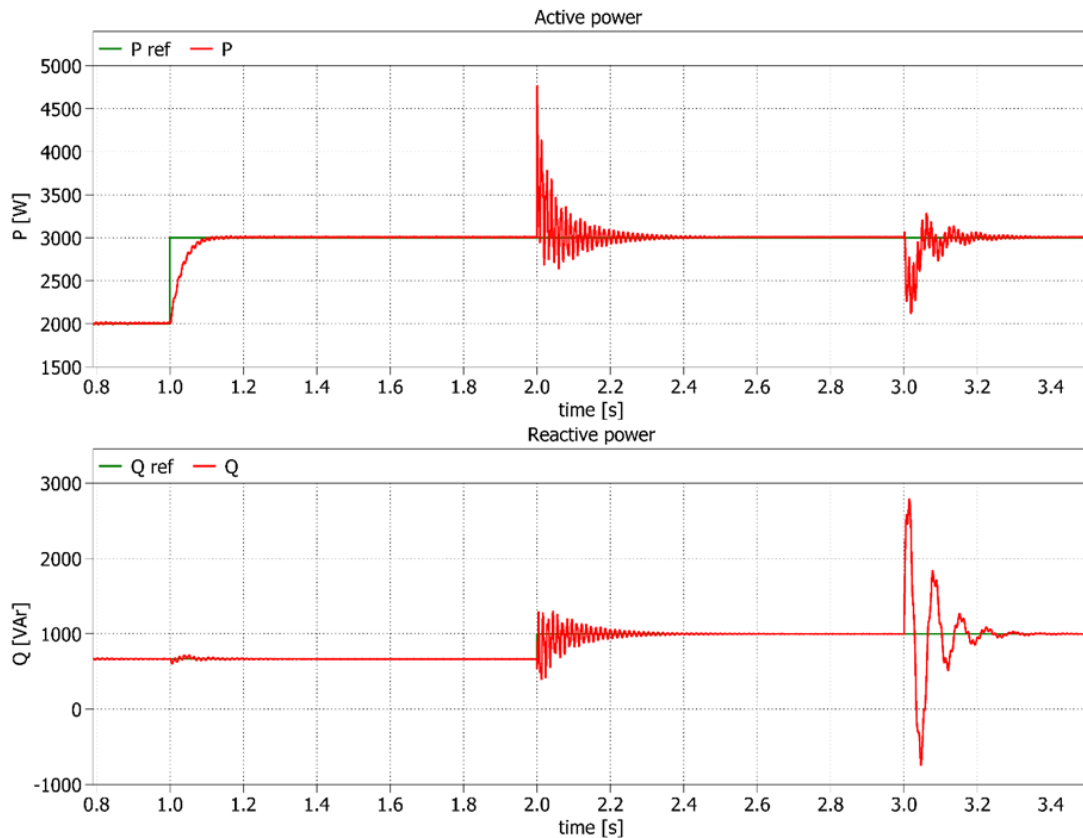


Figure 1.3.1-2 Grid following converter control: active and reactive power dynamics at a step reference variation.

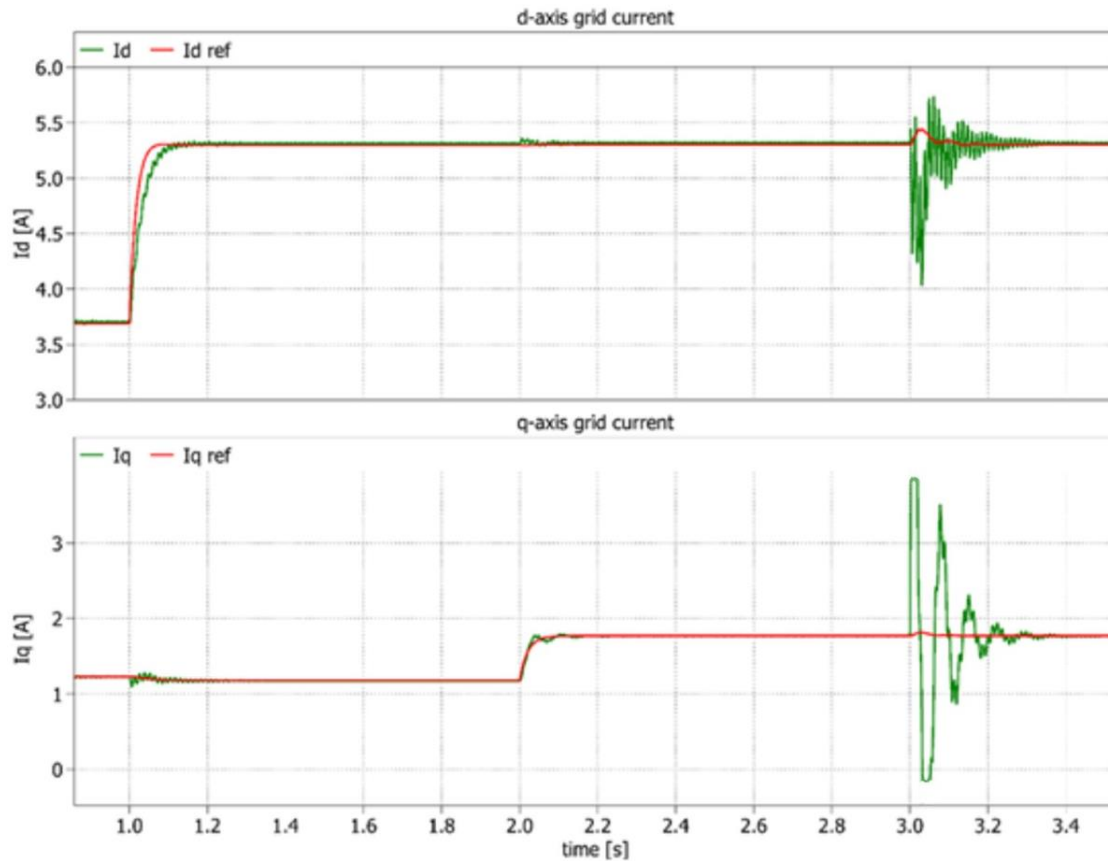


Figure 1.3.1-3 Grid following converter control: dq-axis current dynamic at a step reference variation.

The request of power is satisfied using a current loop control. It can be observed that the d-axis current mainly determines the active power. The reactive power, on the other hand, is determined by the q-axis current. When the current reference on one axis changes, during the transient there is also a change in the current of the other axis because of the cross-coupling. In addition, the frequency variation imposed on the grid voltage only temporarily modifies the power fed into the grid, but with wide oscillations. The control's PLL is able to synchronize itself again with the new main frequency and when the estimated frequency reaches the new reference value the converter operates correctly again and re-establishes the same power and current as before the frequency step. This means that the converter has adapted to the new main frequency.

1.3.2 Grid forming - Droop control

The next step is to understand the operating principle of a grid forming control. The schematic block in Figure 1.3.2-1 represents a simple example of this control methodology. It has been realized and used for the simulation.

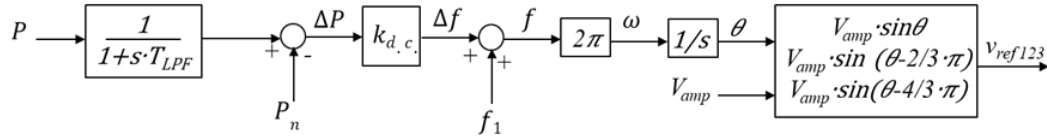


Figure 1.3.2-1 Grid forming converter droop control schematic block.

The baseline solution of the GFM control is a frequency regulation of the active power value. A proportional droop control gain $k_{d.c.} = 0,001$ is introduced after the calculation of the power deviation obtained from the difference between the nominal and the actual value. The current power is calculated through the measurements made in the grid [33]. Its value determines how much frequency variation the converter must add compared to the nominal frequency for the voltage reference generation. [34] [35]

The power measurements are low pass filtered with cut-off pulsation ω_{LPF} before being passed on to droop control. This is done because the high oscillations would make the result of the subtraction with a constant value as oscillating as measures. Adding the nominal frequency f_1 and multiplying for $2 \cdot \pi$, the pulsation ω is obtained. Then, integrating it, the reference angle θ is obtained. The final function works calculating the modulation index requested for the three phases as sinusoidal phases.

$$m_i = \frac{V_{amp}}{\frac{V_{DC}}{2}} \cdot \sin \left[\theta - (k - 1) \cdot \left(\pi \cdot \frac{2}{3} \right) \right] \quad (1.3.2-1)$$

for $k = [1 \ 2 \ 3]$ relative to the three phases.

Because the high frequency dynamic introduced by PWM modulation is neglected, the reference voltages for every phase $v_{ref\ 123}$ is simple obtained multiplying the modulation index for the quantity

$$\frac{V_{DC}}{2} \cdot V_{amp} = \sqrt{2} \cdot 230 \text{ V}$$

It is the amplitude value of the converter reference voltage [36]. So, the reference voltage is

$$v_{ref\ k} = V_{amp} \cdot \sin \left[\theta - (k - 1) \cdot \left(\pi \cdot \frac{2}{3} \right) \right] \quad (1.3.2-2)$$

for $k = [1 \ 2 \ 3]$ relative to the three phases.

A simulation is performed by using a three-phase resistive-inductive load. The topology of the power electric circuit used in this simulation is in Figure 1.3.2-2.

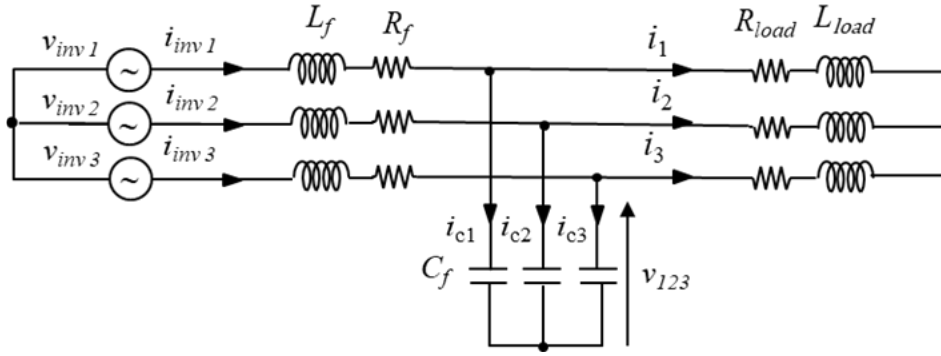


Figure 1.3.2-2 Topology of the power electric circuit used in simulation: converter connected to the RL grid trough RLC filter.

In the simulation:

- an initial reference value for power and frequency has been set

$$P_n(t = 0) = 15,6 \text{ kW}$$

$$f_1(t = 0) = 50 \text{ Hz}$$

- at time $t = 1 \text{ s}$, the load request step is obtained by halving the value of the load resistance.

$$R'_{load} = \frac{R_{load}}{2}$$

$$\Delta P_{ref} = 50\%$$

- at time $t = 2 \text{ s}$, the nominal power's value in the summer is modified by doubling it.

$$P_n = 2 \cdot 15,6 \text{ kW}$$

- at time $t = 3 \text{ s}$, the nominal frequency's value in the summer is modified by decreasing it of the 10%.

$$\Delta f_1 = -10\%$$

- at time $t = 4 \text{ s}$ the reference voltage amplitude is decreased by the 10%.

$$\Delta V_{amp} = -10\%$$

The plots of the power and of the frequency are reported in Figure 1.3.2-3, where reference values, P_n and f_1 , are represented in green and the instantaneous performed values, P and f , are represented in red.

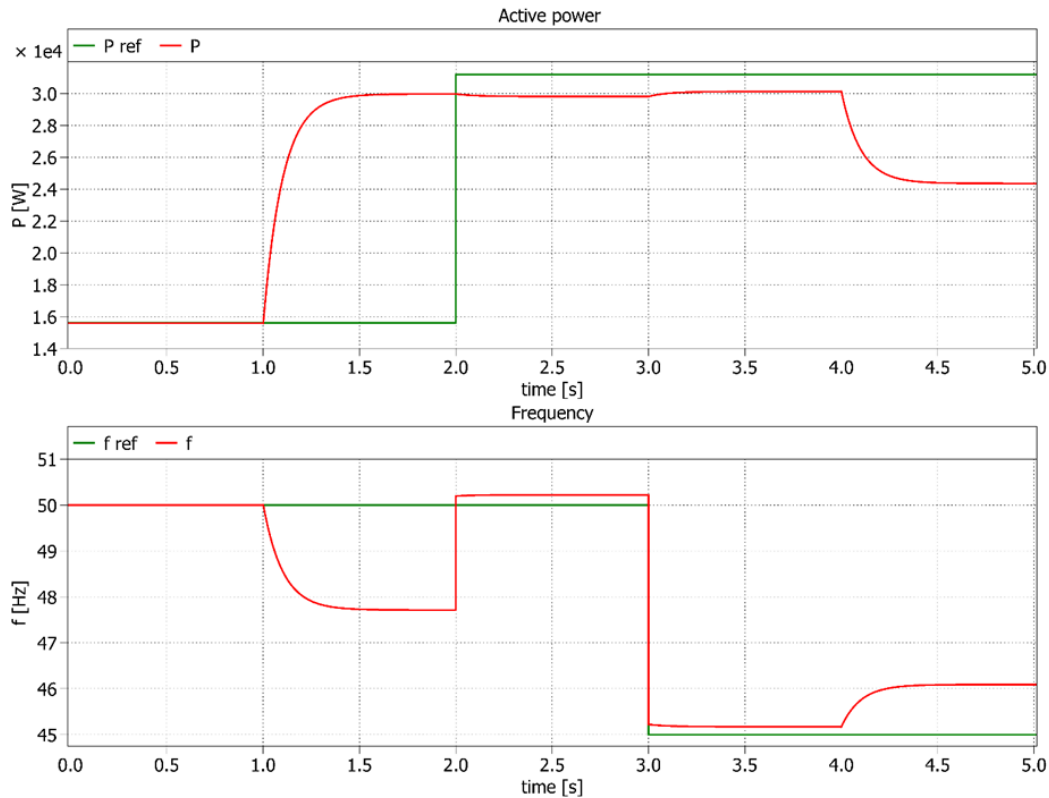


Figure 1.3.2-3 Grid forming converter control: active power and frequency dynamic at step load request, reference power, frequency reference and voltage drop variations.

Initially, since the power on the grid is the same as the reference power, $P = P_n$, the present frequency is also the same as the reference frequency, $f = f_n$. When the load power changes, the control reacts by changing the frequency at which the reference voltage is generated. The frequency variation applied is proportional to the power variation and it is calculated as distance from the reference values set, equal to the nominal ones.

This is also evident in the waveforms of the voltage and of the current measured on the grid, below reported in Figure 1.3.2-4. When the power and frequency's reference values, P_n and f_1 , of the control are changed, the droop-control line of the frequency-power graph, represented in Figure 1.3.2-3, is shifted causing the converter to operate at a new operating point. The effects on the current power and frequency are of different magnitude because of the droop-gain value. The voltage drop creates a reduction in the main power and so the converter reacts by returning higher frequency waveforms.

The voltage and current measurements are shown in Figure 1.3.2-4.

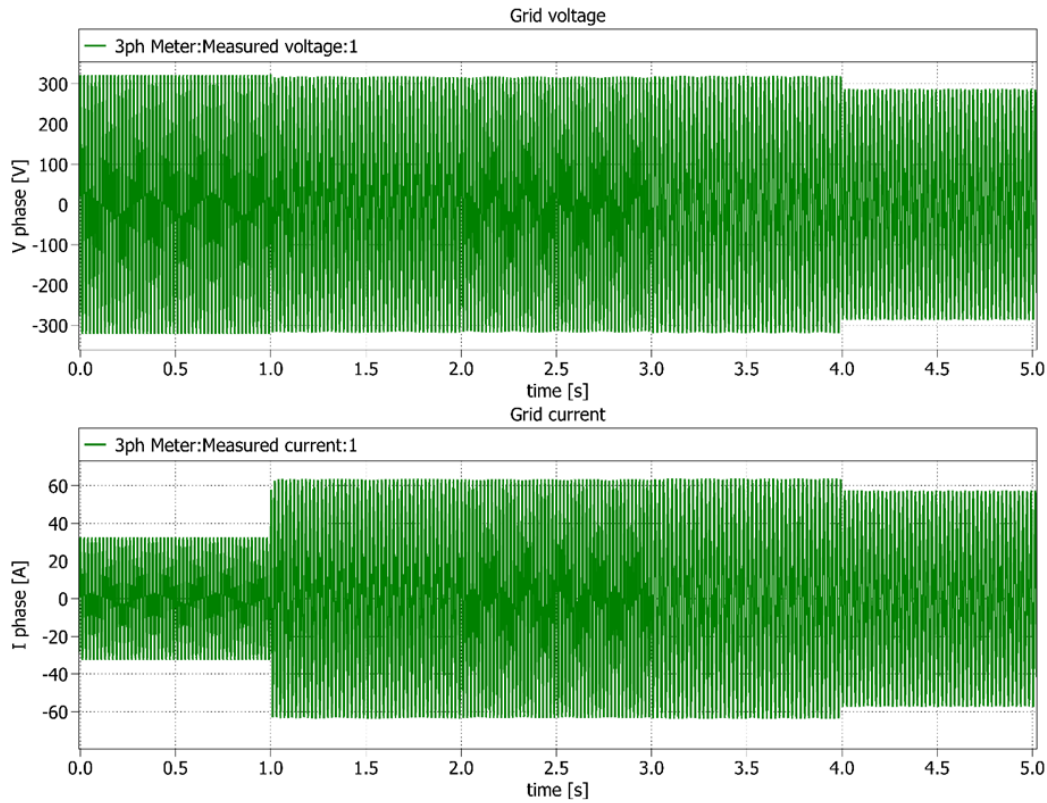


Figure 1.3.2-4 Grid forming converter control: phase voltage and current dynamic at step load request, reference power, frequency reference and voltage drop variations.

The ultimate expression of grid-forming control is inspired by the virtual emulation of the dynamics and control of a synchronous alternator. The general idea is to control the converter signals to behave like a synchronous machine. This emulation of the synchronous machine transforms the converter into a virtual synchronous machine using an algebraic model of a synchronous machine where there is an analogy between the converter's terminals voltage and the generator's stator voltages.

1.4 The Virtual Synchronous Machine control

As required by grid codes, the power balance between the power generation and the power demand following a frequency variation event must be reached in a fast enough way such that the frequency excursions remain close to the reference frequency of 50 Hz or 60 Hz.

As it has just been seen in the Chapter 1.1, during a load power variation event a frequency drop is also generated. The primary control must arrest the fast frequency decline, its nadir, in the timescale of seconds, and then the secondary frequency regulation restores the frequency in some minutes.

When the frequency drops, synchronous generators, autonomously, turn slower and reduce the kinetic energy stored in their rotors and deliver a kinetic power, thus

helping the system to mitigate the frequency drop and to eliminate the frequency deviation, restoring the nominal value [37].

As the penetration level of renewable energy sources grows, inertia decreases. The effect of the primary control is contributed by both frequency drop and inertia, but inertia is an inherent property of synchronous generators and not of static converter. For this reason, is mandatory to give to this technology the inertia sensibility. This could be done implementing an algorithm that works elaborating a power variation reference equal to the mechanical power that an equivalent synchronous machine would deliver.

A method by which a converter can be controlled to mimic the behavior of a synchronous machine is the Virtual Synchronous Machine control. The equations used in it are the same used for the frequency regulation made with alternators, including the swing equation (1.1-1) that introduces the dynamic of the regulation and the link between the power's difference and the frequency's variation. If a converter that uses this kind of control is connected to the grid no difference would be felt from the grid side.

Disadvantage of the use of a VSM control is that, as a synchronous machine, a loss of stability due to under excitation or load-angle too big could occur. Advantage, over the introduction of inertia in the system, is that it's possible to choose the parameters, such as inertia, droop coefficients and so on [38] [39] [40] [16].

To understand how to regulate the frequency using a converter and introducing also the typical dynamics of regulation using synchronous alternators, the dynamic model of the frequency regulation made with synchronous generators is merged into the Grid Forming control. The grid configuration, the control structure and the turbine simulation parameters remain the same previously used.

The block schematic of the implemented control is shown in Figure 1.4-1. It shows the Virtual Synchronous Machine control block diagram realised for the simulation:

- the part coming from a typical GFM control is highlighted in orange.
- the part that simulates the behaviour of the synchronous machines in frequency regulation, using p.u. values, is highlighted in green.

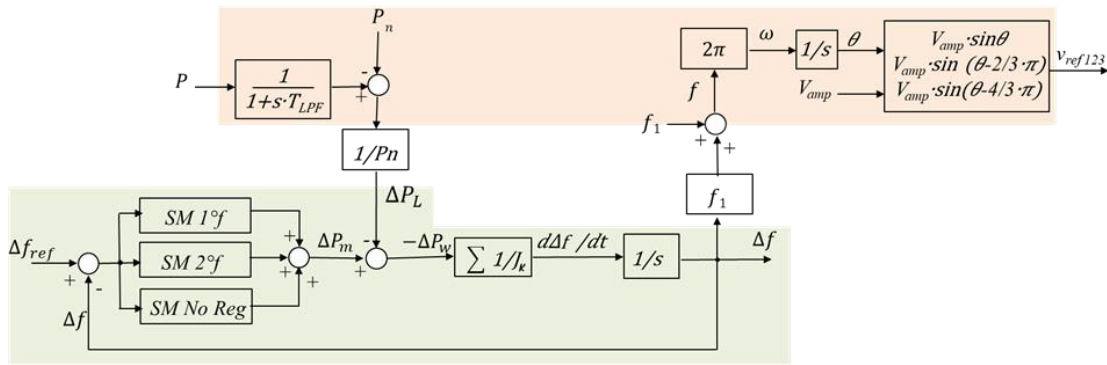


Figure 1.4-1 Grid forming converter Virtual Synchronous Machine control schematic block: in orange the part coming from a typical GFM control; in green the part that simulates the synchronous machine frequency regulation's behavior.

After calculating the load power variation from the nominal value, the signal is sent as input to the block that simulates the closed-loop frequency regulation done with synchronous generators. It returns the frequency variation from which, once the reference frequency value is known, the instantaneous frequency and the electrical angle that the regulator must apply to the voltage reference are calculated. The converter then feeds the grid, generating the desired three-phase voltage at the same frequency and with the same dynamics that the simulated machine would have if a real and identical one has been placed in its place. In this way the new load power demand is satisfied.

A simulation is carried out where, using a resistive-inductive grid, a 10% increase in load power is required at time $t = 10$ s by decreasing the load resistance R_{load} value by 10%.

Because it is intended to emulate the same dynamics as in the example given in Chapter 1.1, the same values for the control parameters (Table 1.4-1) have been used in the block of the emulated inertia dynamic.

Figure 1.4-2 shows the plots of the phase grid current near the power step's time.

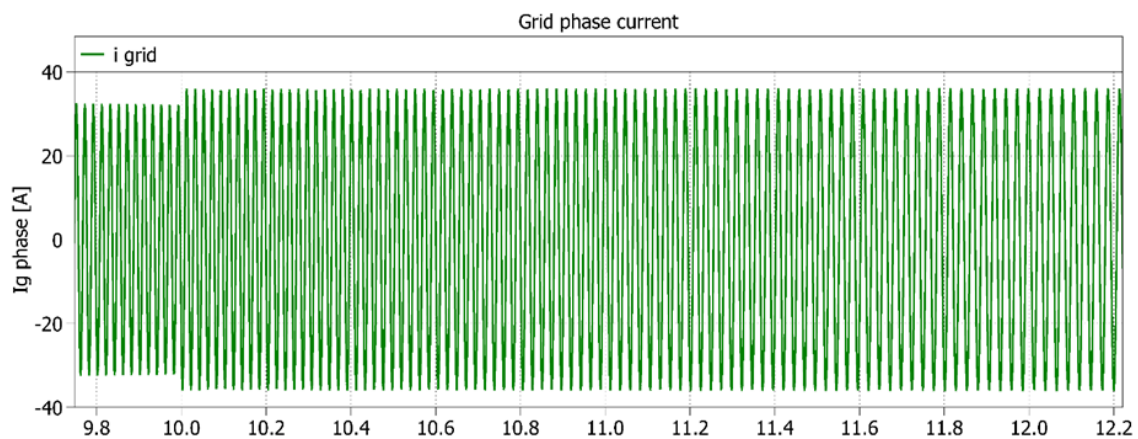


Figure 1.4-2 Grid Forming Virtual Synchronous Machine converter control: phase current dynamic at step load request.

Figure 1.4-3 shows the power and frequency calculated by the measures on the grid.

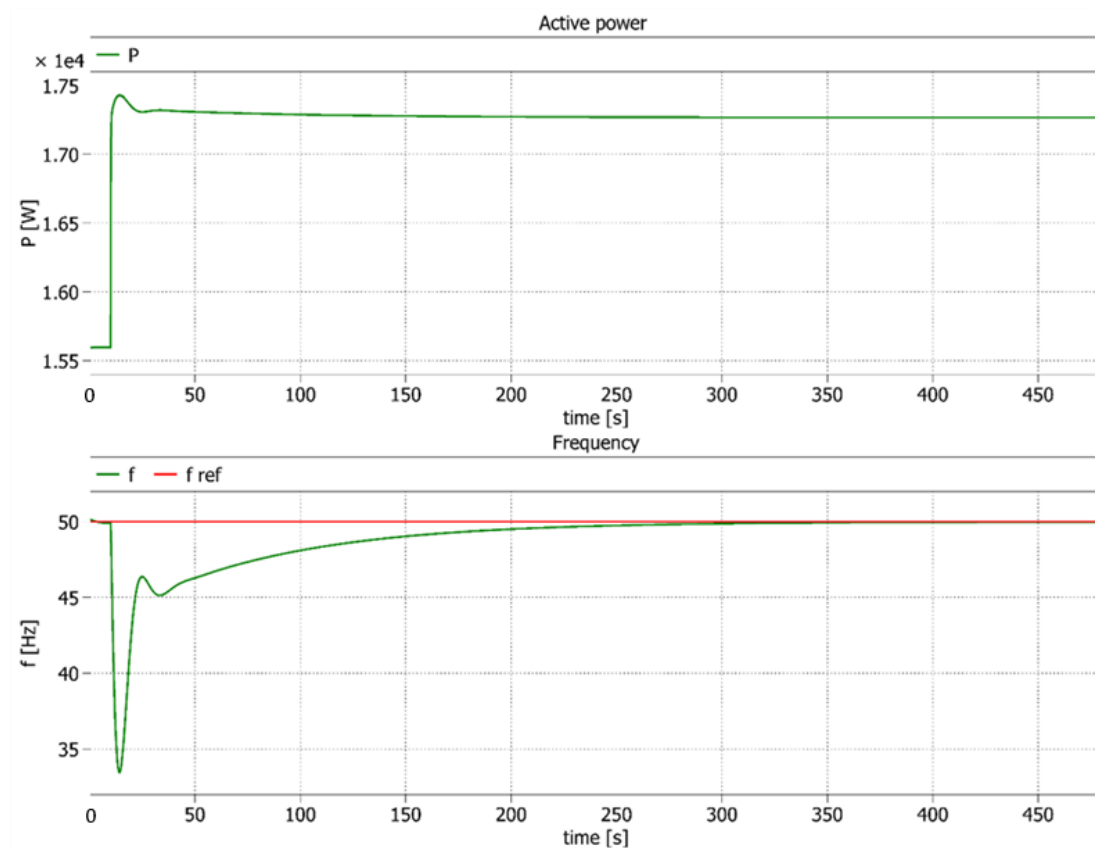


Figure 1.4-3 Grid Forming Virtual Synchronous Machine converter control: power and frequency dynamics at step load request.

Figure 1.4-4 shows the frequency and power deviations calculated by the emulation block of the synchronous machines system.

All the plots are below commented.

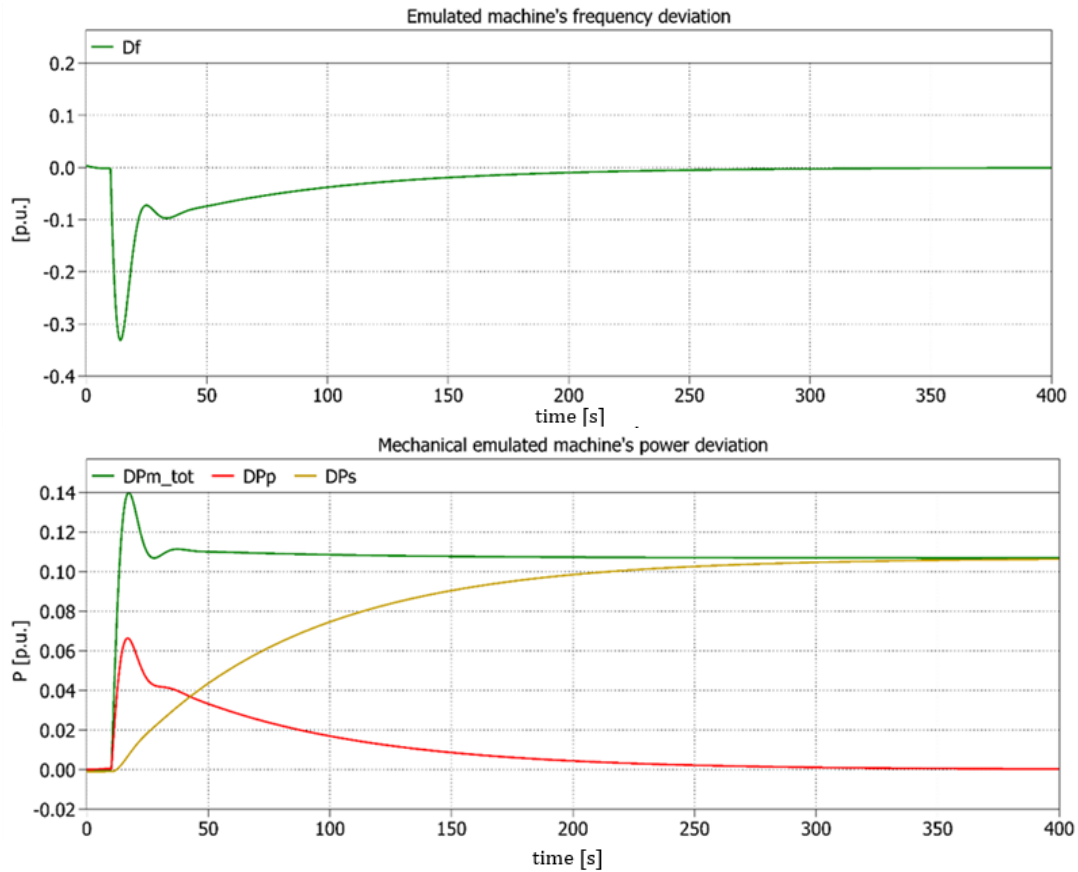


Figure 1.4-4 Grid Forming Virtual Synchronous Machine converter control: dynamic of the power and frequency responses of the simulated machines system -dynamic response at step load request.

As can be seen from the figures, the power variation is realized by an increase in the amplitude of the current flowing in the grid as a result of a step reduction in the load equivalent resistance R_{load} . At the demand for more power requested by the load, the turbine simulation block calculates how much the frequency change should be, calculating it as if the virtual turbine is connected with droops b_T b_P and time constants T_a of the allocated controllers. The simulated mechanical power variation ΔP_m is used to calculate the virtual inertia power ΔP_W and then, using the system inertia value of the virtual machine J , the speed variation Δf that this machine would have in that situation is obtained. The converter generates voltage at the calculated frequency and imposes it on the grid, which will have AC voltages and currents at the same frequency as the converter.

In fact, the frequency plots show that the main frequency in Figure 1.4-3 has the same waveform as that simulated by the virtual machine control in Figure 1.4-4. This is what distinguishes the virtual synchronous machine GFM control from others.

More significantly, the graph in Figure 1.4-4 showing the dynamics of the power variation of the emulated synchronous generators in green (with primary and secondary regulation respectively in red e yellow) actually follows the one of the measured power on the grid in Figure 1.4-3. This demonstrates that the converter manages to behave exactly as if in its place there is a frequency regulation system

with synchronous machines equal to those emulated, and that the grid does not feel any difference due to the use of the converter as a power source. This validates the use of the control.

2 Average model of string inverters

2.1 Motivation

TRUST-PV is a project created to increase the performance and reliability of PV components and PV systems in large distributed and/or utility-scale PV areas.

In the framework of the PV TRUST project activities, it has been proposed to carry out with Enel a system study involving a detailed power system with increasing levels of PV penetration using different strategies, such as grid following, grid forming, and a mixture of them, to assess the grid support and ancillary services that the power plant controllers and inverters can provide. To do this task, has been asked to start a joint activity in which Huawei would provide a generic but detailed model. Huawei agreed to plan the joint activity from the inverter level to the power system solution [41] [42].

As Huawei's strengths are in inverter controls, the company aimed to design control strategies, possibly based on existing techniques, to evaluate grid-following strategies with grid support, and grid-forming strategies, e.g. by introducing virtual inertia, to be tested in a large grid system. Above all, one of Huawei's main interests in PV h2020 Trust is to show virtual inertia capabilities for frequency regulation, leaving some margin in dispatching or transient overload to IGBTs and also oversizing DC capacitors.

Enel, on the other hand, proposed to build it and integrate it into an existing electrical system. They will additionally contribute with power system studies and detailed modelling for all components to be included in the simulation [43].

At the end of the project, the results would be evaluated by both companies together.

2.2 Averaging versus switching models

Switching or average model are two different approaches to represent the behaviour of the system under observation. Both the two models are able to represent the functionality of the controller in the same way. From the viewpoint of the power stage, the only difference between them is that the switching model uses the detailed three-phase component of the inverter's power electronics device to emulate its behaviour, whereas the average model uses three signal-controlled voltage sources.

Depending on the task, the type of device or controller under test and the computing power available, the choice can fall on one model or the other.

If it is intended to realise the control of the inverter itself, the switching dynamics must also be analysed and so a switching model is preferable. However, a higher resolution is required.

On the other hand, if it is desired to develop controllers for grid studies and to investigate energy resources, it is preferable to use models for inverters using average values, since that is the level at which the power transfer between the connected devices takes place. For this reason, highly detailed switching models are generally not necessary for that application [44].

By focusing more on the response of the electrical system rather than the behavior of the converter, generic models are provided that well could represent the dynamics of the control loops under relevant conditions. [45]

Moreover, the collaboration of more than one company implies finding solutions that are good for both. In fact, the collaborating company deals more with studies related to grid, transmission, distribution, generation, industrial plants which are at slow dynamic and they neglect high frequency dynamic effects such as discontinuities introduced by the converter's modulation technique or the delays introduced by the converters in use for sampling the useful variables for the control. In fact, it is used to make simulations with software such as DIgSILENT.

Overall, this case study requires to work with models at average values. By doing so, the level of detail of the inverter control goes up to the current control. The main focus remains on the AC part of the grid that is composed by power loops (active/reactive), inertial emulation loops, internal current loops. The action of the current loop control returns a voltage reference or a modulation signal to convert the DC-link voltage and that injects a dependent three-phase voltage as a source in the AC side of the power system model. After this voltage source, an LCL filter must be inserted and the current control loop must consider its presence. Assuming proper sizing of the LCL filter, it is permissible to neglect high frequency phenomena since they do not modify the response of the power transfer between the grid and the connected devices. In simulations of mass power systems with PV, converter's DC dynamic is not considered unless there is a sudden change in irradiation reaching the PV panels. For these reasons, the DC-link voltage control, placed between the converter and the PV source, is structured to be sensitive to variations in power generation.

In this regard, it has been chosen to realize an average model using the simulation program PLECS that can be easily adapted to other tools.

2.3 Lumped model of a string

When setting up a photovoltaic system, it must be ensured that the output voltage and current are at the required levels. This determines the configuration of the circuit and the connection of the photovoltaic panels to each other. The first way to connect the panels together is in series until the desired voltage is reached. An example of string PV is in Figure 2.3-1.

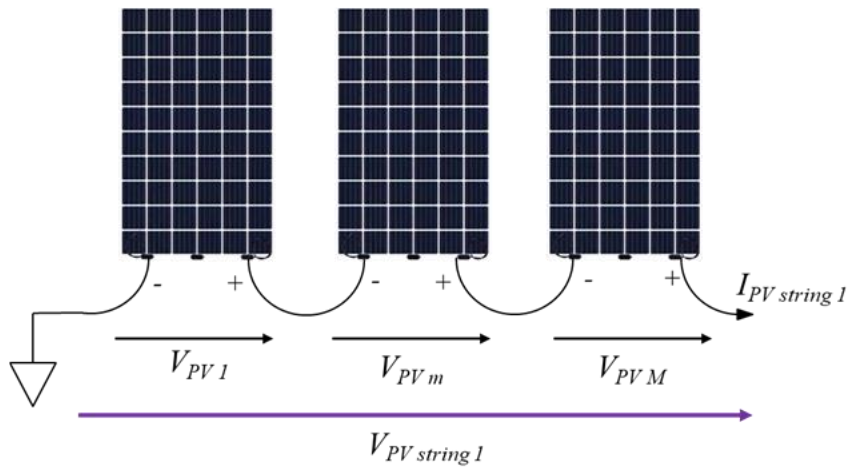


Figure 2.3-1 String PV obtained connecting several PV panel in series.

Proceeding in a similar way, in order to obtain more power than the one that a single string of panels in series can provide, several strings with the same number of PV panels are connected each other in parallel forming a PV module [46], as shown in Figure 2.3-2. They forms a PV module.

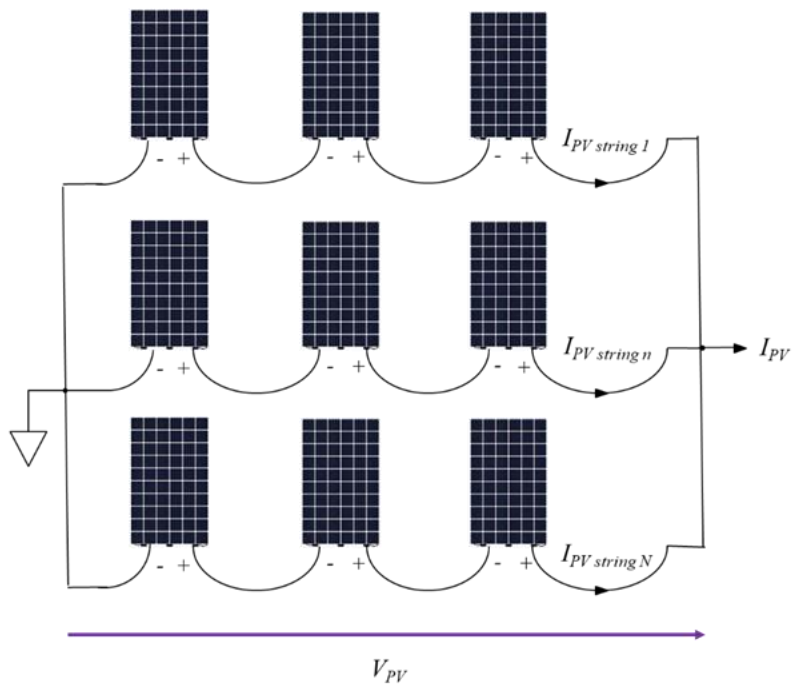


Figure 2.3-2 Parallel of more string PV. Output current and voltage are managed by a converter.

This is also what is to realize in the company's project. In fact, it is planned to use string PV panels connected to an inverter that manages them to work at stable power levels.

Then, more inverters are connected together to deliver a higher power level. The interconnected converter complex acts as a bridge between the energy

production of the photovoltaic panels and the grid. Each converter is connected to the grid through an LCL filter, whose task is to reduce current ripple on the line.

The representation of the AC power system of an inverter connected to the grid is shown in Figure 2.3-3.

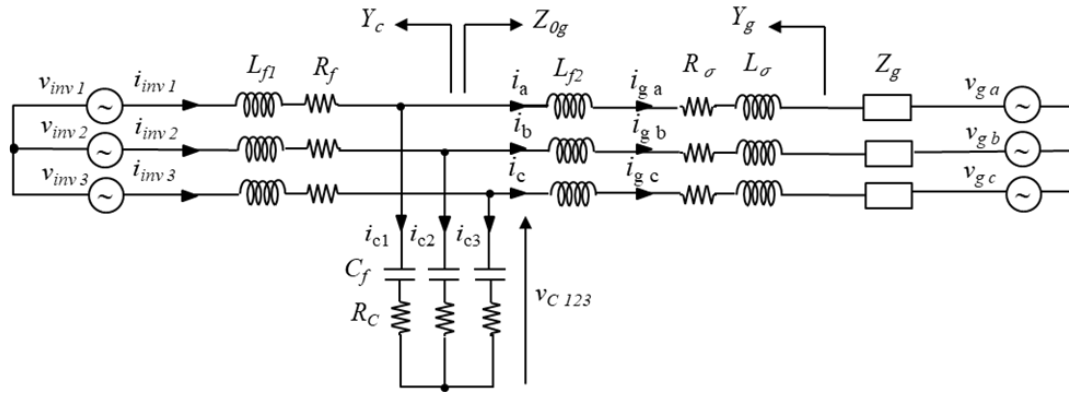


Figure 2.3-3 Electrical circuit of the power system formed by a converter connected to the grid through a LCL filter.

The converter used is a voltage source converter (VSC).

In the Figure 2.3-3 the voltages $v_{g abc}$, $v_c 123$ and $v_{inv 123}$ represent the solid grid, the voltage in the point of connection and the VSC's voltages, respectively. The LCL output filter is formed by the converter side inductive filter, the capacitance and transformer leakage inductance.

The inductive filter in the converter's side is defined by the series inductance L_{f1} and resistance R_f . L_{f2} is the output inductance of the filter but in the calculation it can be neglected because of its small value respected to other variables. The capacitance is given by a parallel capacitance C_f in series with a small equivalent series resistor R_c .

The transformer model is given by a leakage inductance L_σ and an equivalent winding resistor R_σ in series.

The grid impedance is represented by Z_g , which depends on power system circuit and grid conditions.

Converter control commonly consists of an outer DC-link voltage control loop and an inner current control loop. For some applications with line current feedback, the well-known PI controller in the synchronous reference dq frame can be employed. However, the inner PI-based current control is not suitable for many applications, depending on the ratio of LCL resonance frequency to control frequency.

The VSC is an active component. Due to its discrete operation and PWM modulation technique, the effectiveness of the control is increasingly reduced as the frequency increases because system delays and non-linear effects tend to compromise its passivity property. However, these effects can be minimized by including the LCL filter as part of an external VSC admittance. This hypothesis is supported by the fact that at high frequencies the disturbances generated at the

connection point are absorbed by the LCL capacitor branch, and therefore, are not able to create positive feedback in the VSC.

The LCL resonant pulsation is [47]

$$\omega_{res} = \sqrt{\frac{L_{f1} + L_{\sigma}}{L_{f1} \cdot L_{\sigma} \cdot C_f}} \quad (2.3-1)$$

The selection of ω_{res} involves a trade-off between control interactions and filtering. At low values of the ratio of LCL resonance frequency to control frequency, the feedback of the converter's PI current control can lead to instability. For these applications, active resonance damping gets integrated into the current control loop. Typically, the control action calculation also includes an v_c voltage feedforward v_{ff} double path, with the objectives of provide a filtered value of the main grid component, to improve the initial transient and an active damping action based on capacitor voltage derivative term.

Design for passivity is approached as a reliable method to assure the stability of LCL grid-connected VSC working in power systems with potential resonances. Its frequency region for design is reconsidered by having into account non-linear ZOH and PWM effects and the nature of the LCL filter topology.

This proposed method models the converter control and the LCL filter as an equivalent admittance Y_c . The rest of the grid is modelled as an equivalent impedance Z_{og} . The stability condition is given by the fact that, considering Z_{og} to be formed by passive elements only, the whole system formed by $Y_c Z_{og}$ is stable if Y_c is also passive. In practice, design for passivity aims to define converter control actions that shape Y_c to be passive in a specified range of frequencies.

Considering the LCL grid-connected VSC, the outer admittance Y_c sets the dynamics by its interactions with Z_g .

The outer admittance is given by

$$Y_g = (j\omega \cdot C_f + Y_c) // \frac{1}{j\omega \cdot L_{\sigma}} \quad (2.3-2)$$

The term $j\omega \cdot C_f + Y_c$ is the inner admittance and has been defined as the parallel of the converter admittance Y_c and the filter capacitor branch, considering null the series resistance. Only Y_c models the converter control actions, but the remaining Y_g components are passive. As the capacitive branch admittance increases with frequency, the assumption $|j\omega \cdot C_c| \gg |Y_c|$ becomes reasonable at frequencies above ω_{res} . At high frequency the capacitor branch becomes dominant and mainly sets the admittance seen by v_{c123} to the voltage source converter. Having stability means that the high frequency components in the main side flow principally through the capacitor branch and they go hardly into the voltage source current path of the converter. In this way, the consequences on the control resulting from the disturbance are minimal and not sufficient to cause positive feedback or instability. To satisfy this assumption, $|Y_c|$ should be small at high frequencies, which is achieved by the passivity method.

A second issue that arises comes from the digital sampling for measurements of electrical quantities useful for the control. The function in the frequency domain that describes the practical signal reconstruction done by a conventional digital-to-analog converter (DAC) is the Zero Order Hold (ZOH) [48].

$$ZOH(\omega) = \frac{1 - e^{-j\omega T_s}}{j\omega T_s} \quad (2.3-3)$$

Its frequency response is non-linear and aliasing occurs at frequencies higher than half of the main frequency. It's shown in the Figure 2.3-4. The aliasing area is highlighted in yellow.

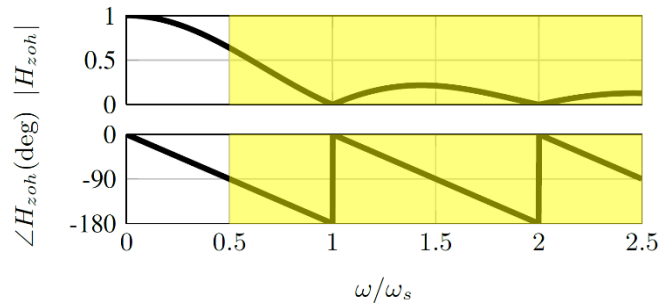


Figure 2.3-4 ZOH frequency response. The yellow zone corresponds to alias region [49].

Anti-aliasing filters are designed so that the frequencies close to $\omega_s/2$ are well attenuated, which implies a high order analogue filter with a cut-off frequency well below $\omega_s/2$. The filter is a low-pass filter and it adds a significant phase delay in the closed loop, and so it can compromise the stability properties. For this reason the frequency region in which anti-aliasing is effective should be outside the working range of the control.

Another problem of non-linearity is given by PWM operation because it generates voltage harmonics at multiple frequencies. They are dependent on the fundamental component amplitude and angle and the carrier phase angle.

The internal admittance of the VSC can be modelled by a reduced-order filter in the Z-domain, which depends mainly on the proportional damping and active (controller) gains.

To create a passivity model with admittance expressions for the converter Y_c and for the grid Y_g , it is taken into account that the non-linearities of the ZOH and the PWM operation depend on the references of the fundamental components. Therefore, these non-linearities can behave as a disturbance in the frequency region for the design.

It is also assumed that:

- the reference current of the controller is zero in the range of frequencies at which a passive behaviour of the current controller is wanted (i.e., above the theoretical closed loop bandwidth);
- the analytical expression of Y_c is calculated by an v_c impulse responses considering it linear in the design region;

- the effect of anti-aliasing filters is negligible in the design region.

Under these assumptions, the admittance of the converter in the Z-domain is described by a third-order expression with zeros and poles depending on the active damping gain k_{ad} and the proportional gain k_p , respectively, of the controller [49].

$$Y_c(z) = \frac{i_c}{v_c} = \frac{0.5 \cdot z^3 + 0.5 \cdot z^2 - \frac{k_{ad}}{T_s} \cdot z + \frac{k_{ad}}{T_s}}{z \cdot \left(\frac{L_{f1}}{T_s} \cdot z^2 - \frac{L_{f1}}{T_s} \cdot z + k_p \right)} \quad (2.3-4)$$

A convenient combination of k_{ad} and k_p provides a stable pole/zero cancellation, which reduces the $Y_c(z)$ order to a first one.

The polo-zero cancellation is obtained by choosing for the control gains equal to [50]

$$\begin{cases} k_{ad} = \frac{2}{3} \cdot T_s \\ k_p = \frac{2}{3} \cdot \frac{L_{f1}}{T_s} \end{cases} \quad (2.3-5)$$

The admittance of the converter is simplified by becoming first-order.

$$Y_c(z) = \frac{T_s}{2 \cdot L_{f1}} \cdot \frac{z+2}{z} \quad (2.3-6)$$

In this way the passivity of the converter's admittance is obtained. The expression obtained has a zero in $z = -2$ which creates a delay that is greater when the frequency is high. Additionally, despite being a first-order expression, the phase delay reaches -180° at the Nyquist frequency.

According to have a frequency response, it is possible to turn $Y_c(z)$ into $Y_c(\omega)$ simply calculating $Y_c(\omega) = Y_c(z = e^{j\omega T_s})$.

For the project that it's wanted to be realized, the control of a single converter is not sufficient. Given the need to manage a higher power level than a single converter would be able to do, it is necessary to connect several identical converters in parallel. This creates a String Inverter Model [51], as represented in the Figure 2.3-5.

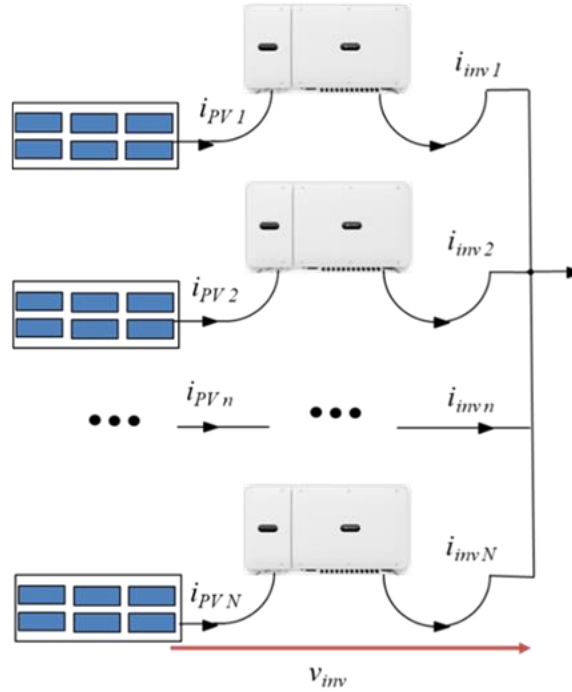


Figure 2.3-5 String inverter obtained connecting N inverter in parallel.

Thus, the problem of having to make an analysis of the overall system arises. Simulations should consider the behavior and control of each individual inverter. The level of detail of the system and the computational power required become enormous. For this reason, a lumped model must be used that is able to represent the behavior of several voltage source inverters connected in parallel through LCL filters to the grid. The advantage of this model is to reduce the order of the system but, because of this, information about individual converters are lost and it is not possible to observe what is happening in one of them.

The aim is to use the equations that govern each individual converter and manipulate them to derive equivalent ones, reduced in number, capable of representing the response that would be obtained if a single converter is used instead of them but with a power output equivalent to that delivered by the converters in parallel.

Considering a generic n LCL filter between the N_{inv} converters connected in parallel, it is formed by a primary and secondary side which will be connected to the converter and the grid respectively. It is represented in Figure 2.3-6 where:

- L_{1n}, L_{2n} are the inductences of the primary and secondary side;
- C_n is the filter's capacitance;
- $i_{1n} = i_{invn}$ and $i_{2n} = i_n$ are the currents of the primary and secondary side of the filter;
- v_{PCC} is the voltage at the point of connection;
- v_{Cn} is the voltage on the filter capacitance;
- v_{invn} is the voltage supplied by the converter.

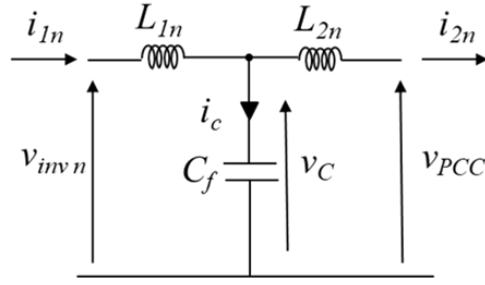


Figure 2.3-6 A generic n LCL filter between the N_{inv} inverter and the point of connection PCC.

The control equations for the state variables of a generic n converter among the N_{inv} connected in parallel are [52]

$$\begin{cases} a) \frac{d}{dt} \mathbf{i}_{1n} = -\frac{v_{Cn}}{L_{1n}} + \frac{v_{invn}}{L_{1n}} \\ b) \frac{d}{dt} \mathbf{i}_{2n} = \frac{v_{Cn}}{L_{2n}} - \frac{v_{PCC}}{L_{2n}} \\ c) \frac{d}{dt} v_{Cn} = \frac{\mathbf{i}_{1n}}{C_n} - \frac{\mathbf{i}_{2n}}{C_n} \end{cases} \quad (2.3-7)$$

To these must be added the equation that interconnects the converter complex with the grid. Let L_g, \mathbf{i}_g, v_g be the total inductance, the current and voltage on the grid. Resistances are neglected.

In Figure 2.3-7 is shown the point of connection of the N_{inv} inverters composing the string inverter.

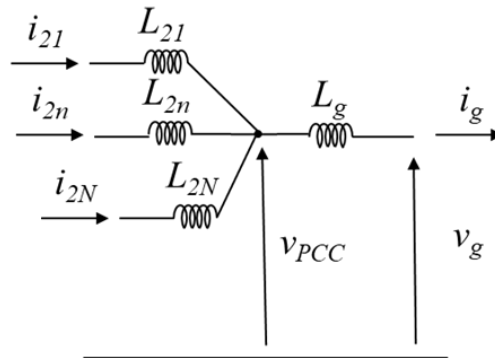


Figure 2.3-7 Point of connection of the N_{inv} inverters composing the string inverter.

$$\begin{cases} d) \frac{d}{dt} \mathbf{i}_g = -\frac{v_g}{L_g} + \frac{v_{PCC}}{L_g} \\ \mathbf{i}_g = \sum_{n=1}^{N_{inv}} \mathbf{i}_{2n} \end{cases} \quad (2.3-8)$$

Because of all the converters are equal and they are connected to the same grid via identical LCL filters, it is assumed that all inductances and capacitances seen by every individual converter are equal.

$$\begin{cases} L_{1n} = L_1 \\ L_{2n} = L_2 \\ C_n = C \end{cases} \quad (2.3-9)$$

for every n^{th} inverter between N_{inv} .

Moving from the time domain to the frequency domain, and so using Laplace equations, the derivative function $\frac{d}{dt}$ is replaced by the s complex variable.

Considering the equations b) (2.3-7) valid for every inverter, they are summed up for all N_{inv} converters. The resulting equations is

$$\begin{aligned} b) \quad s \cdot \mathbf{i}_g &= s \cdot \sum_{n=1}^{N_{inv}} \mathbf{i}_{2n} = \frac{1}{L_2} \cdot \sum_{n=1}^N (\mathbf{v}_{Cn} - \mathbf{v}_{PCC}) = \\ &= \frac{1}{L_2} \cdot \sum_{n=1}^{N_{inv}} (\mathbf{v}_{Cn}) - \frac{N_{inv}}{L_2} \cdot \mathbf{v}_{PCC} \end{aligned} \quad (2.3-10)$$

As lumped model's assumptions are considered the average value for the voltage of the capacitance \mathbf{v}_c and for current in the inductor \mathbf{i}_1 .

$$\begin{cases} \mathbf{v}_c = \frac{1}{N} \cdot \sum_{n=1}^{N_{inv}} (\mathbf{v}_{Cn}) \\ \mathbf{i}_1 = \frac{1}{N} \cdot \sum_{n=1}^{N_{inv}} (\mathbf{i}_{1n}) \end{cases} \quad (2.3-11)$$

Thus, equation b) of the equivalent aggregate converter is

$$b) \quad s \cdot \mathbf{i}_g = \frac{N}{L_2} \cdot (\mathbf{v}_c - \mathbf{v}_{PCC}) \quad (2.3-12)$$

So, it is possible to obtain the value of \mathbf{v}_{PCC}

$$\mathbf{v}_{PCC} = \mathbf{v}_c - \frac{s \cdot \mathbf{i}_g}{\frac{N}{L_2}} \quad (2.3-13)$$

Substituting \mathbf{v}_{PCC} (2.3-13) into equation d) (2.3-12) it is obtained the first equation, B) (2.3-12), that describes the full system.

$$B) \quad s \cdot \mathbf{i}_g = -\frac{\mathbf{v}_g}{L_g} + \frac{1}{L_g} \cdot \left(\mathbf{v}_c - \frac{s \cdot \mathbf{i}_g}{\frac{N_{inv}}{L_2}} \right) = \frac{\mathbf{v}_c - \mathbf{v}_g}{L_g + \frac{L_2}{N_{inv}}} \quad (2.3-14)$$

The second global equation comes from a) (2.3-7) and it is influenced by the type of control that the converter uses. Let there be a generic control function with terms for the voltages of the capacitances and currents passing through the filter inductor.

$$\mathbf{v}_{invn} = K_V \cdot \mathbf{v}_{Cn} + K_I \cdot \mathbf{i}_{1n} + K_F \cdot F_n(s) \quad (2.3-15)$$

Equations a) (2.3-7) becomes

$$a) \quad s \cdot \mathbf{i}_{1n} = \frac{1}{L_{1n}} \cdot ((1 - K_V) \cdot \mathbf{v}_{Cn} + K_I \cdot \mathbf{i}_{1n} + K_F \cdot F_n) \quad (2.3-16)$$

Summing for all the N_{inv} converter and using the lumped model hypothesis before expressed in (2.3-9), it's obtained

$$s \cdot \sum_{n=1}^{N_{inv}} \mathbf{i}_{1n} = \frac{1}{L_{1n}} \cdot ((1 - K_V) \cdot \sum_{n=1}^{N_{inv}} \mathbf{v}_{Cn} + K_I \cdot \sum_{n=1}^N \mathbf{i}_{1n} + K_F \cdot \sum_{n=1}^{N_{inv}} F_n)$$

$$A) \quad s \cdot \mathbf{i}_1 = \frac{1}{L_1} \cdot ((1 - K_V) \cdot \mathbf{v}_C + K_I \cdot \mathbf{i}_1 + K_F \cdot F) \quad (2.3-17)$$

The last equation is obtained simply by using the lumped model assumptions (2.3-9) and summing up the equations c) (2.3-7) for all the N_{inv} converters.

$$s \cdot \sum_{n=1}^N \mathbf{v}_{Cn} = \frac{1}{C} \cdot \sum_{n=1}^N (\mathbf{i}_{1n} - \mathbf{i}_{2n})$$

$$C) \quad s \cdot \mathbf{v}_C = \frac{1}{C} \cdot (\mathbf{i}_1 - \frac{\mathbf{i}_g}{N}) \quad (2.3-18)$$

$\mathbf{v}_C, \mathbf{i}_1, \mathbf{i}_2$ are the state variables. Other variables are inputs, except F_n that depends on the control.

The obtained A,B,C equations are valid for a lumped model of a string converter with a generic control strategy.

The control for passivity, before explained and used in the current loop of the developed control, has

$$\mathbf{v}_{inv n} = k_{ad} \cdot s \cdot \mathbf{v}_{Cn} + k_p \cdot (\mathbf{i}_{1n ref} - \mathbf{i}_{1n}) \quad (2.3-19)$$

Finally, substituting (2.3-19) in the A,B,C equations, the equations of the lumped model of the string converter with the control strategy used in this work are obtained.

$$\left\{ \begin{array}{l} A) \quad s \cdot \mathbf{i}_1 = \frac{1}{L_{1n}} \cdot \mathbf{v}_C + \frac{1}{L_{1n}} \cdot \left(-k_p + \frac{k_{ad}}{C}\right) \cdot \mathbf{i}_1 - \left(\frac{k_{ad}}{N_{inv} \cdot L_{1n} \cdot C}\right) \cdot \mathbf{i}_g + \frac{k_p}{L_{1n}} \cdot \mathbf{i}_{1 ref} \\ B) \quad s \cdot \mathbf{i}_g = \frac{1}{L_g + \frac{L_2}{N_{inv}}} \cdot \mathbf{v}_C - \frac{1}{L_g + \frac{L_2}{N_{inv}}} \cdot \mathbf{v}_g \\ C) \quad s \cdot \mathbf{v}_C = \frac{1}{C} \cdot \mathbf{i}_1 - \frac{1}{C \cdot N_{inv}} \cdot \mathbf{i}_g \end{array} \right. \quad (2.3-20)$$

2.4 Current control

The AC system operating in three phases is composed of a string converter, LCL filters and a connection with the grid trough a step-up transformer. It's considered a nominal power of the grid equal to $P_n = 2 MW$.

The Figure 2.4-1 represents the power arrangement.

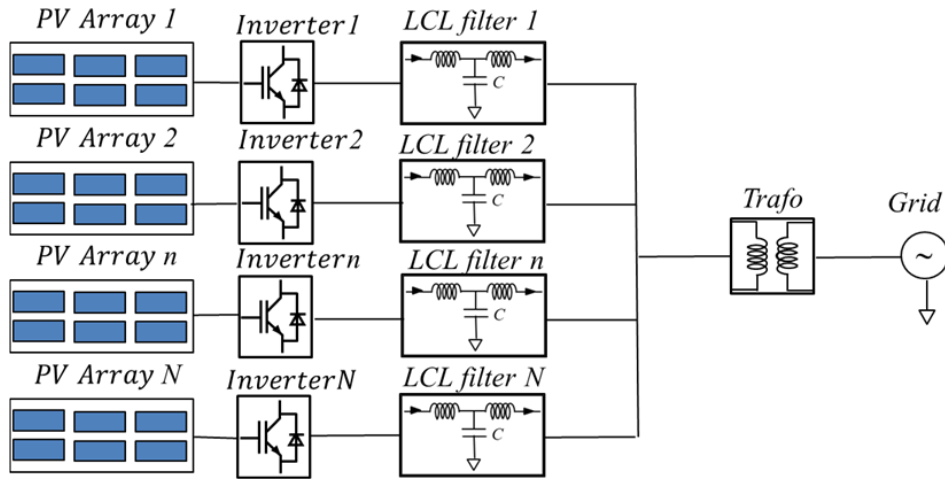


Figure 2.4-1 Power arrangement: PV generation for N inverters composing a string; LCL filters between inverters and point of connection; transformer to connect with the grid.

The string converter is considered an aggregated model of $N_{inv} = 20$ inverters. Each inverter has:

- nominal power $P_n = 100kW$;
- output filter 's capacitance $C_f = 10 \mu F$;
- filter's inductances $L_{f1} = 300 \mu H$ and $L_{f2} = 10 \mu H$.

Because of the parallel connection, the equivalent inductance is simplified with an LC equal to:

$$C_{f_{tot}} = C_f \cdot N_{inv} = 200 \mu F$$

$$L_{f1_{tot}} = L_{f1}/N_{inv} = 15 \mu H$$

The effect of L_{f2} inductances can be neglected.

The primary side of the transformer is connected to the output of the converter, working at the nominal voltage of $V_n = 460 V$. It is considered a short circuit complex power equal to $N_{sc} = 20$ times the nominal one.

$$S_{sc} = N_{sc} \cdot P_n = 20 \cdot 2 \cdot 10^6 = 40 MVA$$

The short circuit impedance is obtained [54]

$$Z_{sc} = \frac{V_n^2}{S_{sc}} = 5,3 m\Omega \quad (2.4-1)$$

Supposing that the short circuit impedance is only an inductance, the short circuit inductance of the transformer is

$$L_\sigma = \frac{Z_{sc}}{2 \cdot \pi \cdot f_n} = 16.83 \mu H \quad (2.4-2)$$

This value is very similar to that of the filter.

To implement a control algorithm, the output voltage \mathbf{v}_{123} and current $\mathbf{i}_{inv\ 123}$ of the converter and currents on the grid \mathbf{i}_{abc} are measured. The Figure 2.4-2 represents the equivalent electric circuit of the system described above.

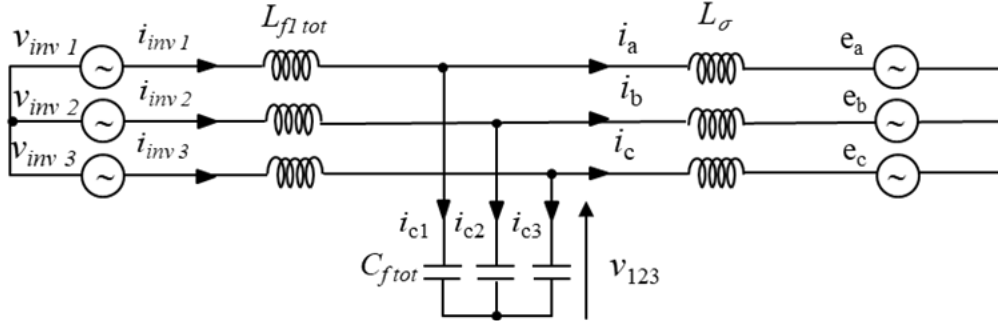


Figure 2.4-2 Equivalent AC system arrangement.

The presented control works in the two-phase dq reference system rotating at the grid frequency. For this reason, the measured quantities are transformed using Parke transformations, from the three-phase frame, abc or 123 , to the $\alpha\beta 0$ orthogonal frame.

$$T_{123 \rightarrow \alpha\beta 0} = \frac{2}{3} \cdot \begin{bmatrix} 1 & -1/2 & -1/2 \\ 0 & \sqrt{3}/2 & -\sqrt{3}/2 \\ 1/2 & 1/2 & 1/2 \end{bmatrix} \quad (2.4-3)$$

In the transformation, the $\frac{2}{3}$ coefficient is used to have a transformation that maintains invariant the vector's amplitude. Because of the star connection, the unidirectional component, resulting from the 0 sequence, is considered null.

The rotational transformation rotates the spatial vector described by the fixed axes $\alpha\beta$ of the angle θ to the dq rotating reference frame.

$$R(\theta)_{\alpha\beta \rightarrow dq} = \begin{bmatrix} \cos(\theta) & -\sin(\theta) \\ \sin(\theta) & \cos(\theta) \end{bmatrix} \quad (2.4-4)$$

To determine the angle of rotation θ , a Phase locked loop (PLL) is used which receives as input the measured three-phase voltage \mathbf{v}_{123} . In this way, it is possible to work in the dq reference frame.

The three-phase AC circuit is described by the following equations.

$$\frac{d}{dt} \mathbf{i}_{inv\ 123} = \frac{1}{L_{f1\ tot}} \cdot (\mathbf{v}_{inv\ 123} - \mathbf{v}_{123}) \quad (2.4-5)$$

$$\frac{d}{dt} \mathbf{v}_{123} = \frac{1}{C_{f\ tot}} \cdot (\mathbf{i}_{inv} - \mathbf{i}_{abc}) \quad (2.4-6)$$

$$\frac{d}{dt} \mathbf{i}_{abc} = \frac{1}{L_{\sigma}} \cdot (\mathbf{v}_{123} - \mathbf{e}_{abc}) \quad (2.4-7)$$

By applying the transformations, the equations that describe the system in the frequency domain are expressed as follow, where:

- j represents the complex variable
- ω represents the pulsation.

They are the cause of the cross-coupling terms resulting from the rotational transformation.

The dynamic of the converter's output current in the dq frame is described by the equation

$$s \cdot \mathbf{i}_{inv\ dq} = \frac{1}{L_{f1tot}} \cdot (\mathbf{v}_{inv\ dq} - \mathbf{v}_{dq}) + j\omega \cdot \mathbf{i}_{inv\ dq} \quad (2.4-8)$$

In the steady state the Laplace variable tends to zero and the pulsation is equal to the nominal value:

$$s \rightarrow 0$$

$$\omega \rightarrow 2 \cdot \pi \cdot f_1$$

The converter's output voltage is

$$\mathbf{v}_{inv\ dq} = \mathbf{v}_{dq} - j \cdot (2 \cdot \pi \cdot f_1) \cdot \mathbf{i}_{inv\ dq} \cdot L_{f1tot} \quad (2.4-9)$$

Replacing the voltage \mathbf{v}_{dq} with the constitutive capacitance equation, and so with the integral of its regime equation

$$\mathbf{v}_{dq} = \frac{1}{s \cdot C_{ftot}} \cdot (\mathbf{i}_{inv\ dq} - \mathbf{i}_{dq}) \quad (2.4-10)$$

the final equation for the reference volteges of the current loop is obtained.

$$\mathbf{v}_{inv\ dq} = \frac{1}{s \cdot C_{ftot}} \cdot (\mathbf{i}_{inv\ dq} - \mathbf{i}_{dq}) - j \cdot 2\pi f_1 \cdot \mathbf{i}_{inv\ dq} \cdot L_{f1tot} \quad (2.4-11)$$

To have a single input – single output (SISO) system, also eliminating the additive disturbance, it is obtained the matrix $G(s)$.

$$G(s) = \mathbf{i}_{inv\ dq}(s)/\mathbf{v}_{dq}(s) = \frac{1}{L_{f1tot} \cdot s} \cdot \begin{bmatrix} 1 & 0 \\ 0 & 1 \end{bmatrix} \quad (2.4-12)$$

A proportiona integral (PI) controller is used to obtain the voltage reference from the error between the reference current and the measured one at the output of the inverter.

$$K_i(s) = k_{p_i} + \frac{k_{i_i}}{s} = \frac{s \cdot k_{p_i} + k_{i_i}}{s} = k_{p_i} \cdot \frac{s + \frac{k_{i_i}}{k_{p_i}}}{s} = k_{p_i} \cdot \frac{s + \omega_z}{s} \quad (2.4-13)$$

A medium time delay $\tau_d = 1.5/f_s$ due to the discrete-time operation is considered. f_s represents the frequency of samplings. In the case under

consideration, it's value is $f_s = 2 \cdot 18 \text{ kHz}$. The Laplace function with added the effects of the delay is [55]

$$\mathcal{L}(f(t - \tau_d)) = \mathcal{L}(f(t)) \cdot H_d(s) = \mathcal{L}(f(t)) \cdot \frac{1 - \frac{\tau_d \cdot s}{2}}{1 + \frac{\tau_d \cdot s}{2}} \quad (2.4-14)$$

The cascade of all transfer functions gives the current open loop transfer function.

$$H_{ol_i}(s) = K_i(s) \cdot H_d(s) \cdot G(s) \quad (2.4-15)$$

A damping value bigger than $\zeta \geq 0,5$ is mandatory to ensure negative feedback and system stability. The proportional gain k_{p_i} determines the crossover frequency and the bandwidth of the current regulator. This must be smaller than the converter's bandwidth that is set at $p_{conv} = -1/\tau_d$. To have $H_{ol_i}(s)$ calculated at the crossover pulsation ω_c with a Bode plot that falls with a slop of -20 db for frequency decade guarantees the stability and a phase margin $pm \geq 45^\circ$.

$$H_{ol_i}(s \rightarrow j \cdot \omega_c) = \frac{k_{p_i}}{j \cdot \omega_c} \cdot 1 \cdot \frac{1}{L_{f1tot}} = 1$$

Choosing the crossover pulsation equal to

$$\omega_c = \frac{1}{\tau_d} = \frac{f_s}{1,5}$$

and so, working with critical damping $\zeta = 0,5$ and $pm = 45^\circ$, the proportional gain is set as

$$k_{p_i} = \frac{f_s}{1,5} \cdot L_{f1tot} \quad (2.4-16)$$

Subsequently, the regulator's integrator gain must be set having into account the design rule

$$k_{i_i} \geq 2 \cdot k_{p_i} \cdot \omega_1 \quad (2.4-17)$$

where ω_1 is the fundamental frequency.

In closed loop, the zero of the regulator $\omega_z = \frac{k_{i_i}}{k_{p_i}}$ of the equation (2.4-13) attracts the closed loop poles to the right half plane of the complex-plane. The gain has to move the main zeros of the PI controller as far as possible from the right half-plane by identifying the critically. For this reason, it is chosen a value of [34]

$$k_{i_i} = 2 \cdot k_{p_i} \cdot \omega_1 \quad (2.4-18)$$

Using the expressed data, the gains have the values of

$$k_{p_i} = 0,384$$

$$k_{ii} = 241$$

A v_{dq} voltage feedforward is added to provide a filtered value of the main grid component to improve the initial transient and an active damping action k_{ad} based on capacitor voltage derivative term. To make this feedforward, should be added the value

$$v_{ff\ dq}(s) = s \cdot k_{ad} \cdot v_{dq} \quad (2.4-19)$$

To avoid the introduction of a derivative term in the system, it is preferable to replace v_{dq} as done in the equation (2.4-10).

$$v_{dq} = \frac{1}{s \cdot C_{ftot}} \cdot (i_{inv\ dq} - i_{dq})$$

In this way the additional feedforward term is

$$v_{ff\ dq}(s) = k_{ad} \cdot \frac{i_{inv\ dq} - i_{dq}}{C_{ftot}} \quad (2.4-20)$$

The value of the active damping gain has been calculated according to the equation (2.3-5)

$$k_{ad} = \frac{2}{3} \cdot T_s = 18,5 \cdot 10^6$$

Figure 2.4-3 represents the current's control loop block diagram.

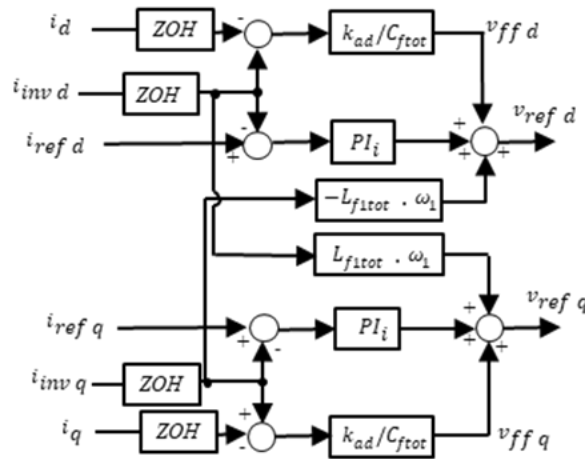


Figure 2.4-3 Current's control loop block diagram.

There is the physical limit of maximum voltage dispensable which depends on the supply DC voltage at the input of the converter. This means that the output of the current controller must be limited to the maximum voltage dispensable by the converter. A saturator block is added to limit the output. Moreover, an Anti-Windup loop is implemented to prevent that during the saturation event the integral part of the PI controller accumulates excess error which must therefore be disposed of. The

controller $K(s)$ can be split into a proper direct feedthrough term k_d and a feedback transfer function $k_{fdb}(s)$

$$K = k_d + k_{fdb}(s) \quad (2.4-21)$$

For a PI controller their values are [56]

$$\begin{cases} k_d = k_p \\ k_{fdb}(s) = \frac{-\frac{k_i}{k_p}}{s + \frac{k_i}{k_p}} \end{cases} \quad (2.4-22)$$

The generated reference voltage $v_{inv dq}$ is limited by the actual present DC-link's voltage, so it is saturated according to have a module value within

$$|v_{dq sat}| = \pm \frac{v_{DC}}{\sqrt{3}} \quad (2.4-23)$$

This value represents the projection of the DC-link voltage in the dq frame.

Because the component in the d-axis voltage $v_{ref d}$ provides the active power P , the d-axis saturation voltage component $v_{d sat}$ has a priority respect the one in the q-axis $v_{q sat}$. According to this, two different saturations references are applied:

$$\begin{cases} v_{d sat} = \pm \left| \frac{v_{DC}}{\sqrt{3}} \right| \\ v_{q sat} = \pm \sqrt{\left(\frac{v_{DC}}{\sqrt{3}} \right)^2 - v_{d sat}^2} \end{cases} \quad (2.4-24)$$

By introducing the Anti-windup mechanism, the control schematic block becomes the following shown in Figure 2.4-4.

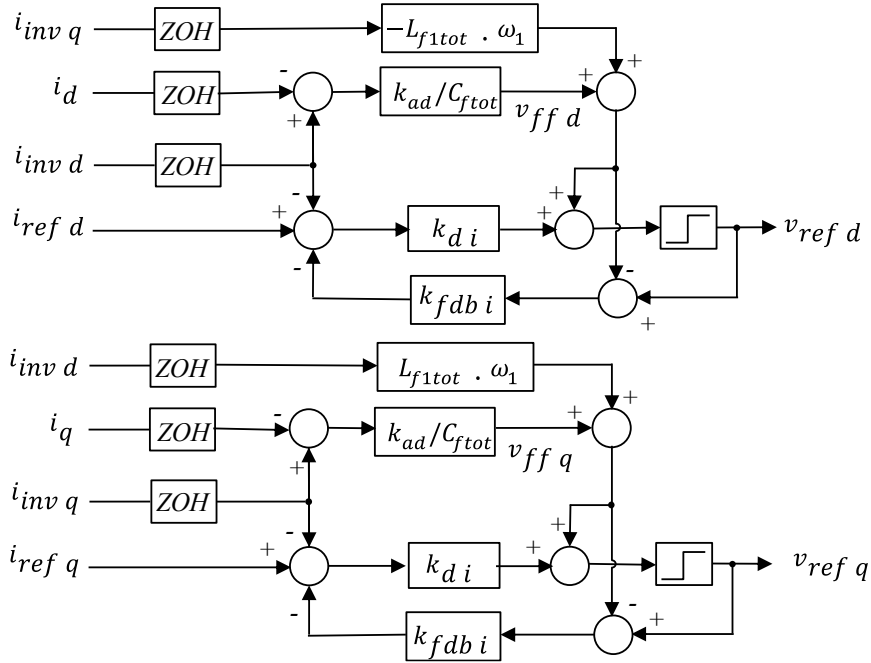


Figure 2.4-4 Current's control loop block diagram with saturators and anti-windup.

The model is validated through a simulation where a step change is made for the current references in both axes $i_{ref dq}$:

- the starting dq current values are

$$i_{ref d}(t = 0 s) = 10 A$$

$$i_{ref q}(t = 0 s) = 10 A$$

- at time $t = 0,5 s$ a d-axis reference current step is applied

$$\Delta i_{ref d} = 50\%$$

- at time $t = 1 s$ a q-axis reference current step is applied

$$\Delta i_{ref q} = 50\%$$

Results are shown in Figure 2.4-5 for the variation of the d-axis reference current and in Figure 2.4-6 for the variation of the q-axis reference current. Reference values are in red while the measured ones are in green.

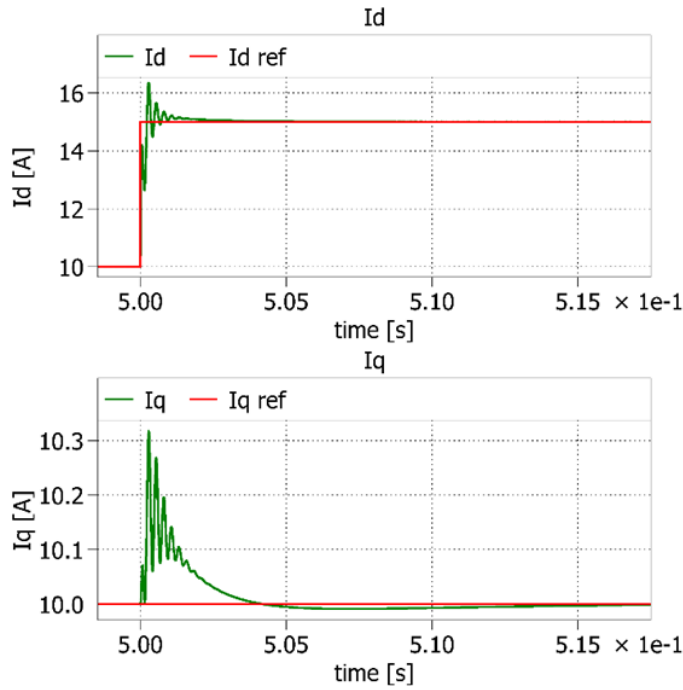


Figure 2.4-5 Plot of currents for a 50% step variation of the d-axis reference current.

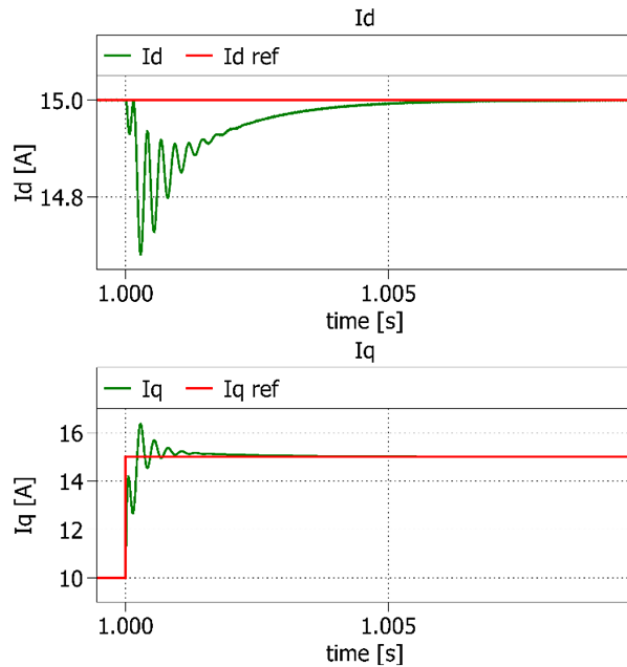


Figure 2.4-6 Plot of currents for a 50% step variation of the q-axis reference current on the right.

The reference values are reached in short time. It's possible to note that during the dynamic in one axis the cross-coupling terms cause some transitory oscillations in the other axis.

2.5 DC-link control

The DC system is composed of the PV power sources connected in parallel to the string converter with common DC link. Each inverter has a capacitance of 1 mF , resulting in a total capacitance of the string inverter of $C_{DCtot} = 20\text{ mF}$.

The overall DC structure is shown in Figure 2.5-1.

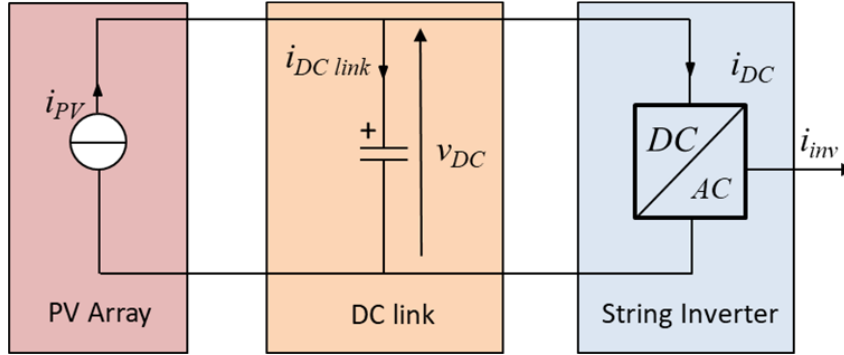


Figure 2.5-1 Equivalent DC system arrangement.

The current supplied by the photovoltaic panels i_{PV} passes through the DC-link which is an electrical energy accumulator that supplies or absorbs power when the power generated by the PV is respectively bigger or smaller than the AC power demand of the grid. So, the current that flows in the DC-link is

$$i_{DC-link} = C_{DCtot} \cdot \frac{d}{dt} v_{DC} \quad (2.5-1)$$

It causes that not all the current generated by the PV, i_{PV} , enters as input in the converter, i_{DC} , and is turned into i_{inv} AC current in the grid.

$$i_{PV} = C_{DCtot} \cdot \frac{d}{dt} v_{DC} + i_{DC} \quad (2.5-2)$$

The voltage present in the DC link capacitor is the one that the converters receive in input, so that then they can work the PWM regulation. But to make a control using the input converter's current $i_{DC}(t)$ as control action is not straightforward because some non-linearities can be introduced. For this reason, it's better to use an energetic approach. The power configuration is shown in Figure 2.5-2.

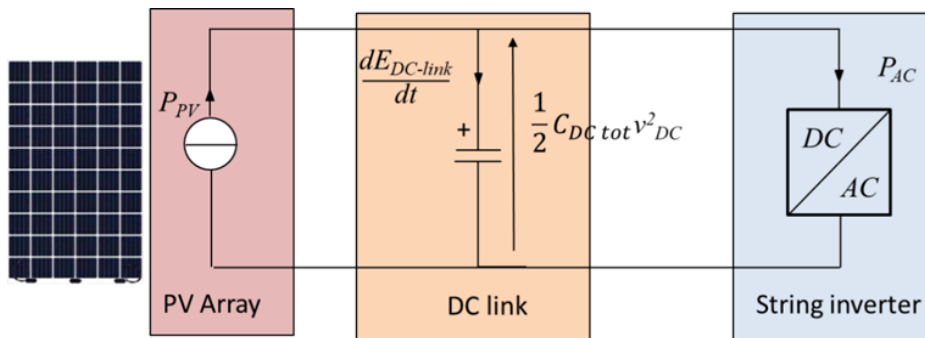


Figure 2.5-3 Equivalent DC system arrangement for power control action.

The square of the voltage v_{DC}^2 is proportional to the energy accumulated in the capacitor and it must be properly controlled to remain at the reference value. For this purpose, the voltage of DC link must be measured. Using $P_{AC}(t) = P_{DC}(t)$ as control action ensures that the system is linear when controlling $v_{DC}^2(t)$

$$P_{PV} = \frac{1}{2} \cdot C_{DCtot} \cdot \frac{d}{dt} v_{DC}^2 + P_{AC} \quad (2.5-3)$$

Another PI controller is used. For the DC link voltage control is a loop external to the current control loop. For this reason, it must have a bandwidth at least smaller than a decade of the bandwidth of the inner loop. In this way, the internal loop can be considered to have unit gain and there is no interference between the two control loops.

The DC controller receives in input the squared voltage of DC link after of being measured and uses a PI controller. The proportional gain k_{pv} is equal to the bandwidth pulsation, while the integral one k_{iv} must be settled according to the limitation of the square voltage when a variation of the PV's power happens. Gains are calculated to have a bandwidth at the frequency of $f_{bandv} = 100 \text{ Hz}$ and a zero at $\omega_{zv} = 25 \text{ rad/s}$.

$$k_{pv} = -2 \cdot \pi \cdot f_{bandv} = -2 \cdot \pi \cdot 100 = -628,3 \quad (2.5-4)$$

$$k_{iv} = k_{pv} \cdot \omega_{zv} = k_{pv} \cdot 25 = -15707,5 \quad (2.5-5)$$

The output is the AC power reference and then the power reference is converted to the d-axis reference current using a division with the voltage amplitude coming from the PLL V_{PLL} . The term $3/2$ is introduced as result of Parke transformation (2.4-3).

$$i_{refd} = \frac{P_{ACref}}{3/2} \cdot \frac{1}{V_{PLL}} \quad (2.5-6)$$

As done for the current loop, a DC link voltage saturator and an anti-windup mechanism are added to the voltage control. The reference power is limited to positive values below the maximum value that can be delivered by string converters. A 20% overload is permitted, $P_{ACsat} = 2,4 \text{ MW}$.

It's important to note that a non-constant v_{DC} causes also that the saturation value of the voltage's references v_{dqsat} in the current loop are not constant. The module of the v_{refdq} is imitated according with the present available DC voltage.

The general block diagram is reported in Figure 2.5-3.

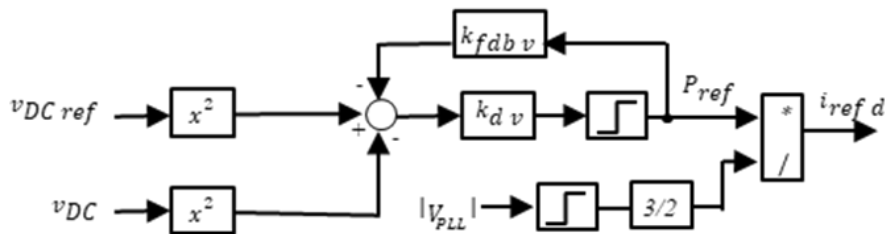


Figure 2.5-4 DC-link voltage's control loop block diagram.

The model is validated through a simulation where a step variation is made for the DC voltage reference.

- The starting values of the DC-link voltage and of the power delivered by the PV are

$$v_{DC-ref}(t = 0 \text{ s}) = 1 \text{ kV}$$

$$P_{PV}(t = 0 \text{ s}) = 0 \text{ W}$$

- At time $t = 0,5 \text{ s}$ a step variation of the PV's power is applied

$$P_{PV} = 1 \text{ MW}$$

- At time $t = 1 \text{ s}$ a step variation of the DC-link reference voltage is applied

$$\Delta v_{DC-ref} = 10\%$$

The plot of the DC-link voltage in green and its reference in red is reported in Figure 2.5-4.

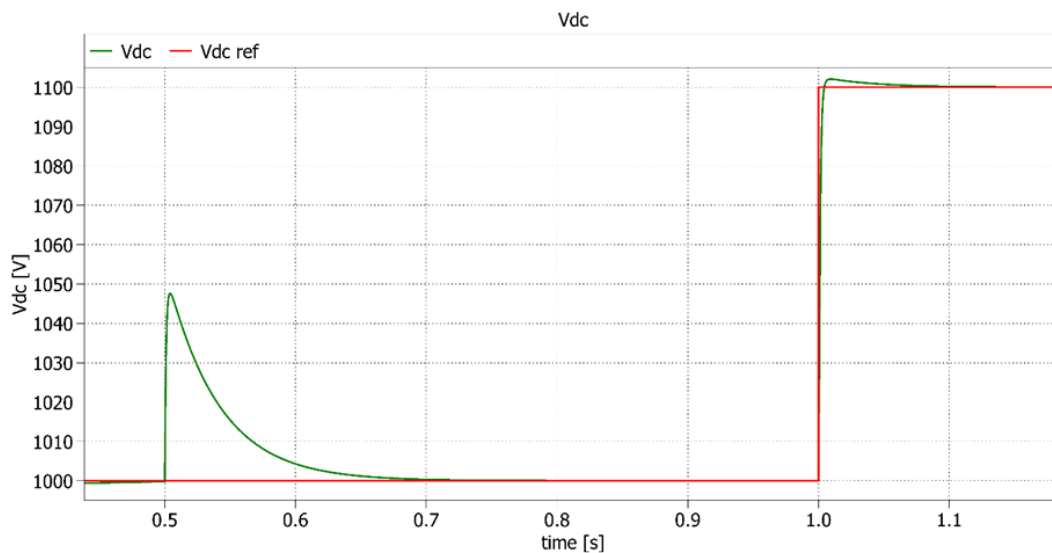


Figure 2.5-5 Plot of DC voltage for a step PV's power of 1MW and 10% step variation of the DC voltage's reference.

At the time of the PV's power introduction, the DC-link starts charging and its voltage grows. Anyway, the control acts to reestablish the reference value.

3 Frequency control with power electronic converter

3.1 Motivation

To assure the power system stability the amount of active power produced by the sources must balance the demand of the loads and restore the nominal frequency to the system. In this way, the change in kinetic energy of the alternators following a load power variation is recovered. This active power support can either come from the mechanical energy of alternators connected to the grid or from the electrical energy stored in the DC-link of converters.

It is wanted that the control of the considered inverters provides inertial support of power systems. The string converter will be connected to the grid using a control strategy that can manage the grid frequency. For this reason, it is good to think of the grid as if it is powered by a synchronous electric machine. According to this, the grid is modelled with a three-phase current source that delivers current $i_{SM abc}$. This allows to have a valid benchmark to test the converter's control when synthetic inertia is introduced in it.

The entire power system looks like in Figure 3.1-1.

R_{load} refers to the request of active power of the grid. The other components are the same used since the Chapter 2.4.

The converter is set in the middle between the PVs and the AC side of the system and in it there is also the equivalent LCL filter, loads and the generation system made by synchronous alternators.

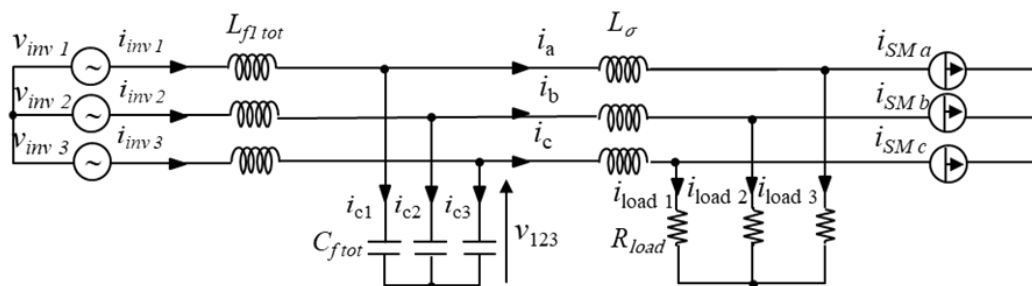


Figure 3.1-1 Entire AC power system: string converter, filter, loads and synchronous alternators in frequency regulation.

The field of work of the converter is in a classic power plant system in which there are loads fed by alternators that work a frequency regulation with their typical slow response. Therefore, it is necessary that the converter could operate following the same dynamics as synchronous generators. For this reason, it is decided to

reproduce a system where the converter operates in parallel with two synchronous machines to supply the loads [57].

More in detail, it's chosen to use two identical isotropic synchronous machines ($L_d = L_q = L_s$) with constant excitation delivered by permanent magnets, with a nominal power of $P_n = 2 \text{ MW}$. It is chosen to use a reference dq frame rotating at the speed of the grid ω and with a direct d-axis in the direction of the magnetic flux.

Considering a nominal voltage of $V_n = 460 \text{ V}$, the nominal magnet flux of the machines has value

$$\lambda_m = \frac{V_n \cdot \sqrt{2}}{2 \cdot \pi \cdot f_1} = 2,071 \text{ V} \cdot \text{s} \quad (3.1-1)$$

From the base impedance Z_b , are calculate the value of stator's resistance and inductance.

$$Z_b = (V_n \cdot \sqrt{3})^2 / P_n = 0,317 \ \Omega \quad (3.1-2)$$

$$R_s = 0,01 \cdot Z_b = 3,17 \text{ m}\Omega \quad (3.1-3)$$

$$L_s = 0,1 \cdot Z_b / (2 \cdot \pi \cdot f_1) = 0,1 \text{ mH} \quad (3.1-4)$$

The equations that describe the synchronous machine's behavior are expressed below. Subscripts s and r indicate stator or rotor membership respectively.

$$\begin{cases} v_d = R_s \cdot i_d + \frac{d}{dt} \lambda_d - pp \cdot \omega_r \cdot \lambda_q \\ v_q = R_s \cdot i_q + \frac{d}{dt} \lambda_q + pp \cdot \omega_r \cdot \lambda_d \end{cases} \quad (3.1-5)$$

$$\begin{cases} \lambda_d = L_d \cdot i_d + \lambda_m \\ \lambda_q = L_q \cdot i_q \end{cases} \quad (3.1-6)$$

$$T_m = \frac{3}{2} \cdot pp \cdot (\lambda_d \cdot i_q - \lambda_q \cdot i_d) \quad (3.1-7)$$

$$T_m - T_{load} = J \cdot \frac{d}{dt} \omega_r \quad (3.1-8)$$

The electrical (3.1-5) and magnetic (3.1-6) equations are used by the model to calculate the currents that must be supplied by the equivalent current sources of $\mathbf{i}_{SM \ abc}$, receiving as input the phase-neuter voltage measured in the stator $\mathbf{v}_s \ dq$. From the estimation of the currents \mathbf{i}_{dq} and the magnetic flux λ_{dq} , the delivered torque T_m is calculated according to equation (3.1-7) [58].

Figure 3.1-2 shows the synchronous machine's schematic block in dq-axes. $\mathbf{X}_0 = \lambda_m$ refers to the initial condition of the integrator.

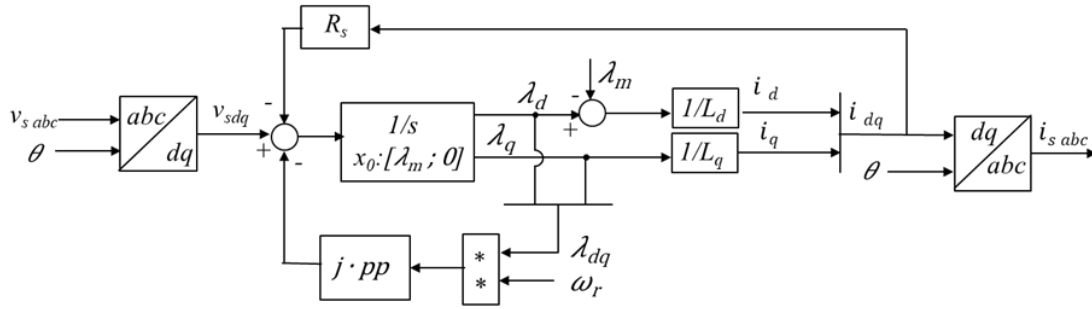


Figure 3.1-2 Synchronous machine's schematic block in dq-axis.

Then, the mechanical equation (3.1-8) provides the mechanical rotor speed ω_r and so also the frequency of the system. Integrating it, the useful angle to perform the rotational transformation of the machine's reference axes in the electrical frame. By integrating the mechanical equation and simplifying it by substituting:

- nominal values of the motor torque

$$T_m = \frac{P_n}{\omega_n}$$

- null load torque

$$T_{load} = 0 N$$

- nominal frequency

$$f_1 = 50 Hz$$

- constant acceleration from a standing start up

$$\omega_0 = 0 rad/s$$

- final speed equal to the nominal speed

$$\omega_n = 2 \cdot \pi \cdot f_1$$

the alternator's inertia J is calculated according to the equation

$$J \cdot (\omega_n - \omega_0) = J \cdot 2\pi \cdot f_1 - 0 = (T_m - T_{load}) \cdot T_a \approx \left(\frac{P_n}{\omega_n} - 0\right) \cdot T_a \quad (3.1-9)$$

$$\rightarrow J = T_a \cdot \frac{P_n}{(f_1 \cdot 2\pi)^2} \quad (3.1-10)$$

These machines have the slow dynamics of frequency regulation performed by steam turbines:

- (SM2) takes part in both the first and second frequency regulation,
- (SM1) takes part only in the first frequency regulation.

The schematic block describing their frequency's control dynamics is shown in Figure 3.1-3 for both machines.

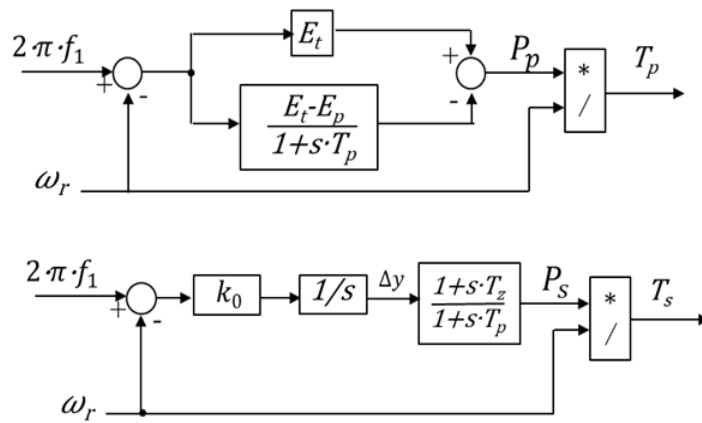


Figure 3.1-3 Block diagram describing the frequency's control dynamics of the machine in first regulation only (upper) and of the one in secondary too (lower).

They are similar to those used in Chapter 1.1 but they don't work with values in p.u. . As input they receive, the error between the nominal speed and the measured rotor speed. Then, the mechanical power values delivered by the machines, P_p for SM1 and P_s for SM2, are returned as output. Finally, dividing by the rotor speed the delivered mechanical torque values are obtained.

The values of the permanent and transient droops and the values of the regulator time constants used for the machines in the simulation are in Table 3.1-1.

	T_p	T_z	b_T	b_p
	[s]	[s]		
SM1 and SM2	10	2,5	0,2	0,05

Table 3.1-1 Data of the droops and time constants of the synchronous machines used in the simulation.

The turbine's regulated permanent and transient energies are calculated as done in equations (1.1-4).

$$\begin{cases} E_p = P_n / (b_p \cdot f_1) \\ E_t = P_n / (b_T \cdot f_1) \end{cases}$$

The following values in Table 3.1-2 are chosen for the synchronous machines to perform the simulations:

	P_n [MW]	J [W · s ²]	T_a [s]	E_p [kJ]	E_T [kJ]
SM1 and SM2	2	202,6	10	800	200

Table 3.1-2 Data of synchronous machines for the simulation.

For the secondary frequency regulation, acted by SM2, are also used the approximate time constant of the regulator T_0 , the energy of rotating loads E_c . From them the gain of the regulator k_0 is obtained. Its value is calculated as the equation (1.1-12).

$$k_0 = (E_p + E_c)/T_0$$

Table 3.1-3 reports the chosen values for the machine in secondary regulation in the simulation.

	T_0 [s]	E_c [kJ]	k_0
SM2	40	20	20,5

Table 3.1-3 Data of the synchronous machine in secondary regulation used in the simulation.

3.2 Power reference generation

The converter, by definition [59], is an amplifier designed to continuously transform one or more electrical quantities in the required form.

It is considered as a non-dissipative component because, if well designed, the level of magnitude of the losses is much lower than the power converted when working at the nominal load.

It is sized to absorb electrical energy from an external source in an efficient and immune manner, that means without inducing additive dissipation in the source circuit as well as without being affected by static and dynamic non-idealities of the same.

In addition, it can operate in a compatible mode with the external environment, meaning without inducing electromagnetic stress in the surrounding environment. In this way, the operating system of all electrically interconnected systems operating in the same electromagnetic environment, where the converter is located, is unchanged and there are no mutual electromagnetic stresses between them.

Having made these considerations and applying them to the case of the DC/AC converter in question, there is the necessity to connect together the DC world, the

power source that feeds the converter, and the AC world, the output that contributes to supply the loads working in the grid. The control loops must also be connected to each other to control the whole operation of the converter.

When the photovoltaic panel produces a certain amount of power, this is fed into the converter. This power is managed by the DC control loop by controlling the square DC-link voltage of the converter. By using a power balance, it is possible to determine how much power can be delivered by the AC side and thus delivered to the grid.

$$P_{PV} = \frac{d}{dt} E_{DC-link} + P_{AC} \quad (3.2-1)$$

where:

- P_{PV} is the power supplied by the photovoltaic panels and it's the only power source of the DC-link;
- $E_{DC-link}$ is the actual DC-link energy of the converter;
- P_{AC} is the power required by the grid, coinciding with converter's DC input power. Obviously, this will have to be saturated to the maximum power value of the string converter, which is $P_{AC sat} = 2,4 MW$.

The DC voltage control it is used receiving as input the energy's values, simply multiplying the square voltages inputs for half of the total capacitance value C_{DCtot} . Then, the DC voltage v_{DC} is calculated knowing load power's value and the power delivered by the PV.

$$v_{DC} = \sqrt{\frac{2}{C_{DCtot}} \cdot \int (P_{PV} - P_{DC}) dt} \quad (3.2-2)$$

The schematic block for the calculation of the DC-link energy and voltage is in Figure 3.2-1. Then it will be used for the generation of the energetic inputs of the DC control regulator.

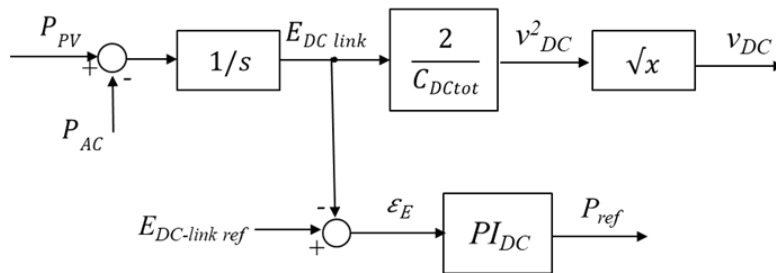


Figure 3.2-1 DC-link voltage and energy calculation schematic block and energetic inputs for the DC voltage control.

Following the described idea, the DC control structure is modified as in Figure 3.2-2.

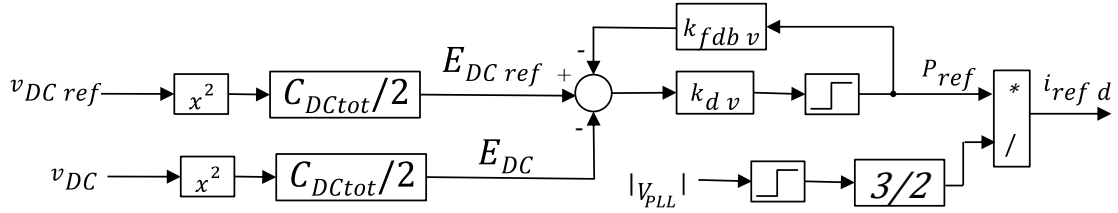


Figure 3.2-2 DC-link voltage control with energetic inputs.

The DC-link voltage control with energetic inputs creates a connection between the DC and the AC side of the converter and generates the value of the reference power.

Assuming that the converter is working ideally, the current DC-link energy varies when the power required by the grid does not coincide with the power generated by the PV system and, as expressed in equation (3.2-2), it is related to the current square DC-link voltage. From the point of view of the grid quality, a low DC-link voltage level results in a limitation of the amplitude of the AC voltage that supplies the grid. On the similar way, from the point of view of the quality of service, an overload or the complete discharge of the stored DC-link energy would lead to an interruption in service.

To avoid these problems, a storage system has been introduced that can accumulate energy or deliver it depending on the energy value of the DC-link and the difference between the power obtained from the PV and the demand of the grid. From the simulations carried out and reported in the following sub-sections, the main limitation is given by the insufficient size of the DC-link capacitance. After a qualitative choice of the various technologies that could be used as storage, it has been decided to introduce Superconducting Magnetic Energy Storage (SMES) system into the simulation. However, whatever type of storage technology is used, it does not change the operation of the converter. The storage is connected to the DC-link and is activated only if the energy level is minimal and it is requested to discharge itself, or the other way round.

The power balance with the introduction of the storage in the system becomes

$$P_{PV} + \frac{d}{dt} E_{storage} = \frac{d}{dt} E_{DC-link} + P_{AC} \quad (3.2-3)$$

where $\frac{d}{dt} E_{storage}$ is the power that is requested at the storage. When it is the condition in which it must be activated, it is requested that the storage exchanges power with the DC-link of the converter.

The equivalent DC system arrangement with the introduction of the storage is in Figure 3.2-3.

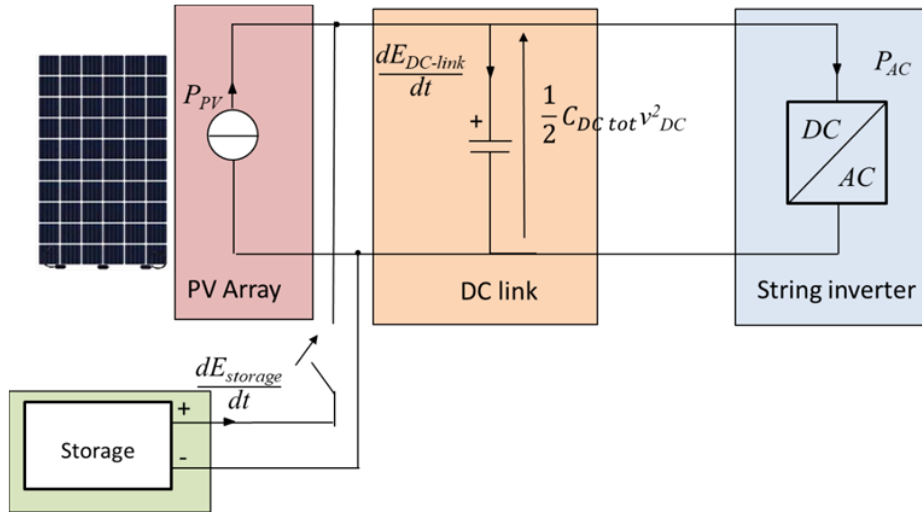


Figure 3.2-3 Storage introduction in the power DC arrangement.

Under these conditions, the power supplied by the storage is commanded to be equal to

$$\frac{d}{dt} E_{storage} = P_{AC} - P_{PV} \rightarrow \frac{d}{dt} E_{DC-link} = 0 \quad (3.2-3)$$

The physical meaning is that the storage provides the amount of necessary power so that the converter can carry on working efficiently without changing its energy level. In practice, power flows from the storage to the DC-link of the converter, which then delivers P_{AC} ensuring the quality of service.

Figure 3.2-4 shows the DC system arrangement and the power flow when the storage is on.

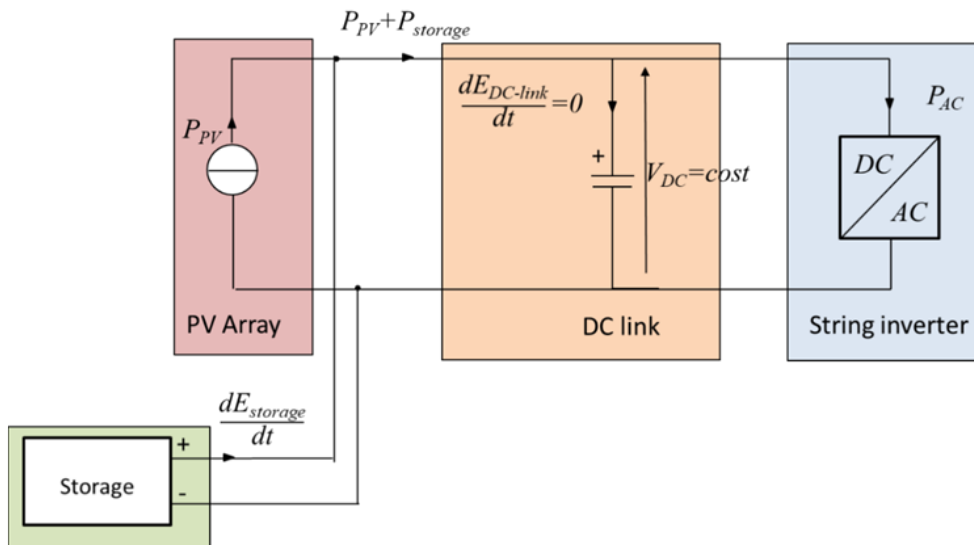


Figure 3.2-4 Power system arrangement with storage in action according with the control strategy.

However, the introduction of the concept of virtual inertia changes the power reference generation performed by the controller. In fact, the control input that generates the power reference is not only the energy error for DC-link voltage

control, but also the virtual inertia energy E_w must be added. For this reason, modifications must be made into the converter's control as shown in the Figure 3.2-5. Please, refer to the next sub-chapter 3.3 to understand how this input is calculated.

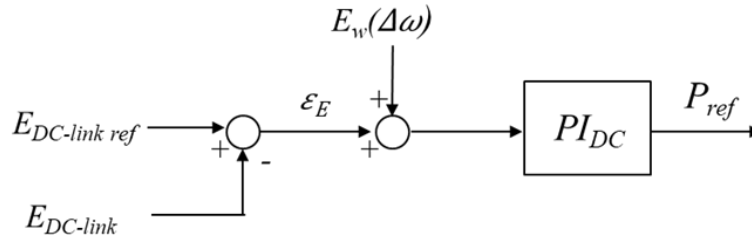


Figure 3.2-5 Emulated inertia energy in the power reference generation.

The reference power generation P_{ref} is affected by the presence of this additional term. While the introduction of storage does not change how the reference power P_{ref} is calculated by the regulator, this additional energetic term E_w is included as an input into the PI controller of the DC-link voltage that generates the reference power P_{ref} , which determines the current reference in d-axis $i_{ref d}$. As E_w depends on the instantaneous difference between the current frequency and the reference frequency, and so between the rotation speed of the synchronous machine and the steady state pulsation, the power reference is dosed as if the converter itself is a synchronous machine. Since it is desired that the converter's exploitation of power should be maximum but never excessive, it is necessary to saturate the regulator output. In addition, the regulating action of the converter is set to be in priority to that of synchronous generators. This means that the synchronous alternators only have to activate their regulation process if the performance limit of the converter is not able to satisfy the power variation required by the system. The aim is to try to avoid the frequency regulation of rotating machines to prevent them from decelerating and thus keep the grid frequency as close as possible to its reference, resulting in an improvement in the quality of service.

The entire control structure of the converter control can be summarised as shown in the Figure 3.2-6.

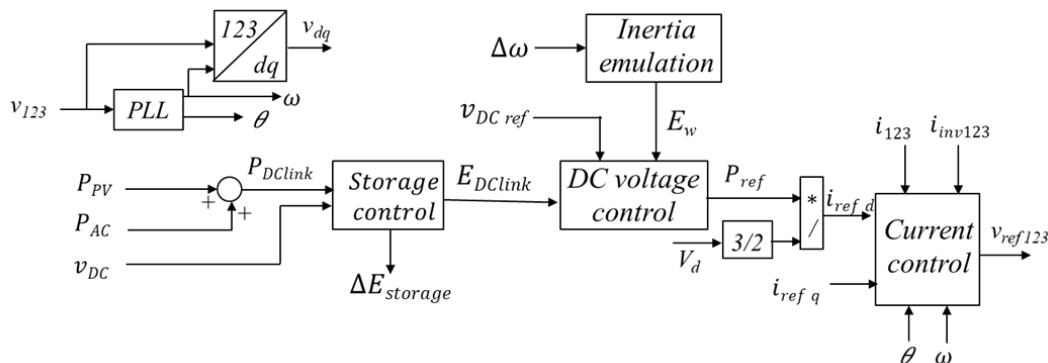


Figure 3.2-6 Schematic block of the entire control structure of the converter control.

The following sub-chapters explain in more detail how these ideas are implemented and what results are obtained from the simulations.

3.3 Modification to the grid control

When the converter makes a frequency regulation, it must be taken into account that in the grid there are already synchronous generators that operate for it. So, the converter must have the sensitivity to the present frequency variation to work together with synchronous alternators. To archive this, the outer control loop must be modified by introducing the energy supplied into the calculation.

A new energy component, E_w , is added to the error between the DC-link reference energy and the energy present at that moment, calculated from the measured voltage on the capacitor. This additional energy is the output of a controller that receives as input the rotational speed error between the reference frequency, constant at 50 Hz, and the current frequency of the synchronous generators.

The gain of the inertial energy branch is calculated from the integration of the mechanical equation (3.1-8) with some simplifications for the torque values .

$$\Delta\omega = \frac{(T_m - T_{load})}{J} \cdot T_{ac} \approx -\frac{1}{J} \cdot \frac{P_w}{\omega_1} \cdot T_{ac} \quad (3.3-1)$$

where:

- P_w indicates the inertial power that is null in the steady state and it's value is proportional at the frequency variation.
- T_{ac} indicates the start-up time of the converter.

From the equation (3.3-1), the inertial power is

$$P_w = -\Delta\omega \cdot J \cdot 2\pi \cdot f_1 / T_{ac} \quad (3.3-2)$$

Integrating this value, the inertial energy E_w is obtained and added to the converter's energy reference. The schematic block that calculates the inertial energy for the power reference generation is in Figure 3.3-1.

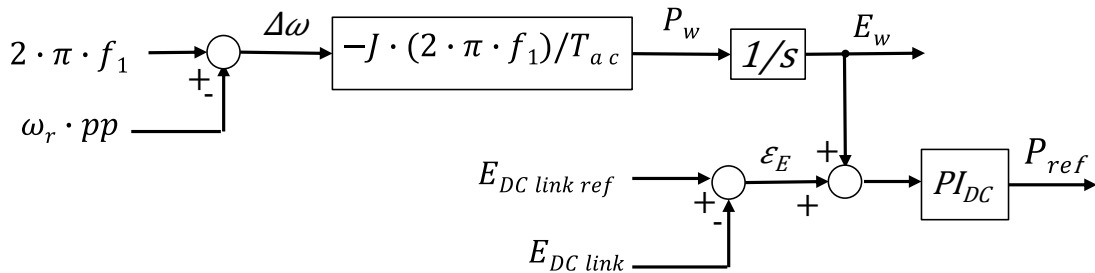


Figure 3.3-1 Inertial energy calculation for the power reference calculation.

An inertia value J equal to the one of the synchronous generators and a starting time of the converter $T_{ac} = 0,25 s$ are used in the simulations.

The complete AC system used in the simulation is represented in Figure 3.3-2.

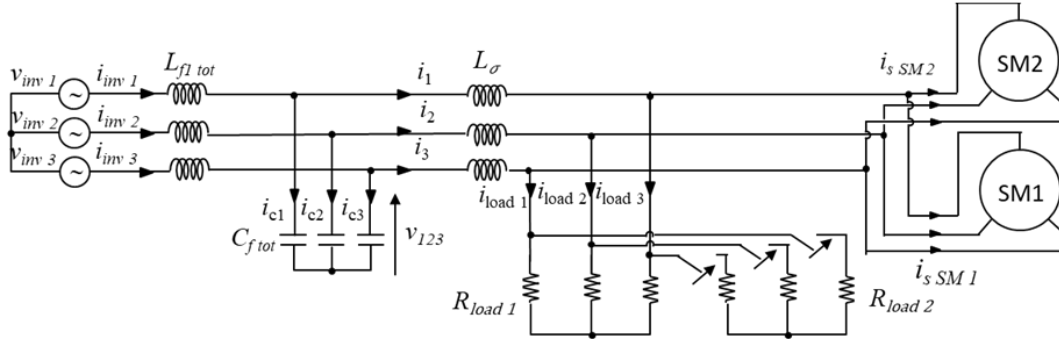


Figure 3.3-2 Complete AC electric circuit: string converter, equivalent filter, short circuit transformer's inductance, load request, synchronous alternator.

The load request is simulated by resistors with resistance equal to

$$R_{load\ 1} = 317\ m\Omega$$

- The initial condition of the DC-link capacitor is to be already charged at the starting voltage reference value.

$$v_{DC\ ref}(t = 0) = 1,1\ kV$$

$$v_{DC}(t = 0) = 1,1\ kV$$

Moreover, the DC-link voltage regulation is always active while the inertial energy's branch is not active at the start.

- At time $t = 0,2\ s$, a step variation of the DC-link voltage reference value is set

$$v_{DC\ ref} = 1,2\ kV$$

- at time $t = 1\ s$, it is set the activation of a power step generated by the PV equal to

$$P_{PV} = 2\ MW$$

- At $t = 1,3\ s$, the branch introducing the inertial energy is activated.
- At time $t = 1,5\ s$, a step variation of the load power is given by connecting another line with resistors of resistance

$$R_{load\ 2} = 158\ m\Omega.$$

Figure 3.3-3 shows the dynamic behavior of the DC-link voltage.

Figure 3.3-4 shows the power requested from the loads and the ones delivered by the converter and synchronous machine,

Figure 3.3-5 shows the rotational speed of synchronous generators, SM2 in green, SM1 in red and converter in blue respectively.

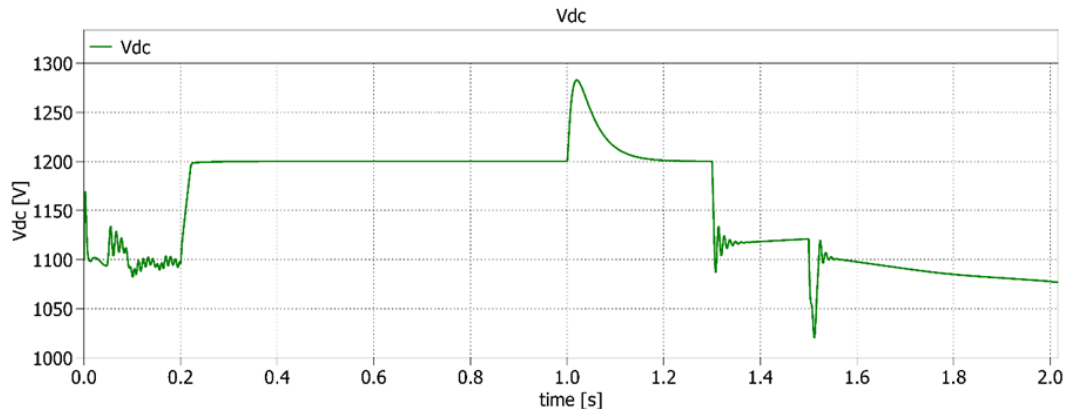


Figure 3.3-3 Dynamic behavior of the DC-link voltage- initial transient.

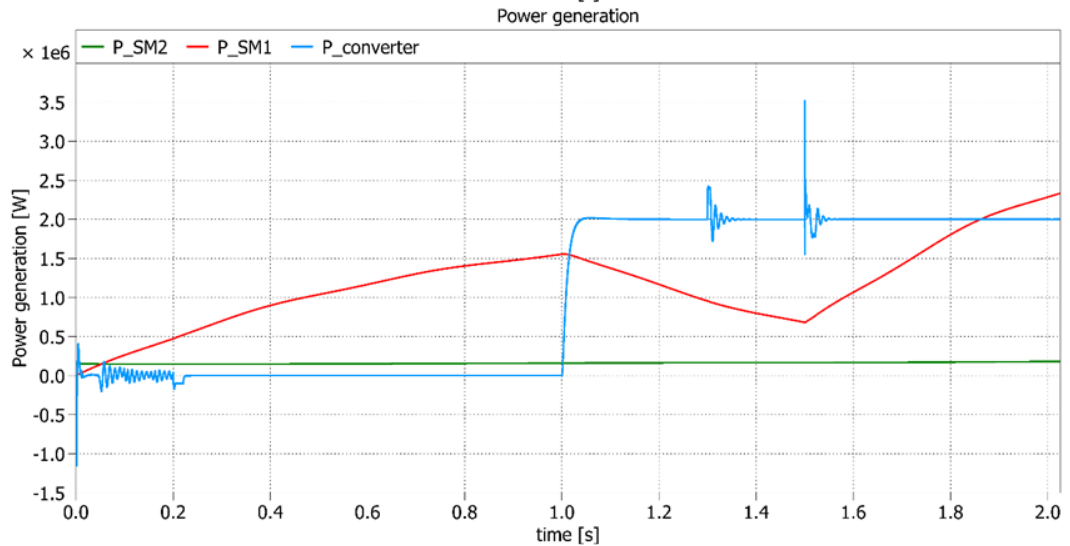
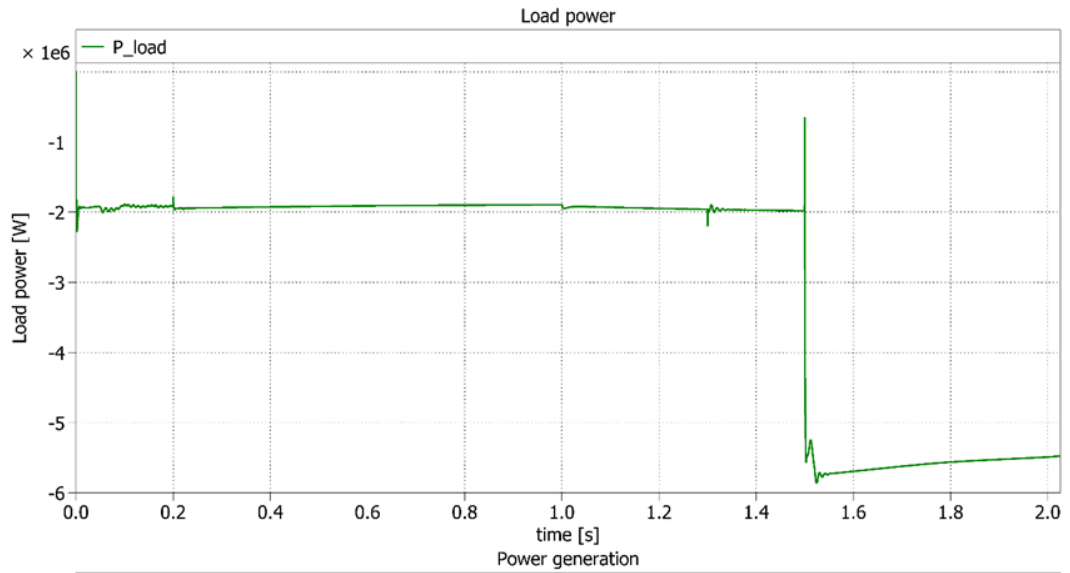


Figure 3.3-4 Dynamic behavior of the load's power and of the sources. - initial transient.

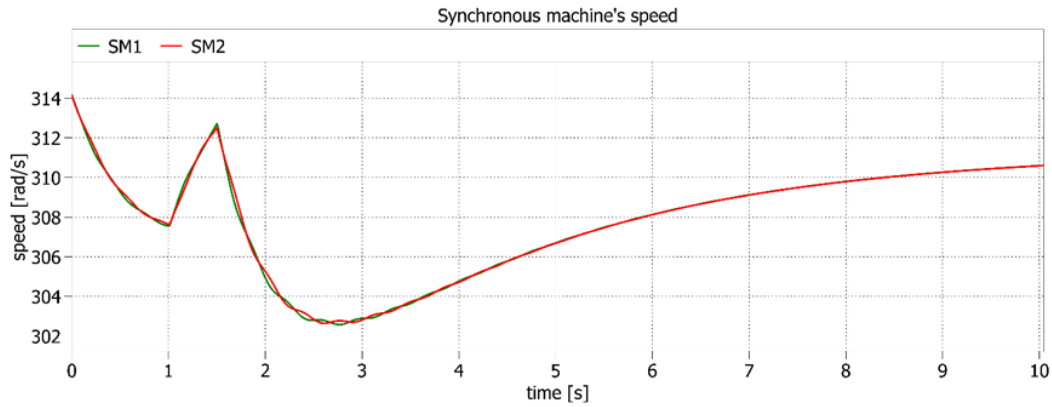


Figure 3.3-5 Mechanical speed measured on both the synchronous machines- initial transient.

Starting to analyze the dynamics of the DC link voltage, in the first few seconds it is observed that the voltage rapidly reacts to the $v_{DC ref} = 1,2 kV$ reference step.

As long as the converter does not receive power from the PV, loads are fed only by the synchronous generators. This creates a decreasing in frequency in an equal mode as in the state of art's frequency regulation.

When power is produced by the PV, synchronous generators are no more alone to supply the loads, but the converter contributes to do it helping to restore the reference frequency. Focusing on the DC-link voltage's dynamic, the DC-link capacitor is charged above the reference. Anyway, the control reacts by restoring the reference value. This dynamic, however, is a problem that must be solved because the plot shows that the voltage can transiently reach unacceptable values. Later, when virtual inertia is introduced, the voltage drops because the converter starts to supply power to the loads, working together with the synchronous generators. However, it tends to rise towards the reference.

The effect of adding an additional component as an energy reference to the converter, at time $t = 1,3 s$, is to request to the converter to take over as much of the required power as possible. In other words, it would like to feed the loads itself, leading to the cancellation of the power supplied by the synchronous generators and to send all the power generated by the PV to the grid. This can be seen from the Figure 3.3-6 representing the trend of the reference power P_{ref} .

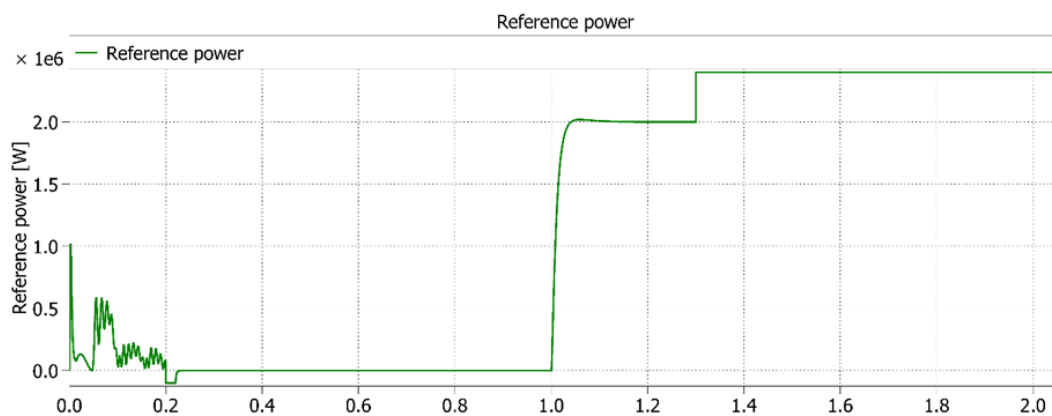


Figure 3.3-6 Dynamic behavior of the converter's reference power- initial transient.

Initially, it can be seen that the reference power P_{ref} coincides with the power supplied by the PV. Once inertial energy is introduced, it is brought to the saturator limit value, set at $P_{AC\ sat} = 2,4\ MW$. The power reference remains saturated for all the time that the synchronous machine participating at the first regulation erogates non-null mechanical power. After this time, the reference power of the power control loop of the converter decreases reaching a value equal to the power developed by the PV at the steady state. It's shown in Figure 3.3-7.

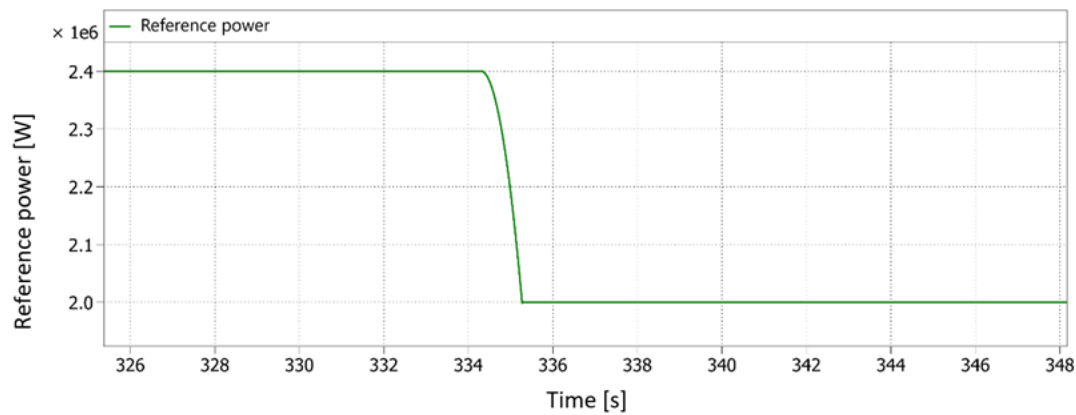


Figure 3.3.7 Dynamic behavior of the converter's reference power- steady state condition.

At the time of the load step $t = 1,5\ s$, again the DC-link voltage falls rapidly. It is important to remember that the AC output voltage of the converter is dependent on the DC voltage. A drop of this voltage would not ensure that the output AC voltage will be of the required amplitude. In fact, as shown in the Figure 3.3-8, representing the peaks of the phase voltages and currents of the load, it is possible to see that voltage's amplitude has the same decreasing behavior of the DC-link's voltage.

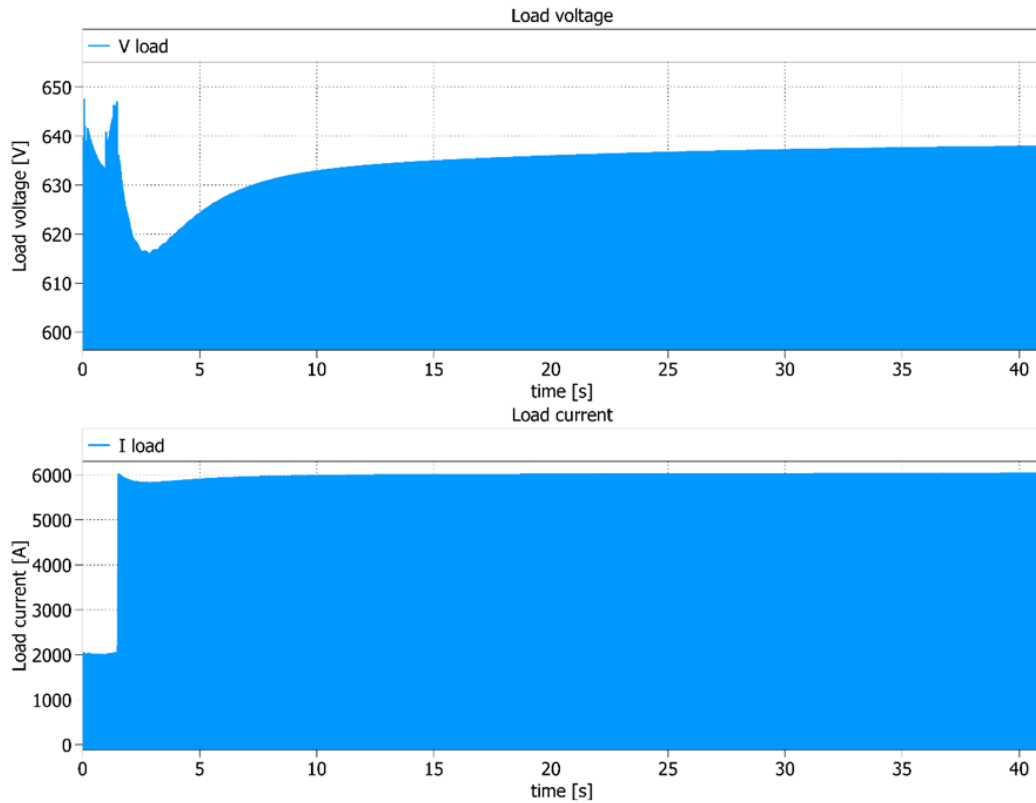


Figure 3.3-8 Dynamic behavior of the phase AC voltage and current.

This voltage drop is only slowed down when the settling time of the converter's power output has elapsed. Synchronous generators react with slower dynamics and this shows that the converter is the first to keep the load request, limiting itself to deliver the power generated by the PV. The explanation of these different load response times is due to the different speeds of the electrical and mechanical variables: synchronous generators react to a mechanical speed variation, while the converter control reacts to a DC-link voltage discharge.

Running a longer simulation, the following results shown in Figure 3.3-9, Figure 3.3-10 and Figure 3.3-11 are given.

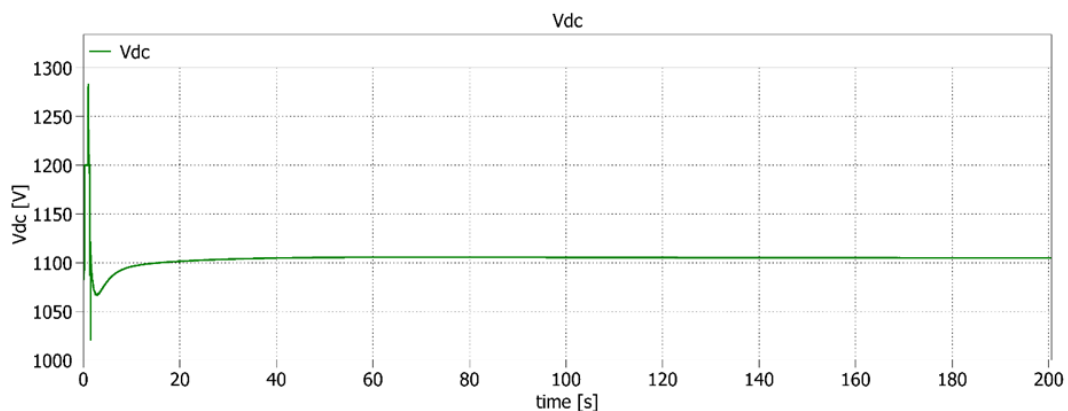


Figure 3.3-9 Dynamic behavior of the DC-link voltage- long time simulation.

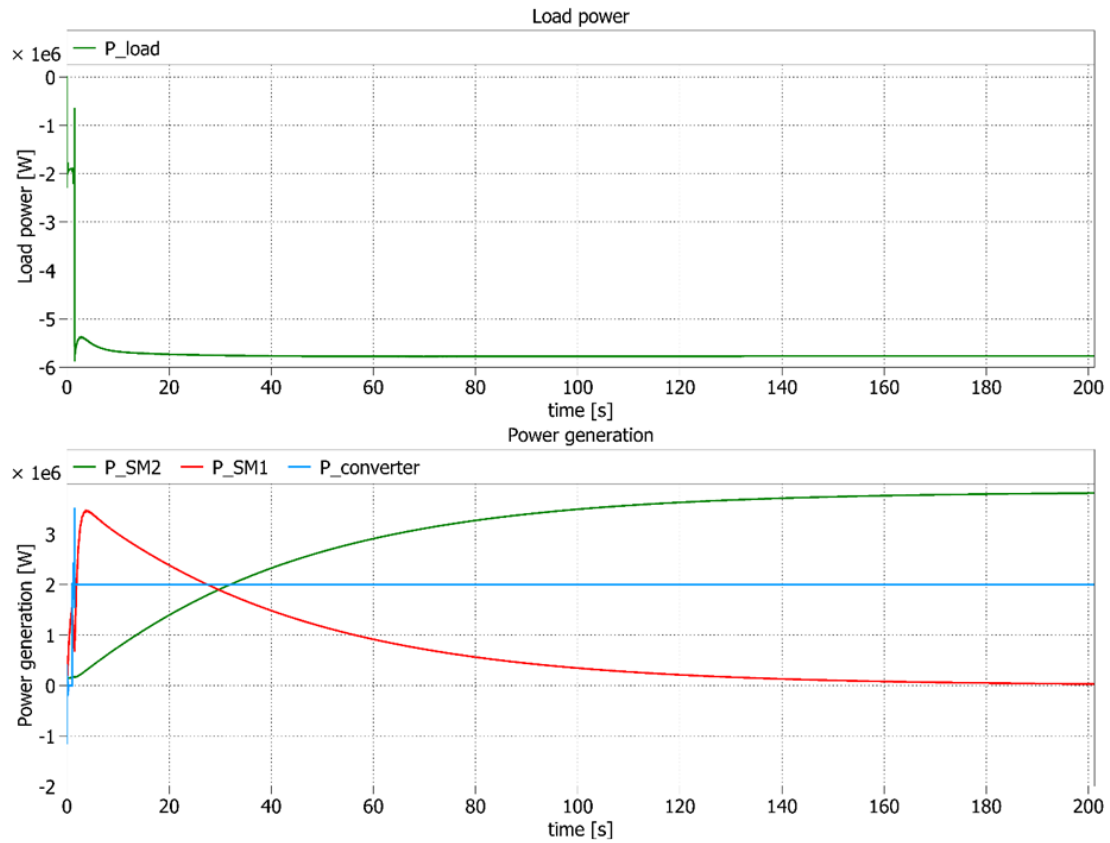


Figure 3.3-10 Dynamic behavior of the load's power and of the sources. - long time simulation.

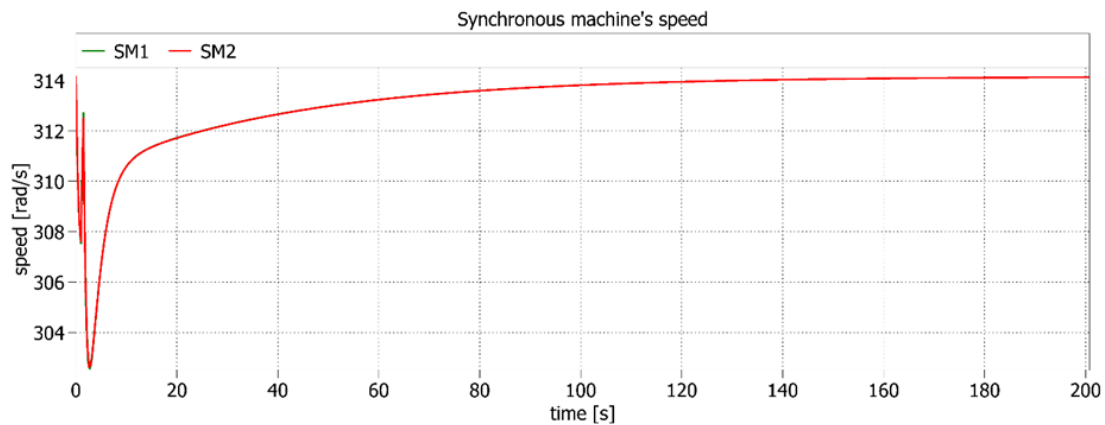


Figure 3.3-11 Mechanical speed measured on both the synchronous machines- long time simulation.

It is immediately observed that the DC-link voltage at steady state does not return to the reference value. This is because all the power supplied by the PV goes to the loads. The variation of energy on the DC-link capacitor is used to power the loads when the alternators have not intervened yet. On the other hand, the introduction of the converter into the system reduces the frequency nadir caused by the power step required by the loads.

Primary and secondary regulation follow their usual dynamics but they only have to supply the power that the PV is unable to provide. Exploitation of the converter under such conditions is maximum. At the steady state, the reference frequency is fully restored.

3.4 Enabling/Disabling state of the storage

As seen in the previous subchapter, once frequency regulation has been introduced to the converter's control, there are still a few points to be solved:

- overvoltage of the capacitor beyond the maximum permissible value at the variation of the power supplied by the PV;
- unacceptable voltage drop at the time of the load request;
- help the converter's insertion into the system, which causes a large variation in the power required from it.

The proposed idea is to introduce an energy storage into the system. This is placed in parallel with the DC-link of the converter and it is activated only when a logical condition is triggered.

First of all, it's evaluated which type of storage is appropriate to solve these problems. The Figure 3.4-1 shows a graph of the working area of the various technologies according to power output and discharging time.

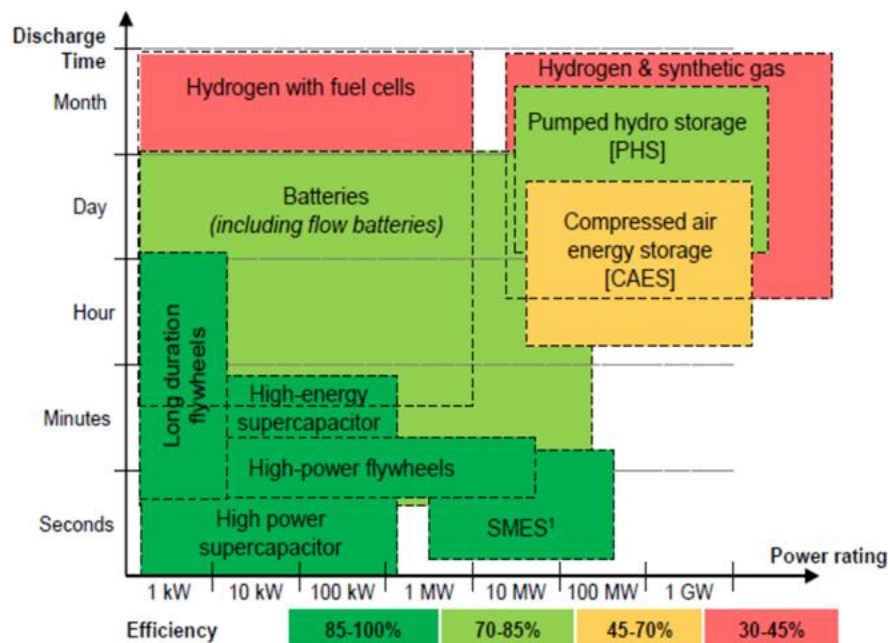


Figure 3.4-1 Working area of storage technologies [60].

The technology that has been decided to use in the simulations is that of a SMES (Superconductor Magnetic Energy Storage) because it is able to supply and receive power at the same level required by the system in consideration, in a short time and with very low losses due to the use of superconductivity material. It stores energy in the magnetic field by sending current into a coil composed of a superconducting material.

As done with the DC-link capacitor, the equation linking the electrical state variable, that in this case is the current fed into the storage, with the change in energy is used to create a model. From this equation it's possible to know the dynamic of the current in function of the power.

$$\int P_{storage}(t) dt = \Delta E_{storage} = \frac{1}{2} L_{storage} i_{storage}^2 \quad (3.4-1)$$

The activation of the device is determined by the state of charge of the DC-link capacitor and the sign of the power required from it [61].

A power balance is carried out at the DC-link point.

$$P_{DC-link} = P_{PV} - P_{AC} \quad (3.4-2)$$

This power is required by the converter, but if an emergency condition occurs, the storage unit is activated to supply or to store the same amount of power by exchanging current with the DC-link capacitor.

The Figure 3.4-2 shows the block diagram of the storage activation control.

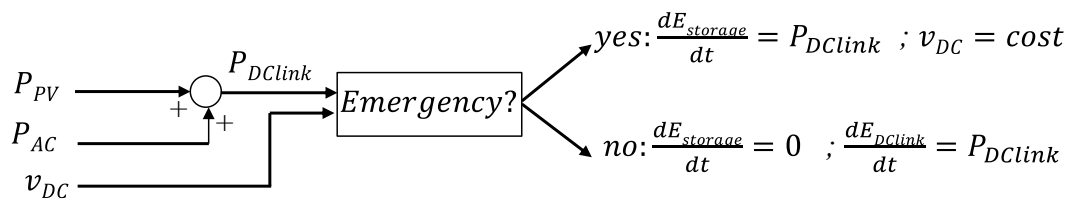


Figure 3.4-2 Schematic block of the storage activation control.

A range between a minimum $V_{DC min}$ and a maximum $V_{DC max}$ values that the capacitor must maintain is chosen. An emergency condition is entered, to store or deliver power from the storage to the converter, respectively, if:

- Storage: The DC-link voltage is at its maximum value and the DC-link is required to store power ($P_{DC-link} < 0$).
- Supply: The DC-link voltage is at its minimum value and the DC-link is required to supply power ($P_{DC-link} > 0$).

In this way, when in emergency, the power demand is allocated to the storage. This power is passed on to the converter, which can work without energy variations, thus keeping the DC-link voltage constant. Using the energy equation (3.4-1) for inductive storage, the current in the storage can be calculated.

A simulation similar to the previous one was carried out, assuming that:

- the storage inductance has a value of

$$L_{storage} = 15 H$$

- initially the storage is already charged with an energy of

$$E_{storage}(t = 0 s) = 2 MJ$$

- the DC-link voltage range is chosen to have values between the maximum and minimum values

$$V_{DC\ min;max} = [1080; 1220]V$$

- at time $t = 60\ s$, it's set another step change of PV's power of

$$\Delta P_{PV} = 200\ kW$$

These values have been chosen because they make the storage's contribution clear.

The results are given below.

Figure 3.4-3 shows the dynamic behavior of the DC-link voltage.

Figure 3.4-4 shows the power requested from the loads and the ones delivered by the converter and synchronous machine, SM2 in green, SM1 in red and converter in blue.

Figure 3.4-5 shows the phase voltage and current in the measuring point.

Figure 3.4-6 shows the rotational speed of synchronous generators.

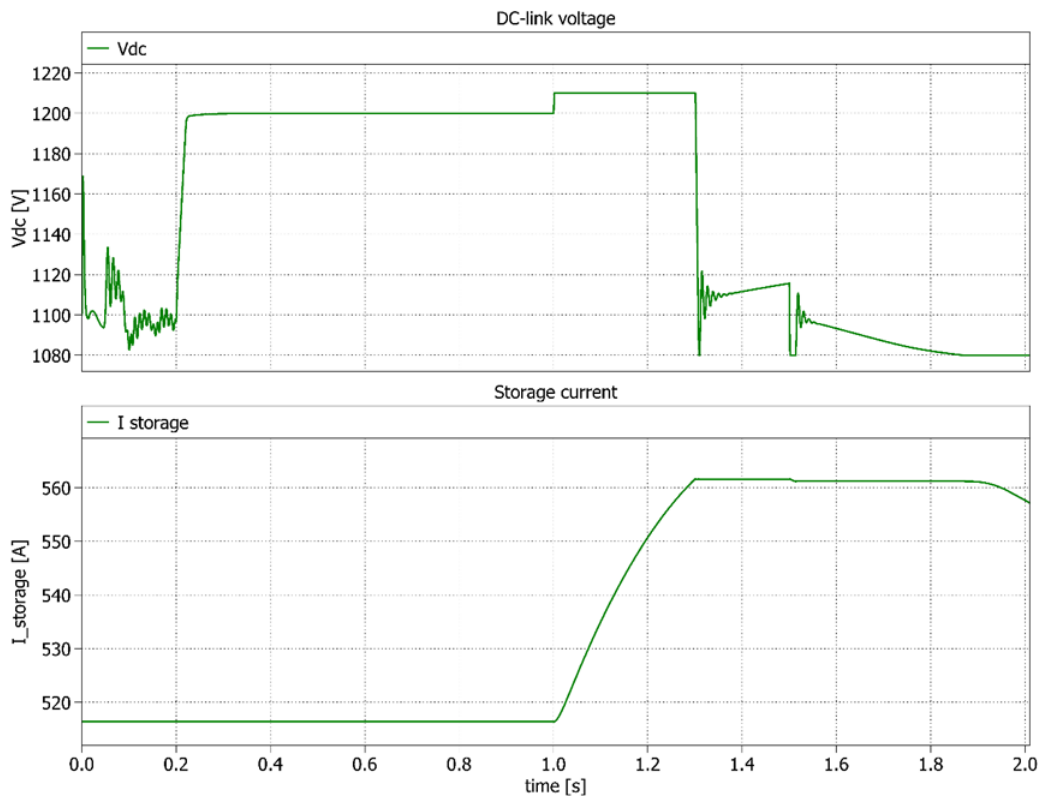


Figure 3.4-3 Dynamic behavior with storage of the DC-link voltage and of the storage's current- initial transient.

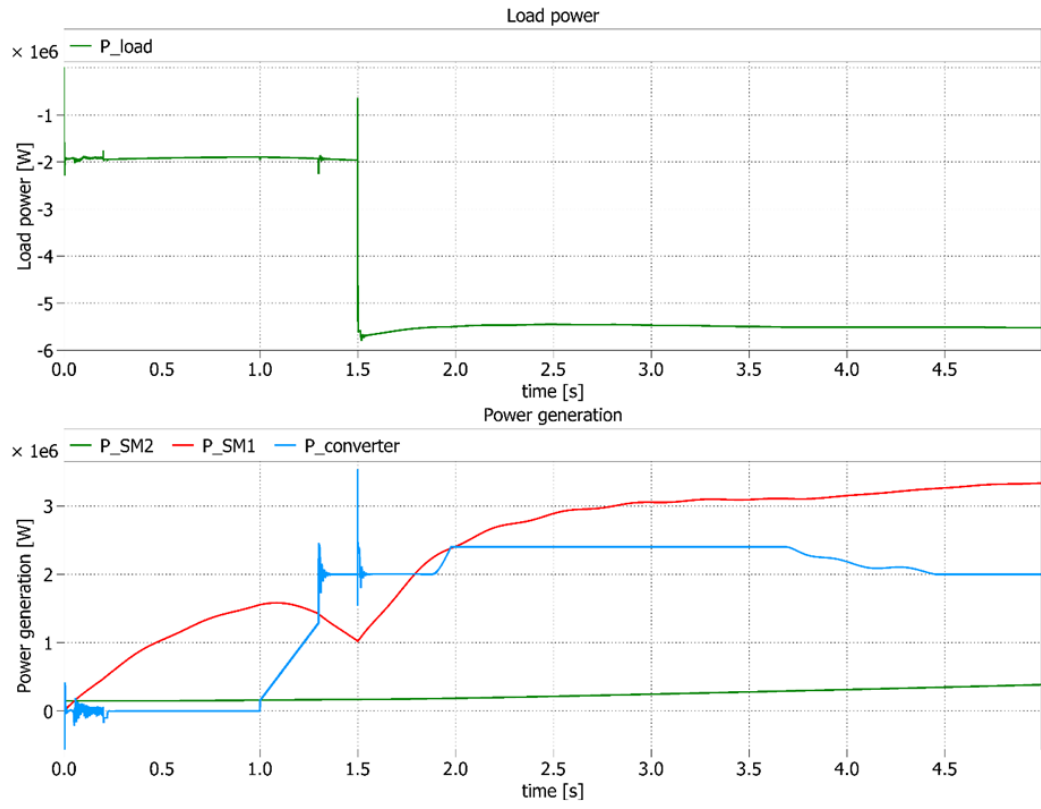


Figure 3.4-4 Dynamic behavior with storage of the load's power and of the sources. - initial transient.

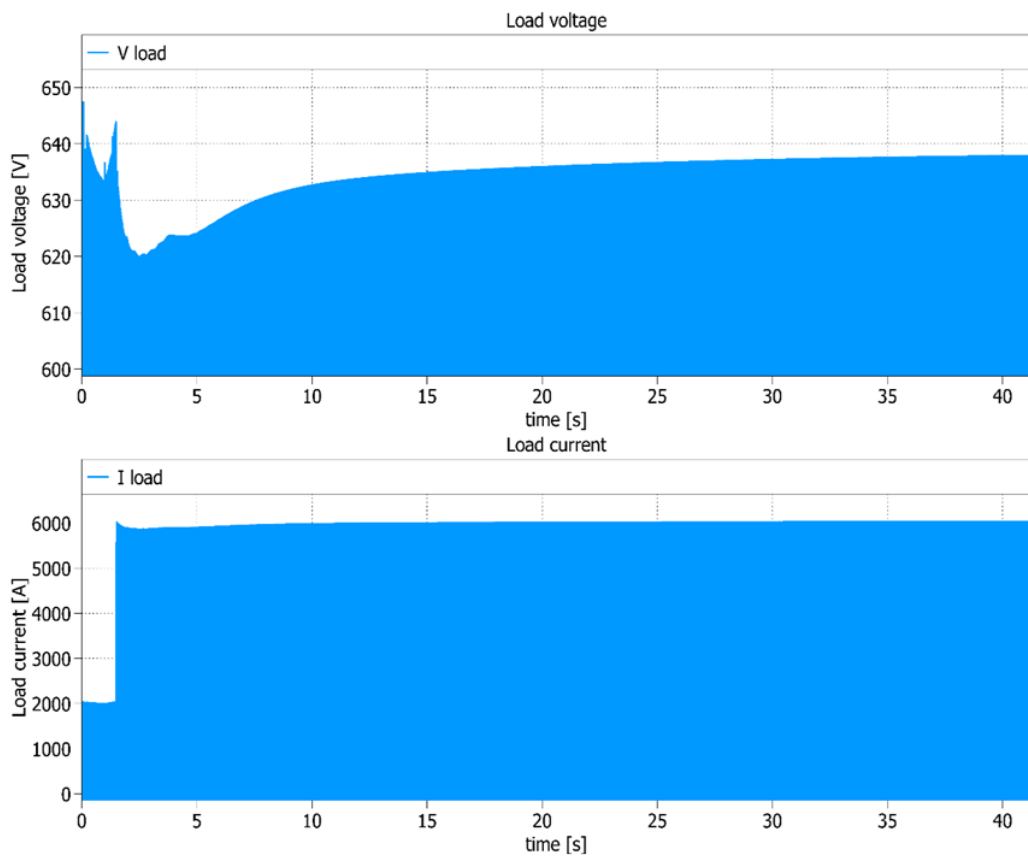


Figure 3.4-5 Dynamic behavior with storage of the phase AC voltage and current.

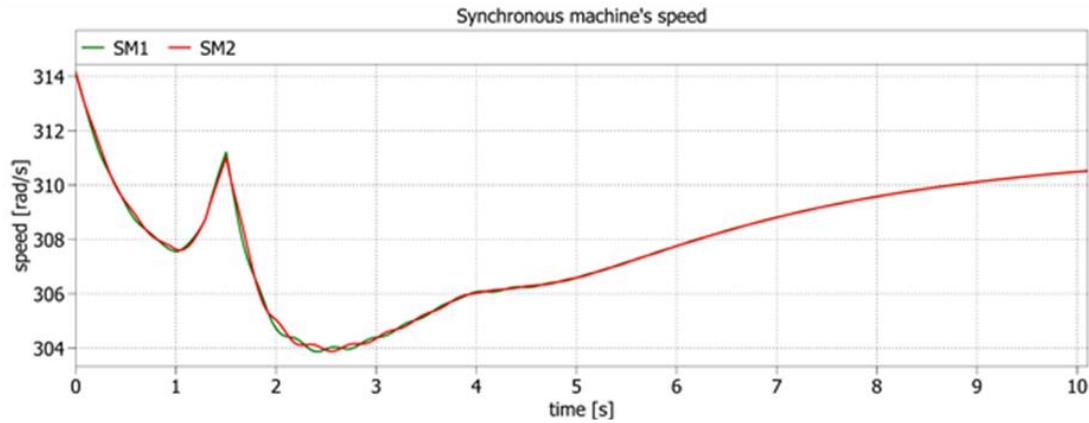


Figure 3.4-6 Mechanical speed measured on both the synchronous machines- initial transient with storage.

Differently of the previous simulation without storage, when the PV starts to deliver power, at $t = 1\text{ s}$, the DC-link voltage is saturated at the maximum value and the excess power is diverted to the storage. Its charge can be observed by the increasing trend of the storage current.

At the same time, it can be seen from the power plot in Figure 3.4-4 that the power supplied by the converter, in blue, is not zero because, if the power given by the PV allows it, the converter still tries to meet the demand of the loads by itself by substituting the action of synchronous generators, which decrease their production. In fact, for $t < 1,3\text{ s}$, the control is still in the time interval where the virtual inertia energy's branch of the converter is not active.

Since the branch that introduces inertial energy is activated, at $t = 1,3\text{ s}$, all the power that is produced by the PV is free to be injected. The storage is no longer charged but, on the contrary, the DC-link voltage drops very quickly as a result of the new power reference. With the storage, however, this drop is limited to the minimum decided value of $V_{DC\ min} = 1080\text{ V}$ because the storage provides power by discharging itself.

The same happens when at $t = 1,5\text{ s}$ the power step variation required by the loads occurs. This has the consequence that the AC voltage of the loads also remains within a certain range. In this example, in fact, the minimum AC voltage amplitude is about $V_{amp} = 620\text{ V}$, higher than in the simulation without storage in Figure 3.3-8.

At time $t = 2\text{ s}$, the DC voltage is saturated to the minimum value again but also the power required by the control reaches the saturation value of $P_{AC\ sat} = 2,4\text{ MW}$. In this case the power supplied by the storage $\frac{d}{dt}E_{storage}$ is also limited.

Finally, from the graph showing the speed of the synchronous machines Figure 3.4-6, it can be seen that the speed nadir is $\omega_{nadir} = 304\text{ rad/s}$, higher than in the case without a converter Figure 3.3-10 of 302 rad/s .

The steady state condition has not changed since the previous simulation.

At time $t = 60 \text{ s}$, another step change of PV's power of $\Delta P_{PV} = 200 \text{ kW}$ occurs. The DC-link voltage and storage's current near the time $t = 60 \text{ s}$ are shown in Figure 3.4-7.

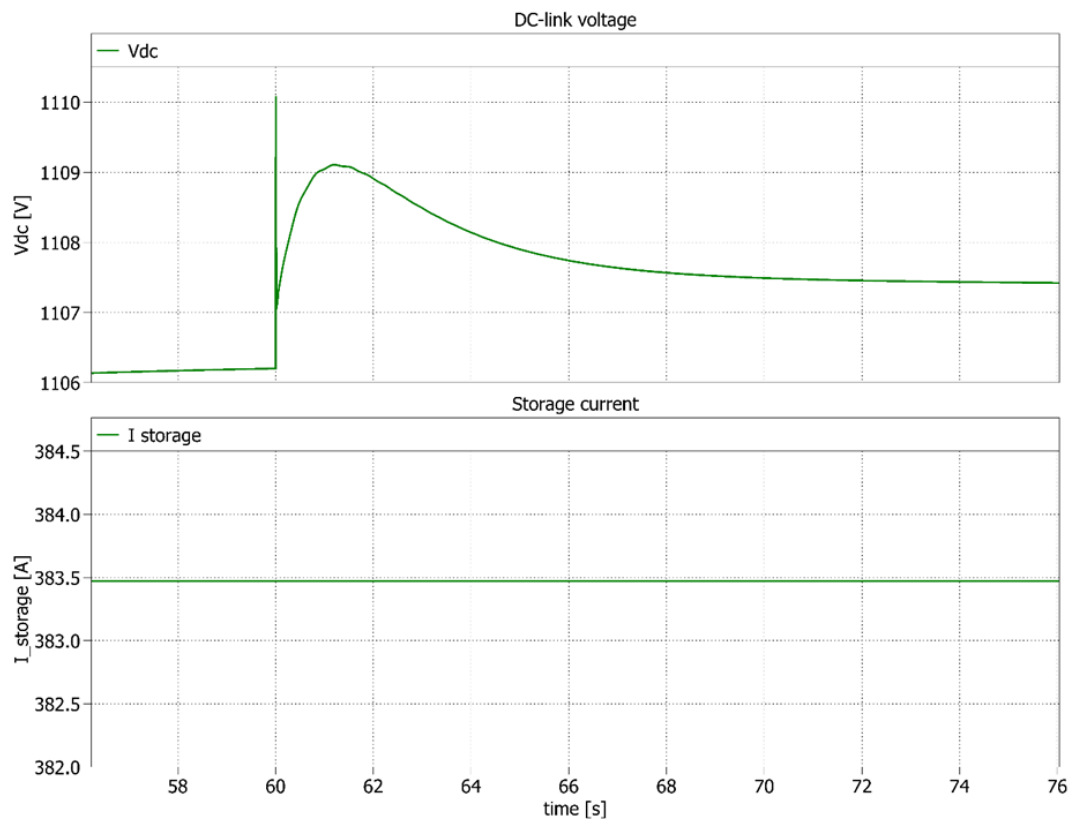


Figure 3.4-7 Dynamic behavior of the DC-link voltage and storage's current- step change of PV's power of 200 kW at time $t = 60 \text{ s}$.

It is interesting to see that if there is a further increase in the power supplied by the PV, the DC voltage is free to increase to a new steady state value without the intervention of the storage. The dual would occur if this PV power has to decrease.

Figure 3.4-8 shows the dynamic behavior of the load's power and of the sources at time $t = 60 \text{ s}$.

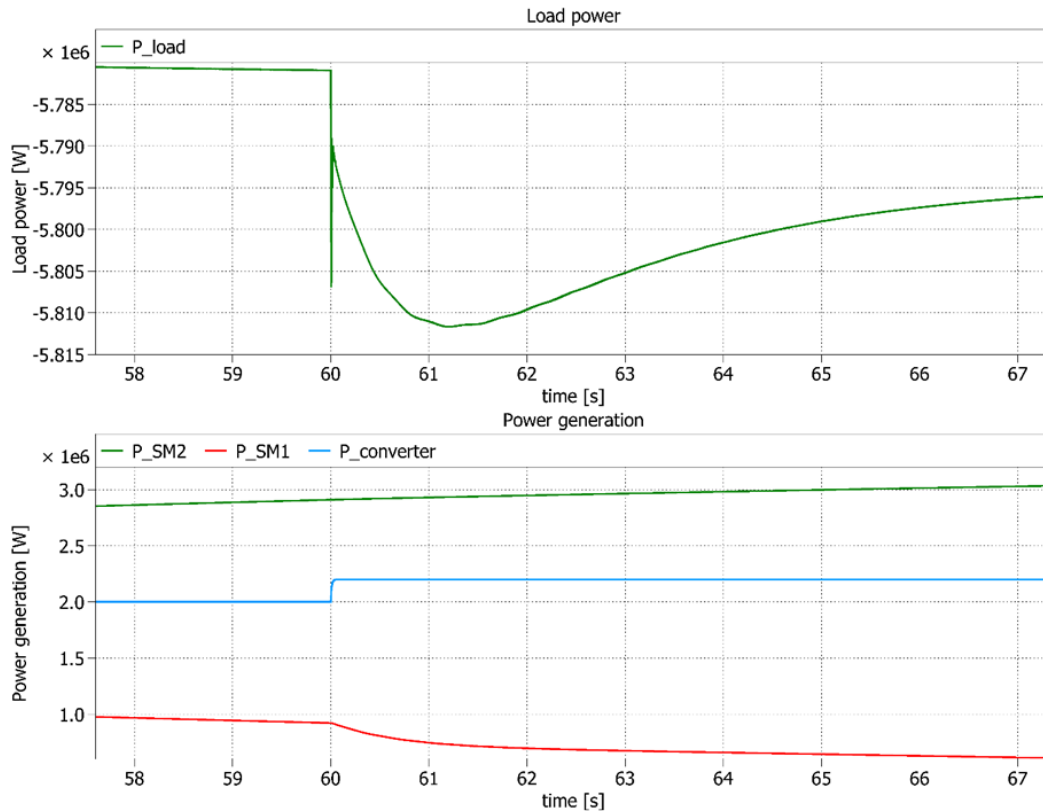


Figure 3.4-8 Dynamic behavior of the load's power and of the sources. - step change of PV's power of 200 kW at time $t = 60$ s

The power regulation of the converter takes place almost immediately, while the rest of the system responds with the typical dynamics of primary and secondary regulation.

To demonstrate that this solution helps the converter's insertion into the system, which causes a large variation in the power required from it, another simulation has been done setting active the branch of the control that takes into account the inertial energy before that the PV delivers power, at start-up when no power is yet produced by the PV:

- at time $t = 0,4$ s the branch of the inertial energy E_w is activated,
- at $t = 1$ s the PV starts to deliver power P_{PV} .

Figure 3.4-9 shows the phase voltage and current at the measuring point.

Figure 3.4-10 shows the power requested from the loads and the ones delivered by the converter and synchronous machine, SM2 in green, SM1 in red and converter in blue.

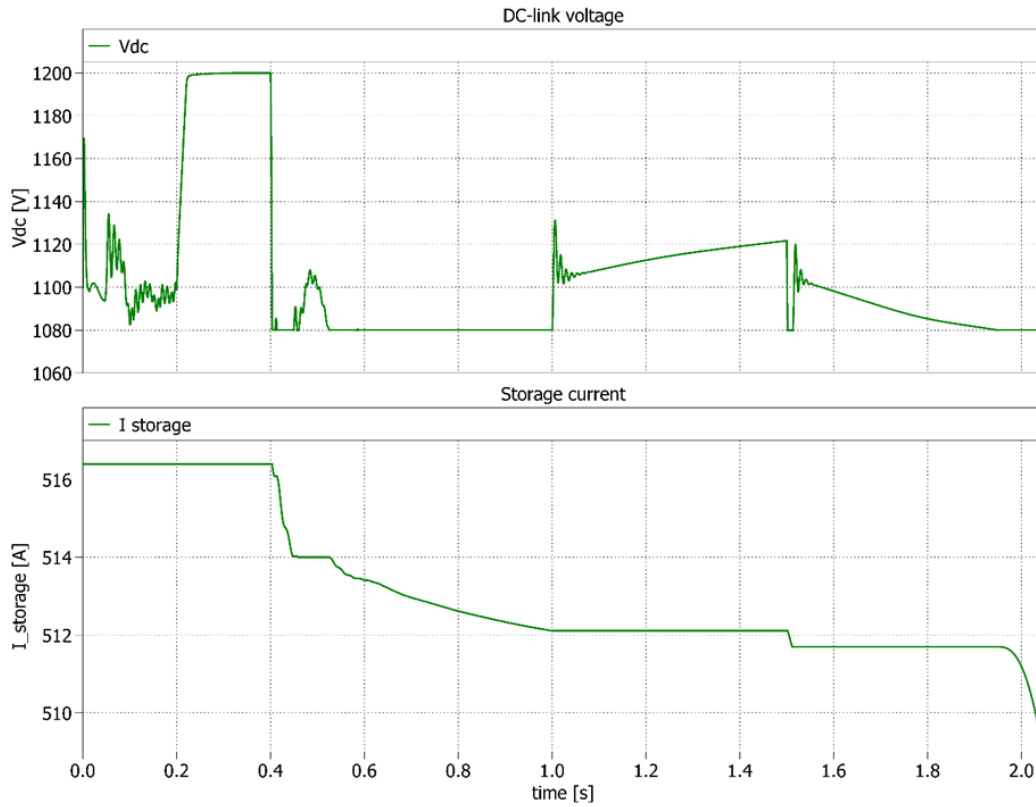


Figure 3.4-9 Dynamic behavior of the DC-link voltage and storage's current- inertial energy is activated at time $t = 0,4$ s.- initial transient.

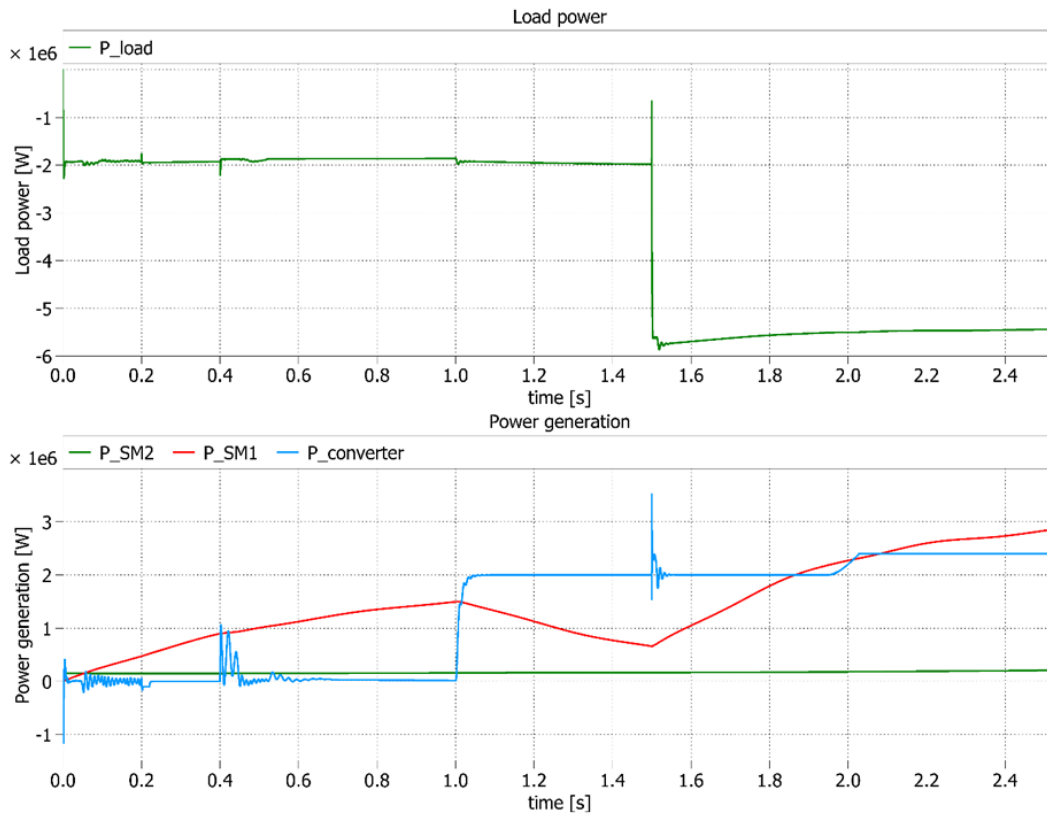


Figure 3.4-10 Dynamic behavior of the load's power and of the sources - inertial energy is activated at time $t = 0,4$ s.- initial transient.

It can be noted that, as soon as the virtual inertia energy's branch of the control is activated, the insertion of the DC-link capacitor into the control system is supported by the storage and therefore the power supplied by the converter remains zero. When the PV starts to deliver power at $t = 1$ s the capacitor is free to charge without overvoltage and storage intervention.

3.5 Case PV's power generation bigger than load's request

The worst disadvantage of using a photovoltaic renewable energy source is that it is intermittent, in the meaning that it is not possible to predict when the power delivered by the PV increases or decreases.

So far, the situation in which the converter in consideration contributes to feed into the grid only part of the entire power demand has been analyzed. Now it's wanted to analyze the situation in which there is a PV power overproduction compared to the load's demand, $P_{PV} > P_{load}$.

Two simulations have been carried out where the converter is used:

- without the storage in sub-chapter 3.5.1
- with the addition of storage to the DC-link in sub-chapter 3.5.2.

The parameters chosen for the simulations are the same as the previous ones. The only differences are on the value of load demand:

- the load request is simulated by resistors with resistance equal to

$$R_{load\ 1} = 1,585\ \Omega$$

- the initial condition of the DC-link capacitor is to be already charged at

$$v_{DC}(t = 0) = 1,1\ kV$$

with the starting voltage reference value of

$$v_{DC\ ref} = 1,2\ kV$$

- the DC-link voltage regulation is always active while the inertial energy's branch is not active at the start.
- at time $t = 0,2$ s, a step variation of the DC-link voltage reference value is set to

$$v_{ref\ DC} = 1,2\ kV$$

- at time $t = 1$ s, the activation of a power step generated by the PV is set to

$$P_{PV} = 2\ MW$$

- at $t = 1,3$ s, the branch introducing the inertial energy is activated.

- at time $t = 1,5 s$, the step variation of the load power is given by connecting another line with resistors of resistance

$$R_{load\ 2} = 792\ m\Omega$$

The values of the load resistors are five times bigger than the ones in the previous simulation in the sub-chapter 3.4, so it's expected a load power request five times smaller.

3.5.1 Without energy supplier

The results of the simulation where the PV delivers more power than the one requested by the loads and no storage is used are reported.

The dynamic behavior of the DC-link voltage is shown in the Figure 3.5.1-1.

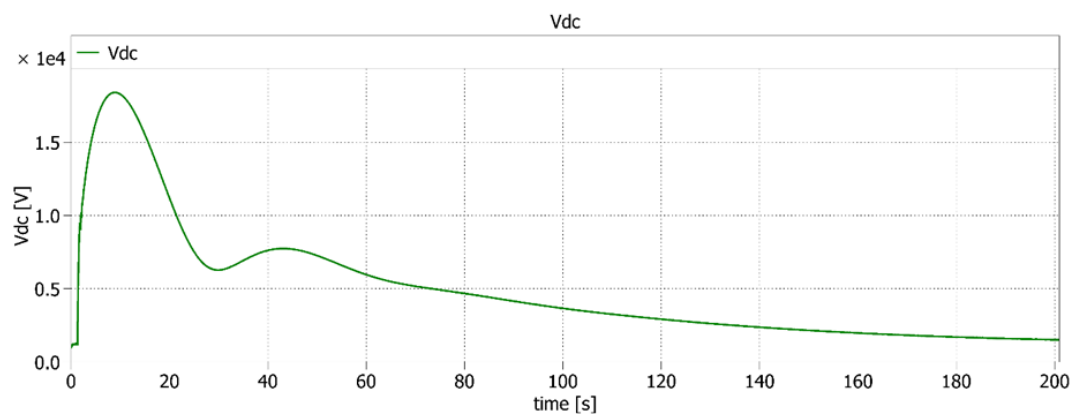


Figure 3.5.1-1 Dynamic behavior of the DC-link voltage- power generation bigger than load's request.

As there is no limit to the maximum DC-link voltage, as soon as power is produced by the PV, it starts to rise to unacceptable values. This reason alone makes it clear that the application is unusable without storage.

Assuming, however, that the energy that can be stored is infinite, the voltage decreases until it reaches the reference level at full power. This is due to the action of the voltage control but has consequences on the other components of the system, as can be seen from the power dynamics graph.

The load power and the power delivered by the converter and the synchronous machines is shown in Figure 3.5.1-2.

The rotational speeds of synchronous machines are shown in the Figure 3.5.1-3.

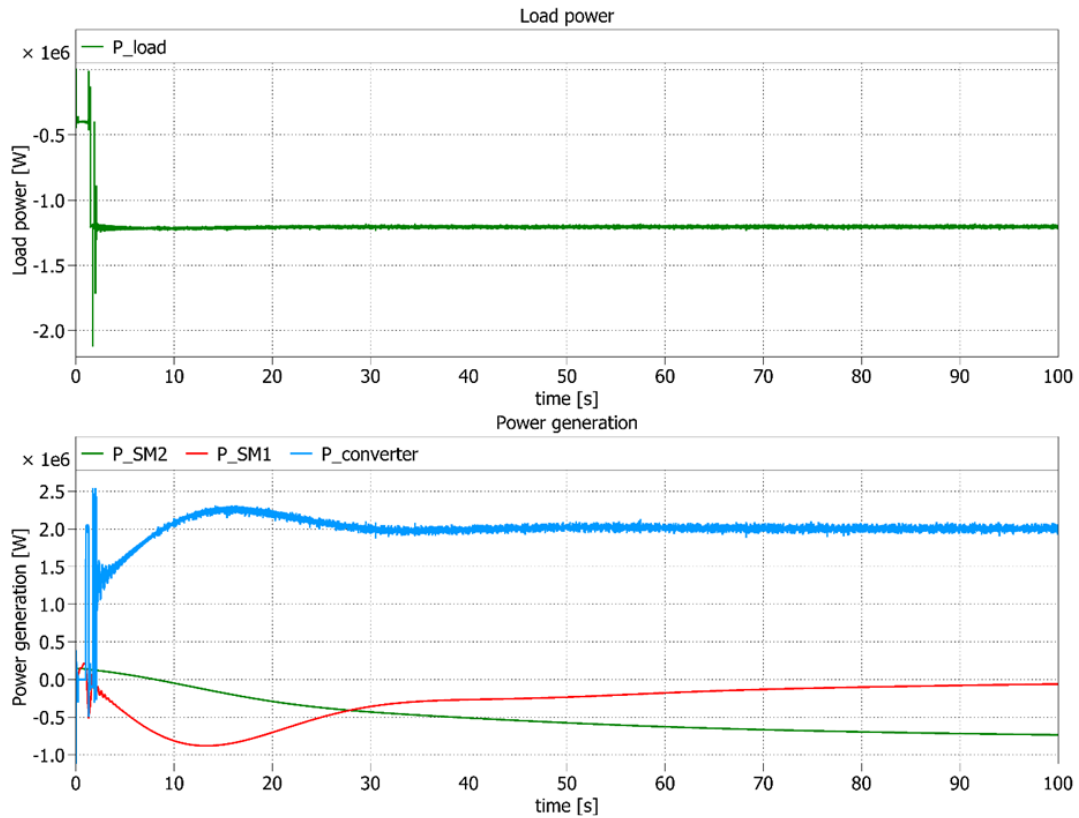


Figure 3.5.1-2 Dynamic behavior of the load's power and of the sources - power generation bigger than load's request.

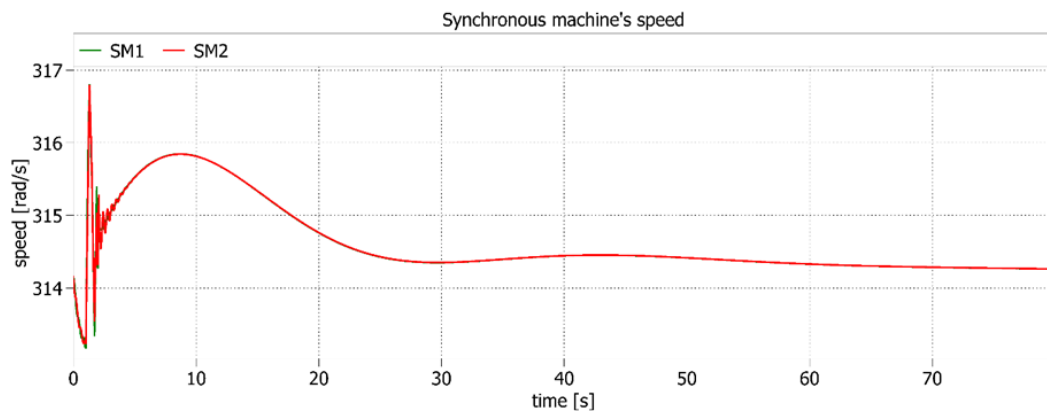


Figure 3.5.1-3 Mechanical speed measured on both the synchronous machines- power generation bigger than load's request.

At the steady state, the power delivered by the converter reaches the value of the power delivered by the PV. This means that whatever is the value of the power required by the loads, the converter is inclined to feed everything it has available into the grid, even if it is more than necessary. This means that synchronous generators start to absorb this extra power and accelerate.

This behavior can also be seen in the plot of the power required by the converter in Figure 3.5.1-4.

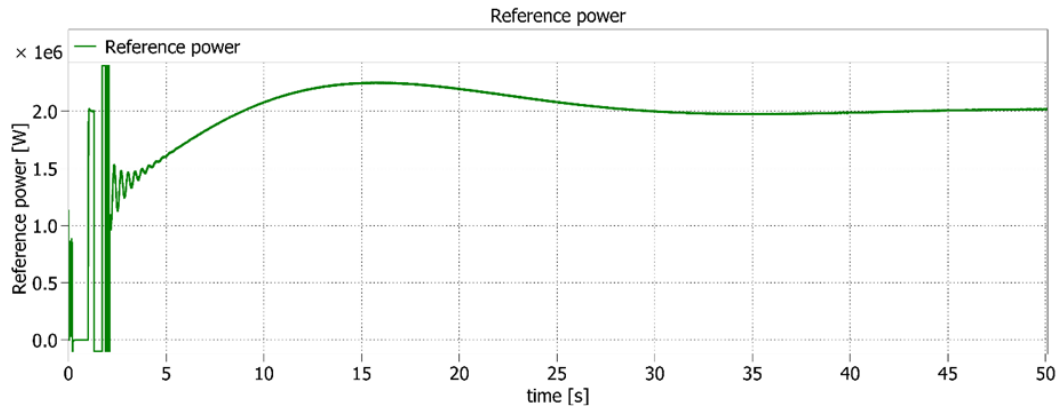


Figure 3.5.1-4 Dynamic behavior of the converter's reference power- power generation bigger than load's request.

In this simulation, as the PV's power can power the whole system by itself, the reference power of the converter is saturated at $P_{sat} = 2,4 MW$ for only a few time during the first seconds and then it reaches the level of the power generated by the PV, P_{PV} . In the case of overproduction, therefore, the reference power P_{ref} has an average value independent on the load demand but it is proper calculated so that the converter generates all the power that feeds it, coming from PV production.

Detailing the first few seconds of the plots of the load power and the power delivered by the converter and alternators, reported in Figure 3.5-5, it can be seen better that synchronous generators and converter establish a power exchange.

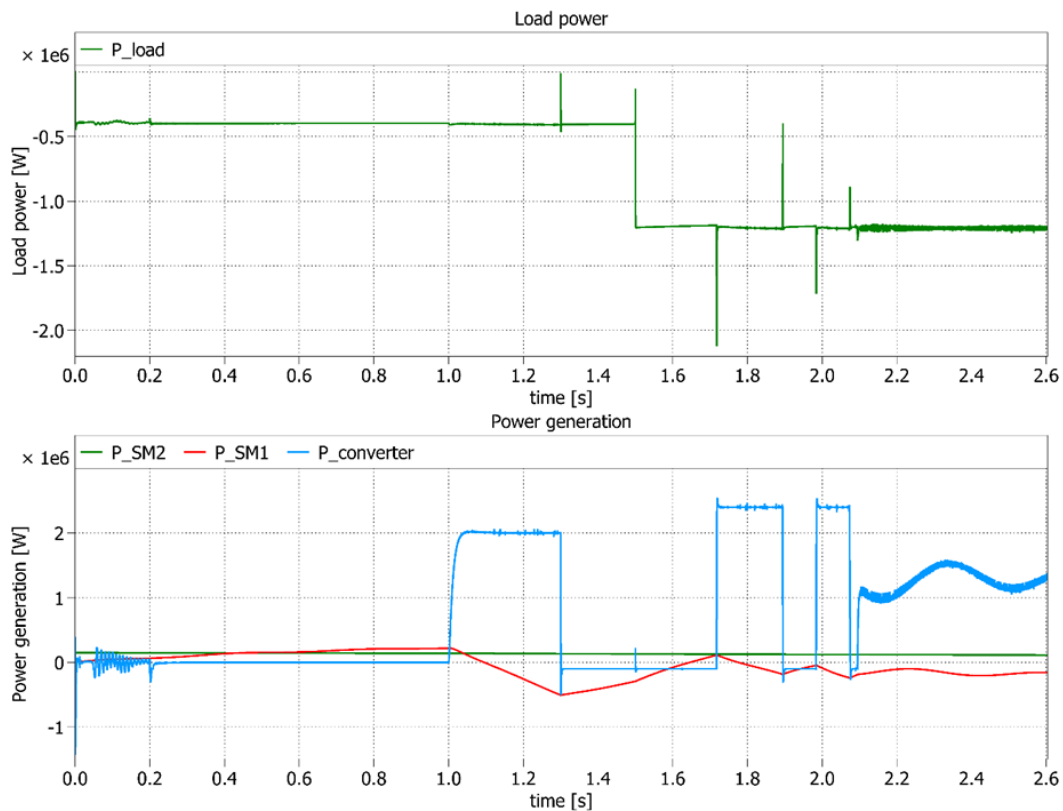


Figure 3.5.1-5 Dynamic behavior of the load's power and of the sources - power generation bigger than load's request- initial transient.

3.5.2 With energy supplier

The results of the simulation where the PV delivers more power than the one requested by the loads and the storage is connected to the DC-link are reported.

The dynamics of the DC voltage and of the storage current are reported in Figure 3.5.2-1.

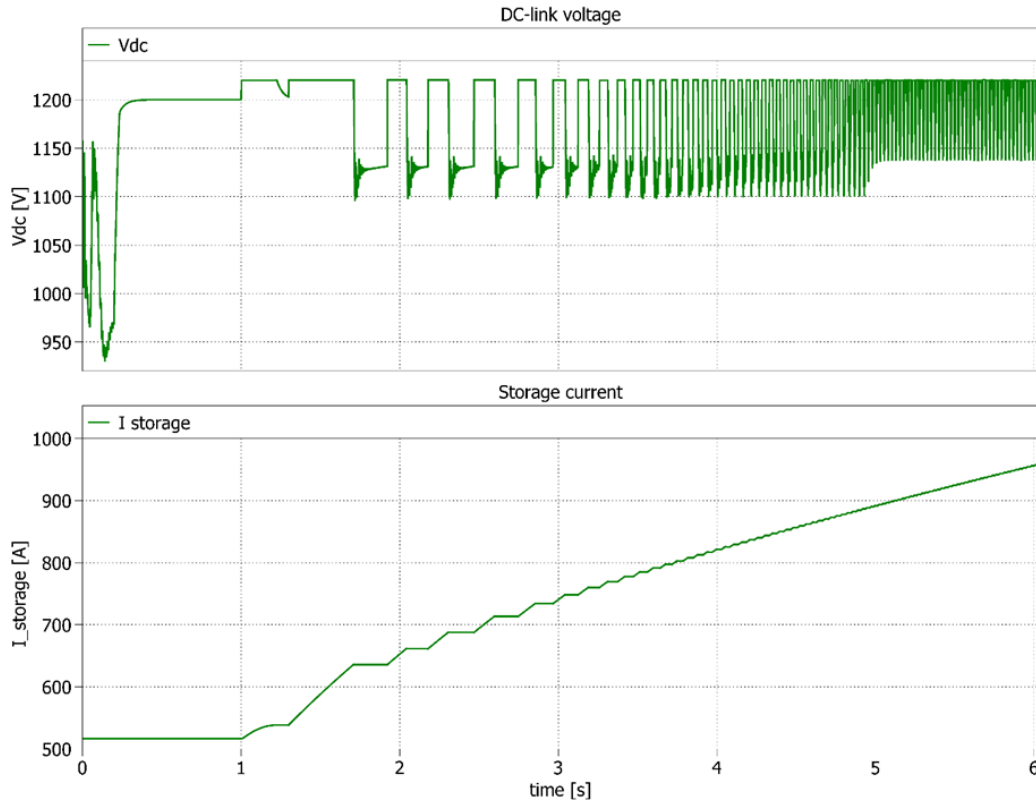


Figure 3.5.2-1 Dynamic behavior of the DC-link voltage and storage's current-power generation bigger than load's request.

Looking at the DC voltage dynamic, at $t = 1$ s, when the PV starts to deliver power, the maximum acceptable voltage value $V_{DC\ max}$ is reached without overvoltage. This is because the excess power coming from the PV is stored in the storage, which increases its energy.

Initially, the voltage has a dynamic with an almost rectangular waveform and with increasing frequency over time. The minimum peak is saturated a lot of times but for less and less time and then has an increasing value until it reaches a constant minimum peak at $v_{DC} = 1030\ V$ at the steady state.

The steady state situation is after $t = 5$ s, where the waveform stabilizes at a constant duty cycle without any more oscillations after every voltage drop. The average value of the rectangular waveform corresponds to $v_{DC} = 1160\ V$.

The current accumulated by the storage has a variation when the DC-link voltage is inclined to go out of the chosen acceptable range $V_{DC\ min-max}$ and it has a periodic triangular waveform with an increasing average value. Before reaching

the steady state at about $t = 5 \text{ s}$, there are increasing and decreasing current intervals because there are saturations at the lower voltage value $V_{DC \text{ min}}$. Later, when the voltage saturation occurs only for the maximum value, there are increasing and constant current intervals. The frequency of the storage current's variation follows the one of the DC-link voltage.

The Figure 3.5.2-2 shows the load power and of the power delivered by the converter and by the synchronous alternators.

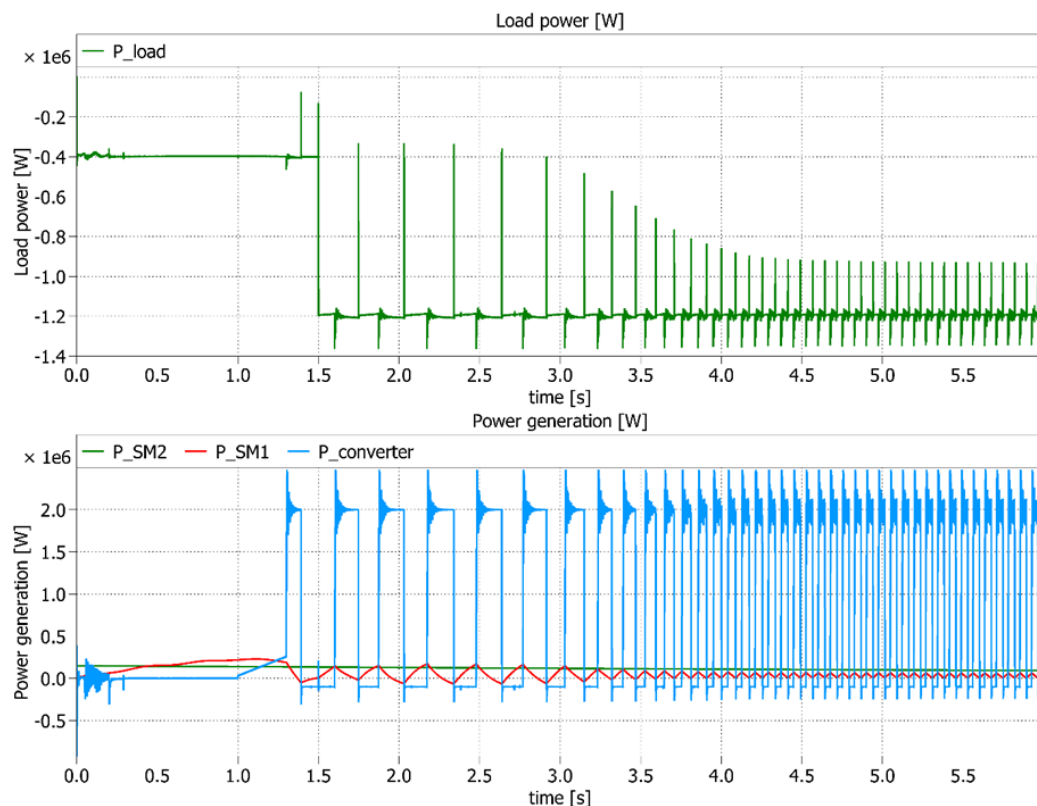


Figure 3.5.2-2 Dynamic behavior of the load's power and of the sources with storage- power generation bigger than load's request- initial transient.

Unlike without storage, the power generated by the PV, P_{PV} , is now delivered for a certain time to the AC system, P_{AC} , and for another time to the energy storage, $\frac{d}{dt} E_{storage}$. Synchronous generators are activated by absorbing a small amount of power when the converter feeds power into the AC grid. They deliver the same amount of energy previously stored as power to the loads just at the time intervals when the converter is delivering power to the storage. This creates a stable periodic situation where the average power required by the synchronous generators is zero, and the average power fed into the AC grid by the converter is equal to that required by the loads.

This can be seen from the converter's reference power P_{ref} plot in Figure 3.5.2-3.

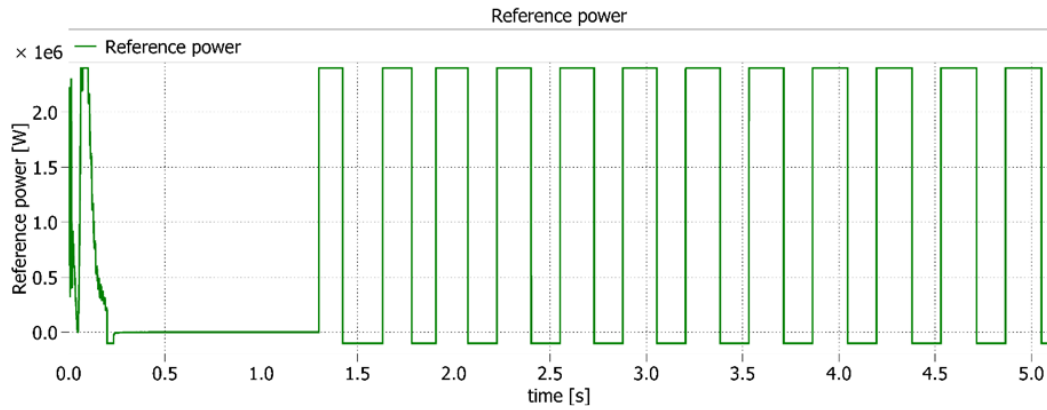


Figure 3.5.2-3 Dynamic behavior of the converter's reference power with storage-power generation bigger than load's request.

Differently from the case without storage, this time it is a rectangular waveform that saturates at the maximum and minimum values permissible for the converter. The average value no longer coincides with the power supplied by the PV, but it is equal to the sum of the load demand, $P_{load} = 1,2 MW$, plus the temporary demand of the synchronous generators, tending to become null at the steady state.

There are advantages also for the frequency dynamics, which can be observed from the speed of the synchronous generators in Figure 3.5.2-4.

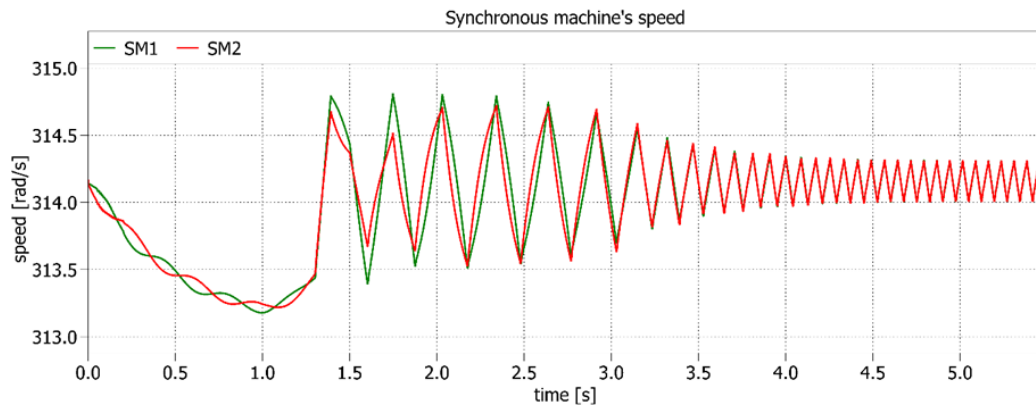


Figure 3.5.2-4 Mechanical speed measured on both the synchronous machines-power generation bigger than load's request using the storage.

The oscillations have a gradually decreasing amplitude, starting from a maximum value of $\Delta\omega = 0,5 rad/s$. The wide variations in speed that used to occur without storage are no longer present; on the contrary, the average value over time settles down very quickly to the reference value of $\omega_1 = 2 \cdot \pi \cdot 50 rad/s$.

Conclusions

The aim of this thesis has been to design the string converter control model for the PV TRUST project in which the Huawei Nuremberg Research Center participates to increase the amount of renewable energy produced by photovoltaic panels and thus the penetration of electrical power converters into the grid.

My personal contributions are listed below:

- Studying the currently used state of the art of frequency regulation done with synchronous alternators through simulations with MATLAB and PLECS software. The total inertia value of the interconnected machine system makes the response to the load power step more damped. Secondary regulation is essential to cancel the frequency variation at steady state caused by rotating loads and friction.
- Understand what problems arise in the future perspective of high-density non-synchronous generation grids, such as possible loss of synchronism and low short circuit current in case of faults. Implementing the Grid following converter control allowed to understand how to calculate the voltage references of the converter as a function of the frequency. Implementing the Grid forming control, in particular the Virtual Synchronous Machine control, has helped to understand how to introduce the typical frequency regulation dynamics of a synchronous machine to a static converter by receiving as input the value of electrical power present at the measurement point.
- Design a lumped average model of the string inverter to be implemented in the TRUST PV project that ensures stability of the converter model and reduces the order of complexity of the model. This is achieved by giving appropriate values to the active damping coefficient and making simplifying assumptions. The current loop is designed considering these assumptions. The voltage loop is an outer loop in cascade with the current loop that generates a power reference by the value of the energy of the DC-link and thus controlling the square value of its DC voltage.
- Design of the frequency regulation actuated by the converter by introducing virtual inertial energy. Simulations have been carried out where the converter works with synchronous alternators. The response to the power steps reveals the need to limit the value of the DC-link voltage in the transient to a limit band; Help the converter's insertion into the system, which causes a large variation in the power required from it. To evaluate the introduction of a storage to the DC-link and to add to the control model its activation/deactivation. This solution resolves the issues that have arisen when it is not used, and it allows to have a energy storage in the case of photovoltaic overproduction. This avoids the acceleration/deceleration of

synchronous alternators and keeps the grid frequency closer to the reference value. The advantage of having a converter that anticipates the action of the synchronous machines in case of small power variations is that it helps to keep their speed constant and thus also the grid frequency.

The model produced satisfies all the requirements of the project and it should be tested in the next points of the PV TRUST project.

References

- [1] J.J.Grainger e W.D.Stevenson, Power system analysis, McGraw Hill.
- [2] R.Marconato, Electric power systems. Vol.1 - Background and basic components, CEI - Comitato Elettrotecnico Italiano.
- [3] R.Marconato, Electric power systems. Vol. 3 - Dynamic behaviour, stability and emergency controls., CEI - Comitato Elettrotecnico Italiano.
- [4] R.Marconato, Electric power systems. Vol. 2 - Steady-state behaviour controls, short circuits and protection systems., CEI - Comitato Elettrotecnico Italiano.
- [5] T. Finnigan, «Preparing the grid for a future without coal, blackouts or emissions,» IEEFA Institute for Energy Economics and Financial Analysis, 2021.
- [6] [. EirGrid, «System Non-Synchronous Penetration - Definition and Formulation,» 2018. [Online].
- [7] AEMO, «NEM Engineering Framework,» 2021.
- [8] F. Longatt e J. Rueda, Modelling and simulation of the power electronic converter dominated power system in PowerFactory, Springer-Verlag.
- [9] P. Kundur, J. Paserba, V. Ajjarapu, G. Andersson, A. Bose, C. Canizares, N. Hatziargyriou, D. Hill, A. Stankovic e C. Taylor, Definition and classification of power system stability, 2004.
- [10] P.kunder, Power system stability and control, IEEE, 2003.
- [11] N. Hatziargyriou, J. V. Milanovi, C. Rahmann, V. Ajjarapu, I. Erlich, D. Hill, I. Hiskens, I. Kamwa, B. Pal e P. Pourbeik, Stability definitions and characterization of dynamic behavior in systems with high penetration of power electronic interfaced technologies, IEEE, 2020.
- [12] T. Neumann e I. Erlich, «Short Circuit Current Contribution of a Photovoltaic Power Plant,» Institute of Electrical Power Systems University Duisburg Essen , 2012.
- [13] N. G. ESO, «System operability framework - Impact of declining short circuit levels,» National Grid ESO, 2018.
- [14] F. Viollaz, «Draft 1 OMIB Benchmark SYM versus PV,» Enel, 2021.
- [15] M. Reza, «Stability analysis of transmission systems with high penetration of distributed generation,» Delft University of Technology, 2006.
- [16] F. Mandrile, «Next Generation Inverters Equipped with Virtual Synchronous Compensators for Grid Services and Grid Support,» Politecnico di Torino, 2021.
- [17] ENTSO-E, «Vision on Market Design and System Operation towards 2030,» ENTSO-E.
- [18] P. Mancarella e F. Billimoria, «The Fragile Grid: The Physics and Economics of Security Services in Low-Carbon Power Systems,» *IEEE Power and Energy Magazine*, 2021.
- [19] Longatt, «Innovative Smart Grid Technologies-Asia (ISGT-Asia),» *IEEE*, 2016.

- [20] F. Gonzalez-Longatt, Impact of inertia from wind power on under-frequency protection scheme for future power systems - vol. 4, 2016.
- [21] R. Rosso, X. Wang, M. Liserre, X. Lu e S. Engelken, «Grid-forming converters: an overview of control,» *IEEE*, 2020.
- [22] Y. Zuoa, Z. Yuana, F. Sossan, A. Zecchino, R. Cherkaoui e MarioPaolonea, «Performance assessment of grid-forming and grid-following converter-interfaced battery energy storage systems on frequency regulation in low-inertia power grids,» *Elvesier*, 2020.
- [23] Y. Li, Y. Gu e T. C. Green, «Rethinking Grid-Forming and Grid-Following Inverters: A Duality Theory,» *Cornell University*, 2021.
- [24] F. Freijedo e A. M. Munoz, Interviewees, *Grid following meeting*. [Intervista]. 2021.
- [25] R. H. Lasseter e T. M. Jahns, «Comparison of Grid Following and Grid Forming,» *IEEE*, 2018.
- [26] F. Freijedo e A. M. Munoz, Interviewees, *Grid forming meeting*. [Intervista]. 2021.
- [27] A. M. M. Munoz e F. Freijedo, «WP5- Increase friendly integration of reliable PV plants considering different market segments,» *Huawei Nuremberg Research Center*, 2021.
- [28] F. Freijedo, «Grid-Forming capabilities for next generation of power converters,» *Huawei Power Conversion Technology; Huawei Nuremberg Research Center*, 2020.
- [29] A. G. Radwan, «Resonance and Quality Factor of the RLC Fractional Circuit,» *IEEE*, 2013.
- [30] F. Freijedo, «An overview on power electronics control,» *Huawei Power Conversion Technology; Huawei Nuremberg Research Center*, 2020.
- [31] T. Qoria, «Grid-forming control to achieve a 100% power electronics interfaced power transmission systems,» *HESAM Université*, 2020.
- [32] Z. Yu, R. Ayyanar, V. Vittal e J. Undrill, «Converter model for representing converter interfaced generation in large scale grid simulations,» *IEEE*, 2017.
- [33] K. D. Brabandere, B. Bolsens, J. V. d. Keybus, A. Woyte, J. Driesen e R. Belmans, «A voltage and frequency droop control method for parallel inverters,» *Huawei Technologies Co Ltd ; IEEE Xplore*, 2007.
- [34] L. A. d. S. Ribeiro, F. Freijedo, F. d. Bosio, M. S. Lima, J. Guerrero, F. Member e M. Pastorelli, «Full discrete modeling, controller design, and sensitivity analysis for high-performance Grid-Forming Converters in Islanded Microgrids,» *IEEE*, 2018.
- [35] F. Viollaz, «Performance verifications of grid-connected inverters - Revision 4,» *Enel*, 2021.
- [36] A. Tayybi, F. Dörfler, F. Kupzog, Z. Miletic e W. Hribernik, «Grid-Forming Converters - inevitability, control strategies and challenges,» *CIREN*, 2018.
- [37] J. Fang, H. Li, Y. Tang e F. Blaabjerg, «On the inertia of future more-electronics power systems,» 2019.
- [38] I. Cvetkovic, D. Boroyevich, R. Burgos, C. Li, M. Jaksic e P. Mattavelli, «Modeling of a Virtual Synchronous Machine-based Grid-interface Converter for Renewable Energy Systems Integration,» *Huawei Technologies Co Ltd; IEEE Xplore*, 2021.

- [39] Q.-C. Zhong e G. Weiss, «Synchronverters: inverters that mimic synchronous generators,» Huawei Technologies Co Ltd. ; IEEE Xplore, 2011.
- [40] Q.-C. Zhong, P.-L. Nguyen, Z. Ma e W. Sheng, «Self-Synchronized Synchronverters: inverters without a dedicated synchronization unit,» Huawei Technologies Co Ltd. ; IEEE Xplore, 2014.
- [41] «Solar PV, performance e reliability,» TRUST PV, 2021. [Online]. Available: <https://trust-pv.eu/>.
- [42] «Project overview - Objectives,» TRUST PV, 2021. [Online]. Available: <https://trust-pv.eu/project-overview/>.
- [43] D. Moser e C. Vedovelli, «EU H2020 TRUST-PV: Increase Friendly Integration of Reliable PV plants considering different market segments,» *Eurac Research*, 2021.
- [44] K. Monar e O. Gagricca, «Switching and average models of grid-connected battery inverter,» Typhoon HIL.
- [45] F. Viollaz, «Analysis of performance of customary inverter model used in interconnection studies,» Enel, 2016.
- [46] J. P. O'Connor, *Off Grid Solar: A handbook for Photovoltaics with Lead-Acid or Lithium-Ion batteries Paperback - ed. 2, Alternative Energy*, 2019.
- [47] J. Dannehl, F. W. Fuchs, S. Hansen e P. B. Thøgersen, «Investigation of active damping approaches for PI-based current control of grid-connected pulse width modulation converters with LCL filters,» IEEE, 2010.
- [48] F. D. Freijedo, E. Rodriguez-Diaz, M. S. Golsorkhi, J. C. Vasquez e J. M. Guerrero, «A Root-Locus design methodology derived from the impedance/admittance stability formulation and its application for LCL grid-connected converters in wind turbines,» Huawei Technologies Co Ltd. - IEEE Xplore, 2017.
- [49] F. D. Freijedo e D. Dujic, «Design for Passivity in the Z-Domain for LCL,» *IEEE*, 2016.
- [50] E. Rodriguez-Diaz, F. Freijedo, J. M. Guerrero, J. Marrero-Sosa e D. Dujic, «Input-Admittance passivity compliance for Grid-Connected Converters with an LCL filter,» *IEEE TRANSACTIONS ON INDUSTRIAL ELECTRONICS*, 2019.
- [51] D. D. Rooij, «String inverters: advantages and disadvantages explained,» *Sino Voltaics*, 2021.
- [52] A. M. Munoz e F. Freijedo, «Several LCL inverters in parallel and a grid: Lumped Model,» Huawei Nuremberg Research Center, 2021.
- [54] B. d. Metz-Noblat, F. Dumas e C. Poulain, *Cahier technique no.158, Schneider Electric*, 2006.
- [55] F. D. Freijedo, A. Vidal, A. G. Yepes, J. M. Guerrero, Ó. López, J. Malvar e J. Doval-Gandoy, «Tuning of synchronous-frame PI current controllers in grid-connected converters operating at a low sampling rate by MIMO root locus,» *IEEE TRANSACTIONS ON INDUSTRIAL ELECTRONICS*, 2015.
- [56] H. Cao, «Modeling, simulation and controller for AC/DC and DAB1 converter,» HUAWEI TECHNOLOGIES Duesseldorf GmbH - Energy Competence Center Europe –ECCE- Nuremberg.
- [57] Q. Yang, D. Han, L. Xiong e T. Yi, «Synthetic inertia control of grid-connected inverter with tailored synchronization dynamics,» *IEEE Transactions on Power Electronics*, 2021.

- [58] A. Holczer, «Current harmonic reduction in PMSM Drive,» HUAWEI TECHNOLOGIES Duesseldorf GmbH - Energy Competence Center Europe (ECCE)- Nuremberg, 2021.
- [59] A. Fratta, Conversione statica dell'energia elettrica, CLUT, 1998.
- [60] S. E. Institute, «Hydrogen based energy conversion,» 2014.
- [61] A. Badel, «Superconducting magnetic energy storage using high temperature superconductor for pulse power supply,» Institut National Polytechnique de Grenoble, 2010.